

Structural and functional characterization of a Major Facilitator Superfamily multidrug resistance transporter (MdfA) from *Escherichia coli*

Dissertation

zur Erlangung des akademischen Grades
doctor rerum naturalium
(Dr. rer. nat.)

vorgelegt der

Naturwissenschaftlichen Fakultät I - Biowissenschaften

der Martin-Luther-Universität
Halle-Wittenberg



von Herrn Kumar Nagarathinam, M.Sc.

geboren am 10. Februar 1987 in Salem, India

Halle (Saale) | Germany | 2020

This research work was initiated in March 2013 and completed in February 2017 at the ZIK-**HALO**mem center for Membrane Protein Structure and Dynamics, Halle (Saale), Germany.

Date of the Doctoral defense: 02.12.2020

Supervisors:

Prof. Dr. Milton.T.Stubbs (Institute of Biotechnology, MLU, Halle)

Dr. Mikio Tanabe (Structural Biology Research Center, KEK, Japan)

Prof. Dr. Klaas Martinus Pos (Institute of Biochemistry, Goethe Universität, Frankfurt)

Examination Board:

Prof. Dr. Dietrich H. Nies (Institute of Biology/Microbiology, MLU, Halle)

Prof. Dr. Andreas Simm (University Hospital, MLU, Halle)

“If you want to shine like a sun, first burn like a sun”

- *Dr. A.P.J Abdul Kalam*

ABSTRACT

Efflux pump-mediated resistance towards antibiotics poses an increasing challenge for the treatment of pathogenic bacterial infections. Efflux pumps also known as multidrug resistance (MDR) transporters are embedded in the bacterial membrane and expel the antibiotics from the cytoplasm to the periplasm or to the extracellular space thereby mediating resistance. A large group of MDR-antiporters belong to the Major Facilitator Superfamily (MFS). These transporters shuttle the substrates across the membrane by the so-called “Alternating access mechanism”, a hallmark of this superfamily.

The main focus of this thesis is to unravel the efflux mechanism of bacterial MFS-type multidrug resistance antiporter. MdfA, a H⁺/multidrug antiporter possesses functional elements conserved in other MFS-MDR antiporters which makes it a model character to study efflux transport. Although many biochemical data are available for MdfA, the absence of structural information impedes a deeper understanding of efflux transport. Before the initiation of this project, the only crystal structure available of the efflux antiporter was EmrD (occluded state) resolved at 3.5 Å resolution. EmrD is biochemically less characterized and does not lend any support to describe an efflux mechanism. We perceived that the structural characterization of MdfA with the available biochemical data will help to provide insights into the mechanism of efflux transport. In order to determine the structure of MdfA, we chose X-ray crystallography for which crystals need to be grown.

Membrane proteins are notoriously difficult to crystallize as they are purified in detergent. Detergents jacket the surface preventing the crystallization process and can also be detrimental for the stability of the protein which can lead to low protein quantity deficient for crystallization trials. Membrane proteins can also be conformationally flexible which hamper the formation of well-ordered crystals. Co-crystallization with antibody fragment (Fab) has shown to yield significant advantages in reducing the conformational flexibility by stabilizing the membrane protein to a single state. Antibody fragment binding also provides an extended hydrophilic portion for crystal-crystal contacts which are often hampered by the detergents used for membrane protein purification. Using the advantages of Fab as a crystallization chaperone by systematic screening, we were able to identify a Fab fragment (YN1074) which formed a stable complex with MdfA. MdfA-YN1074 Fab complex showed high stability assessed by CPM thermostability assay and enhanced crystallization properties compared to the other MdfA-Fab complexes and MdfA wild type (**Manuscript I**).

We assessed the thermostability of MdfA-YN1074 Fab complex as a function of pH. We identified Fab-YN1074 binding to MdfA suppressed pH-dependent thermostability changes of the complex and allowed crystallization screening under a wide range of pH conditions. MdfA wild type and MdfA-Fab complexes were subjected to both vapour diffusion (VD) and lipidic cubic phase (LCP) crystallization techniques. VD grown crystals of MdfA wild type and MdfA-YN1074 Fab complex were of type II packing with weak crystal contacts and poor diffraction behaviour. In contrast, MdfA-YN1074 Fab complex crystals grown in the LCP resulted in crystals of type I packing diffracting to a high resolution of 3.4 Å belonging to the hexagonal space group P6₁22 (**Manuscript II**).

Crystal structure determination revealed an outward-open (O_o) conformation of MdfA with Fab-YN1074 bound to the cytoplasmic side. In 2015, the ligand bound inward-facing (I_F) structures of MdfA were published at high resolution which revealed insights of the substrate-binding site and a model of the transport cycle was proposed. MdfA localized to the inner membrane of *E. coli* consists of 12 transmembrane (TM) helices. The 12 TM helical fold can be split into pseudosymmetrical halves as N- and C-terminal domains with 6 TM helices each connected by a cytoplasmic loop. The two domains enclose a substrate-binding pocket which is

either open to the periplasmic or to the cytoplasmic side of the inner membrane by the rigid body rotation of the two domains along the plane of the lipidic bilayer.

Comparing the O_o state with the published ligand bound inward-facing structure, two relevant structural differences were observed localized to the conserved motifs, “Motif B, Motif C” within the N-terminal domain. These conserved motifs are known to play an important role in the antiport activity of MdfA and other antiporters. The differences show that in the O_o structure that the transmembrane helix (TM) 5 was kinked around motif-C, “APXXGP”, observed only in antiporters and a slight significant expansion of the hydrophobic cluster was observed surrounding Arg112^{TM4} of conserved motif-B, “RXXXG”. Previously identified acidic residues Glu26^{TM1} and Asp34^{TM1} within the binding cavity are known to be involved in the H^+ /substrate coupling.

Based on the structural differences, molecular dynamics simulations studies and transport assay, we propose a conformational switching mechanism for MdfA. Exposure of the binding cavity to low periplasmic pH in the O_o state upon protonation of Asp34^{TM1} is thought to trigger the conformational switching of MdfA from an outward-open to the inward-open state. Changes in the chemical environment around the protonated Asp34^{TM1} may result in the rearrangement of the hydrophobic cluster around motif-B which in turn extends the rearrangements in helix TM4. Further to note motif-C present on helix TM5 achieves different conformations (kinked or straight form) which are associated in dictating the conformational states either as O_o or I_F state respectively. The highly conserved TM5 motif-C appears to play a central role in the relative orientations of the two domains and the conformational switching mechanism proposed here may apply to 12 TM helical MFS type-MDR antiporters comprising the conserved motifs as MdfA (**Manuscript III**).

In this thesis, I describe the process involved in generating well-ordered MdfA-Fab crystals using the lipidic cubic phase method and present the structure of MdfA in an O_o state. Comparing the O_o structure of MdfA with the published I_F structure, provides insights into the conformational switching mechanism which may serve as a template to understand drug efflux in other MFS-MDR type antiporters.

ZUSAMMENFASSUNG

Die Effluxpumpen-vermittelte Resistenz gegen Antibiotika stellt die Behandlung pathogener bakterieller Infektionen vor eine zunehmende Herausforderung. Efflux-Pumpen, welche auch als MDR-Transporter (Multidrug Resistance) bezeichnet werden, sind in die Bakterienmembran eingebettet. Sie vermitteln Resistenzen indem sie Antibiotika aus dem Zytoplasma in das Periplasma oder in den extrazellulären Raum ausschleusen. Eine große Gruppe von MDR-Antiportern gehört zur Major Facilitator Superfamilie (MFS). Diese Transporter transportieren die Substrate durch den sogenannten "Alternating Access Mechanism", ein Markenzeichen dieser Superfamilie, über die Membran.

Das Hauptaugenmerk dieser Arbeit liegt auf der Aufklärung des Effluxmechanismus der bakteriellen Multidrug-Resistenz-Antiporter vom MFS-Typ. MdfA, ein H⁺ / Multidrug-Antiporter, verfügt über Funktionselemente, die gegenüber anderen MFS-MDR-Antiportern konserviert sind. Deshalb kann er als Modell dienen, um den Efflux-Transport zu untersuchen. Obwohl viele biochemische Daten für MdfA verfügbar sind, erschwert das Fehlen von Strukturinformationen ein tieferes Verständnis des Effluxtransports. Vor Beginn dieses Projekts war die einzige verfügbare Kristallstruktur, die des Efflux-Antiporters EmrD (okkludierter Zustand), mit einer Auflösung von 3.5 Å. EmrD ist biochemisch unzulänglich charakterisiert und die verfügbaren Daten lassen keine Rückschlüsse auf einen Effluxmechanismus zu. Wir vermuteten, dass die strukturelle Charakterisierung von MdfA mit den verfügbaren biochemischen Daten dabei helfen könnte, einen Einblick in den Mechanismus des Effluxtransports zu gewinnen. Um die Struktur von MdfA zu bestimmen, haben wir die Röntgenkristallographie gewählt, für welche Kristalle gezüchtet werden müssen.

Membranproteine sind bekanntermaßen schwierig zu kristallisieren, da sie in Detergenz gereinigt werden. Detergenzien umhüllen die Oberfläche und verhindern den Kristallisationsprozess. Sie können auch die Stabilität des Proteins beeinträchtigen, was zu einer geringen, für Kristallisationsversuche unzureichenden Proteinausbeute führen kann. Membranproteine können auch konformationsflexibel sein, was die Bildung gut geordneter Kristalle behindert. Es hat sich gezeigt, dass die Co-Kristallisation mit einem Antikörperfragment (Fab) signifikante Vorteile bei der Stabilisierung des Membranproteins auf einen einzelnen Zustand bringt, indem die Konformationsflexibilität verringert wird. Die Antikörperfragmentbindung bietet auch einen erweiterten hydrophilen Anteil für Kristall-Kristall-Kontakte, die häufig durch die zur Reinigung von Membranproteinen verwendeten Detergenzien behindert werden. Unter Verwendung der Vorteile von Fab als Kristallisations-Chaperon konnten wir durch systematisches Screening ein Fab-Fragment (YN1074) identifizieren, das mit MdfA einen stabilen Komplex bildete. Der MdfA-YN1074 Fab-Komplex zeigte im Vergleich zu den anderen MdfA-Fab Komplexen und dem MdfA-Wildtyp eine hohe, durch ein CPM-Thermostabilitätsassay ermittelte, Stabilität und verbesserte Kristallisationseigenschaften (**Manuscript I**).

Wir untersuchten die Thermostabilität des MdfA-YN1074-Fab-Komplexes in Abhängigkeit vom pH-Wert. Wir identifizierten eine Fab-YN1074 Bindung an MdfA, die pH-abhängige Thermostabilitätsänderungen des Komplexes unterdrückte und ein Kristallisationsscreening in einem weiten Bereich von pH-Bedingungen ermöglichte. MdfA-Wildtyp und MdfA-Fab Komplexe wurden sowohl Dampfdiffusions (VD) als auch Lipid Cubic Phase (LCP) Kristallisationstechniken unterzogen. In VD gezüchtete Kristalle des MdfA-Wildtyps und des MdfA-YN1074 Fab Komplexes wiesen eine Packung vom Typ II mit schwachen Kristallkontakten und schlechtem Beugungsverhalten auf. Im Gegensatz dazu führten MdfA-YN1074 Fab Komplexkristalle, die im LCP gezüchtet wurden, zu Kristallen der Typ I Packung, die mit einer hohen Auflösung von 3,4 Å zur hexagonalen Raumgruppe P6122 gehörten (**Manuscript II**).

Die Kristallstrukturbestimmung ergab eine nach außen offene (O_o) Konformation von MdfA mit Fab-YN1074, welches an die cytoplasmatische Seite gebunden war. Im Jahr 2015 wurden hochaufgelöste ligandengebundene, nach innen gerichtete (I_F) Strukturen von MdfA veröffentlicht, welche die Substratbindungsstelle aufdeckten. Des Weiteren wurde ein Modell für den Transportzyklus vorgeschlagen. Das in der inneren Membran von *E. coli* lokalisierte MdfA besteht aus 12 Transmembran (TM) -Helices. Die 12-TM-Helix kann als N- und C-terminale Domäne in pseudosymmetrische Hälften aufgeteilt werden, wobei 6 TM-Helices jeweils durch eine zytoplasmatische Schleife verbunden sind. Die beiden Domänen schließen eine Substratbindungstasche ein, die entweder zur peri- oder zur cytoplasmatischen Seite der inneren Membrane geöffnet ist. Dies wird durch eine starre Rotation der beiden Domänen entlang der Ebene der Lipiddoppelschicht erreicht.

Beim Vergleich des O_o Zustands mit den veröffentlichten, Liganden-gebundenen nach innen gerichteten Strukturen, wurden zwei relevante strukturelle Unterschiede beobachtet, die auf die konservierten Motive, „Motif B, Motif C“ innerhalb der N-terminalen Domäne beschränkt waren. Es ist bekannt, dass diese konservierten Motive eine wichtige Rolle bei der Antiportaktivität von MdfA und anderen Antiportern spielen. Die Unterschiede zeigen, dass in der O_o Struktur die Transmembran-helix (TM) 5 um Motif-C "APXXGP" geknickt war, eine Struktur, die nur in Antiportern beobachtet wurde. Außerdem wurde eine geringfügige, aber signifikante Ausdehnung des hydrophoben Clusters um Arg112^{TM4} des konservierten Motif-B "RXXXG" beobachtet. Zuvor identifizierte saure Reste Glu26^{TM1} und Asp34^{TM1} in der Bindungstasche sind an der H^+ /Substrat-Kopplung beteiligt.

Basierend auf den strukturellen Unterschieden, den Studien zur Molekulardynamiksimulation und dem Transportassay schlagen wir einen Konformationsumschaltmechanismus für MdfA vor. Es wird angenommen, dass ein MdfA Konformationswechsel von einem nach außen offenen in einen nach innen offenen Zustand dadurch ausgelöst wird, dass die Bindungstasche im O_o Zustand dem niedrigen periplasmatischen pH ausgesetzt wird und es damit zu einer Protonierung von Asp34^{TM1} kommt. Änderungen der chemischen Umgebung um das protonierte Asp34^{TM1} können zur Umlagerung des hydrophoben Clusters um Motif B führen, was wiederum die Umlagerungen in der Helix TM4 und TM5 erweitert. Außerdem kann Motif-C, das auf der Helix TM5 vorhanden ist, verschiedene Konformationen (geknickt oder gerade Form) annehmen, wodurch Konformationszustände entweder als O_o Zustand oder als I_F -Zustand vorgegeben werden. Das hochkonservierte TM5-Motif C scheint eine zentrale Rolle bei der relativen Orientierung der beiden Domänen zu spielen, und der hier vorgeschlagene Konformationsumschaltmechanismus könnte für 12 TM-helikale MFS-Typ-MDR Antiporter mit Motif C gelten (**Manuscript III**).

In dieser Arbeit beschreibe ich den Prozess der Erzeugung gut geordneter MdfA-Fab Kristalle mit der Lipidisch Kubischen Phasen Methode und präsentiere die Struktur von MdfA in einem O_o Zustand. Der Vergleich der O_o Struktur von MdfA mit der veröffentlichten I_F Struktur bietet Einblicke in den Konformationsumschaltmechanismus, der als Vorlage für das Verständnis des Arzneimittelausflusses in anderen Antiportern vom MFS-MDR Typ dienen kann.

LIST OF SCIENTIFIC PUBLICATIONS

* Contributed equally

The following scientific papers are included in this dissertation

- I. Generation of conformation-specific antibody fragments for crystallization of the multidrug resistance transporter MdfA.
Jaenecke F*, Nakada-Nakura Y*, **Nagarathinam K**, Ogasawara S, Liu K, Hotta Y, Iwata S, Nomura N, Tanabe M.
Bacterial Multidrug Exporters. Methods in Molecular Biology, vol 1700, 2018. Humana Press, New York, NY
(Copyright SpringerNature, reproduced with permission)
- II. The multidrug-resistance transporter MdfA from *Escherichia coli*: crystallization and X-ray diffraction analysis.
Nagarathinam K*, Jaenecke F, Nakada-Nakura Y*, Liu K, Hotta Y, Iwata S, Stubbs M.T., Nomura N., Tanabe M.
Acta Crystallogr F Struct Biol Commun. 2017 Jul 1;73(Pt 7):423-430
- III. Outward open conformation of a Major Facilitator Superfamily multidrug/H⁺ antiporter provides insights into switching mechanism.
Nagarathinam K*, Nakada-Nakura Y*, Parthier C, Terada T, Juge N, Jaenecke F, Liu K, Hotta Y, Miyaji T, Omote H, Iwata S, Nomura N, Stubbs M.T., Tanabe M.
Nature Communications 9, Article number: 4005 (2018)

The author also contributed to the following scientific paper not included in this dissertation

- IV. Hyperbolic Pressure-Temperature Phase Diagram of the Zinc-Finger Protein apoKti11 Detected by NMR-Spectroscopy.
Klamt A[#], **Nagarathinam K**, Tanabe M, Kumar A, Balbach J.
J. Phys. Chem. B, 2019, 123, 4, 792-801

Contribution to this manuscript:

Crystal structure determination of zinc-finger protein apoKti11. PDBID: 5AX2.

CONTENTS

ABSTRACT	3
ZUSAMMENFASSUNG	5
LIST OF SCIENTIFIC PUBLICATIONS	7
ABBREVIATIONS	9
LIST OF FIGURES	10
LIST OF TABLES	10
1 INTRODUCTION	11
1.1 Antibiotic resistance	11
1.2 Mechanisms of antibiotic resistance	12
1.3 Bacterial multidrug resistance transporters	13
1.4 The Major Facilitator Superfamily	22
1.4.1 General Overview of MFS transporters	22
1.4.2 MFS-type MDR transporters	25
2 PURPOSE OF THIS THESIS	29
2.1 Aim of this thesis	29
2.2 Membrane protein production and crystallization	29
2.3 Multidrug facilitator Assembly, MdfA	37
3 SUMMARY OF THE RESULTS AND DISCUSSION	41
3.1 Manuscript I	41
3.2 Manuscript II	43
3.3 Manuscript III	47
4 CONCLUSIONS AND FUTURE PERSPECTIVES	53
5 REFERENCES	55
6 PUBLICATIONS	67
6.1 Manuscript I	67
6.2 Manuscript II	69
6.3 Manuscript III	81
7 CONTRIBUTIONS	105
8 CURRICULUM VITAE	112
9 DECLARATIONS	114
10 ACKNOWLEDGEMENTS	116

ABBREVIATIONS

3M3SH	3-methyl-3-sulfanylhexasan-1-ol
AcrAB	Acriflavine resistance protein A/B
ASU	Asymmetric unit
ATP	Adenosine triphosphate
Cm	Chloramphenicol
CMC	Critical Micellar Concentration
CPM	N-[4-(7-diethylamino-4-methyl-3-coumarinyl)phenyl]maleimide
DCCD	Dicyclohexylcarbodiimide
DHA	Drug/H ⁺ antiporter
DMT	Drug/metabolite transporter superfamily
DNA	Deoxyribonucleic acid
DXC	Deoxycholate
<i>E.coli</i>	<i>Escherichia coli</i>
EmrD	Efflux-mediated resistance protein D
EPIs	Efflux pump inhibitors
EPR	Electron paramagnetic resonance spectroscopy
ESKAPE	<i>Enterococcus faecium</i> , <i>Staphylococcus aureus</i> , <i>Klebsiella pneumoniae</i> , <i>Acinetobacter baumannii</i> , <i>Pseudomonas aeruginosa</i> and <i>Enterobacteriaceae</i>
smFRET	single molecule Fluorescence Resonance Energy Transfer
FSEC	Fluorescence size exclusion chromatography
IM	Inner membrane
IMP	Integral membrane protein
I _F	Inward-facing
I _o	Inward-open
LCP	Lipidic cubic phase
LDAO	Lauryldimethylamine-N-Oxide
MAG	Monoacylglycerol
MATE	Multidrug and toxic compound extrusion
MDR	Multidrug resistance
MdfA	Multidrug facilitator assembly
MFS	Major facilitator superfamily
NBDs	Nucleotide binding domains
OM	Outer membrane
O _o	Outward-open
PACE	Proteobacterial antimicrobial compound efflux
P-gp	P-glycoprotein
PMF	Proton motive force
RND	Resistance-nodulation-cell division
SMR	Small multidrug resistance
TM	Transmembrane helix
TMDs	Transmembrane domains
TopoIV	Topoisomerase IV
VD	Vapour diffusion

LIST OF FIGURES

Fig 1. Mechanisms of antibiotic resistance	13
Fig 2. Bacterial multidrug resistant transporters	15
Fig 3. Crystal structures of ABC transporters captured in different conformational states	16
Fig 4. Crystal structures of MATE transporters captured in different conformational states ...	17
Fig 5. Crystal structures of SMR and AbgT family transporters.....	18
Fig 6. Cryo-EM structure of the RND-type tripartite complex	20
Fig 7. Peristaltic extrusion mechanism of AcrAB-TolC complex	21
Fig 8. Conformational states of MFS transporters	23
Fig 9. Sequence alignment of MFS-MDR antiporters.....	26
Fig 10. Crystal structures of MFS-MDR antiporter EmrD and YajR from <i>E.coli</i>	27
Fig 11. Lipidic cubic phase and types of packing in membrane protein crystals.....	36
Fig 12. Inward-facing (I_F) structures of MdfA bound with deoxycholate (DXC) and lauryldimethylamine-N-Oxide (LDAO).....	39
Fig 13. Chloramphenicol bound Inward-facing (I_F) structure of MdfA.....	40
Fig 14. Crystal packing in MdfA crystals	46
Fig 15. Structure of MdfA in the outward open (O_o) and inward facing (I_F) state.....	48
Fig 16. The O_o and I_F conformations differ by local twisting of TM5	49
Fig 17. Small but significant differences are observed in the hydrophobic core near the periplasmic face of the N-terminal domain	50
Fig 18. Molecular dynamics studies of MdfA.....	51

LIST OF TABLES

Table 1. Structures of MFS transporters.....	33
--	----

1 INTRODUCTION

1.1 Antibiotic resistance

Discovery of antibiotics

Antibiotics are indispensable chemotherapeutic agents (<500 Da) used for evading lethal diseases and infections caused by pathogenic microorganisms. Antibiotics have been of great importance and have saved millions of lives from the beginning of the 20th century up today (Sengupta et al., 2013). Discovery of antibiotics is one of the outstanding achievements in the field of medicine. The discovery of Penicillin by Sir Alexander Fleming in 1928 (Fleming, 1929), led to the introduction of several classes of antibiotic through different routes namely, i) soil screening of microorganisms producing secondary metabolites (antibiotics) – Walksman approach (Schatz et al., 1944, de Lima Procópio et al., 2012), ii) chemical modification of natural compounds (Zhanel et al., 2004) and iii) synthetic antibiotics (Fernandes, 2006). The upturn in the discovery of new antibiotics from 1940s to 1960s is undoubtedly the “Golden Age of Antibacterials” (Davies, 2006). These life-saving drugs have undeniably decreased the mortality rate of the people (Oeppen and Vaupel, 2002), not until the development of antibiotic resistance.

Antibiotic resistance crisis

What is antibiotic resistance? The reduction in susceptibility of a pathogenic bacterium to the deleterious effects of an antibiotic is called, “Antibiotic resistance”. The rapid emergence of resistance towards the antibiotics by microorganisms has almost decreased the therapeutic efficacy of most of the drugs discovered in the 20th century (Neu, 1992, French, 2010, Fernández et al., 2011). Antibiotic resistance has been observed in major pathogenic bacteria (Levy, 2005). To highlight, currently the life-threatening pathogens among the gram-positive and gram-negative bacteriae are the ESKAPE organisms (*Enterococcus faecium*, *Staphylococcus aureus*, *Klebsiella pneumonia*, *Acinetobacter baumannii*, *Pseudomonas aeruginosa* and *Enterobacteriaceae*) (Tommasi et al., 2015, Santajit and Indrawattana, 2016) which have developed multidrug resistance (MDR) to the most promising drugs available in the market, creating situations alike the pre-antibiotic era. In the post-antibiotic era i.e. 21st century, extrapolating this alarming situation will result in the death of millions of lives by 2050 (O’ Neil, 2014).

The causes and spread of antibiotic resistance

In order to survive in their environmental niche, bacteria have developed a range of resistant elements whose existence predate the practice of modern medicine (Jacob, 1977, Wiedenbeck and Cohan, 2011). Resistance elements in bacteria are either encoded in their genome or acquired from the bacterial community (D'costa et al., 2011, Cox and Wright, 2013). The intrinsic genetic resistant elements are passed on from mother cell to the daughter cell by cell division known as “vertical gene transfer” (Martínez et al., 2007). Resistance genes are also acquired by bacteria from another microorganism via “horizontal gene transfer” which is uncoupled to cell division, (Davies, 1994, Wiedenbeck and Cohan, 2011). Horizontal gene transfer is mediated via transformation, transduction (attack of bacteriophages) or conjugation (Bennett, 2009). Mobile genetic elements like plasmids or transposons carrying resistant genes are transferred by conjugation between bacteria (Van Hoek et al., 2011). Accumulation of resistant genes by vertical and horizontal gene transfer increases the virulence of the microorganisms making them as “Multidrug-resistant Superbugs” (Nikaido, 2009).

1.2 Mechanisms of antibiotic resistance

Antibiotics act on a specific bacterial target to elicit their action. Bacterial drug targets are present on the cell wall, periplasmic space, and cytoplasm to which antibiotics bind to inhibit the function, resulting in a bacteriostatic or bactericidal effect (Kohanski et al., 2010). An antibiotic to exert its action within the cytoplasm of gram-negative bacteria must permeate the outer membrane (OM) – the first line of defence, periplasm, and then the inner membrane (IM). The peptidoglycan layer of gram-positive bacteria is a coarse mesh which allows permeation of antibiotics in contrast to the OM of gram-negative bacteria. The OM of gram-negative bacteria is a tightly packed lipidic bilayer and acts as a protective barrier reducing the permeation rate of hydrophobic substrates (Nikaido, 1994, Hancock, 1997). Antibiotics enter into the periplasm of gram-negative bacteria through, “Porins” (β -lactams) (Livermore, 1988) or via “Self-promoted uptake pathway” (aminoglycosides) (Delcour, 2009). Further, the antibiotic passively diffuses from the periplasm into the cytoplasm through the IM to act on the target (Hancock and Bell, 1988).

As briefed earlier, bacteria with the innate or acquired resistant genes can circumvent the action of antibacterials by different resistance mechanisms, a) inactivation of the antibiotic by enzymatic hydrolysis or modification, b) alteration of the drug target, c) overproduction of the drug target, d) “bypass” target metabolic pathway, e) reduced intake by decreased outer

membrane permeability and f) efflux of the antibiotic by multidrug resistant transporters (Fig. 1) (Tenover et al., 2006, Giedraitienė et al. 2011).

The focus of this thesis further will be on the efflux pumps mediated resistance towards antibiotics in bacteria.

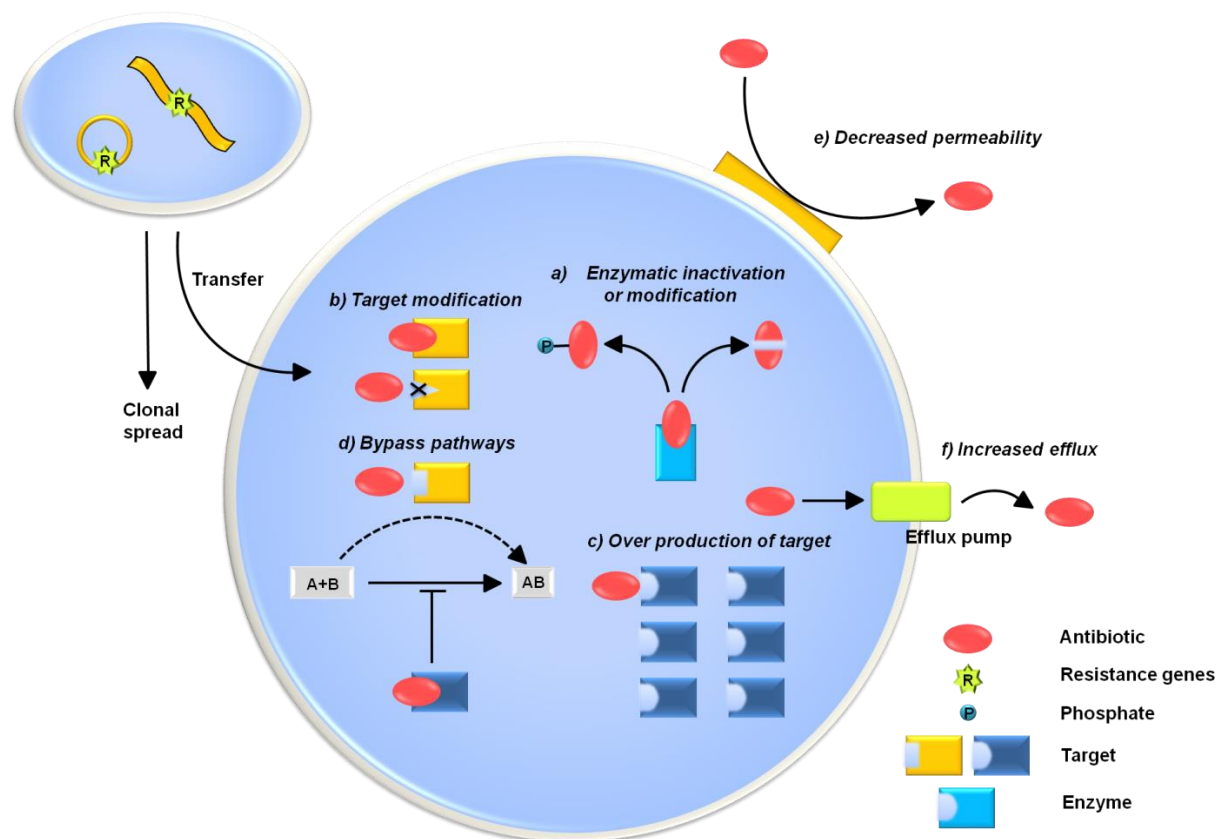


Fig 1. Mechanisms of antibiotic resistance: Resistance genes are transferred between bacteria which reduces the efficacy of the antibiotics by different resistance mechanisms; **a) inactivation of the antibiotic or enzymatic hydrolysis.** For example. β -lactamase hydrolyse the β -lactam ring of Penicillin (Abraham and Chain, 1940), **b) target modification.** For example. Mutations in the gene of the enzymes DNA gyrase or topoIV reduces the binding affinity to quinolones (Drlica et al., 2008), **c) overexpression of the drug target.** For example. Overexpression of AcrAB-TolC efflux pump (Yu et al., 2003), **d) bypassing the target metabolic pathway.** For example. Trimethoprim inhibits the enzyme dihydrofolate reductase which is required for the synthesis of the DNA precursor thymidine. *E.coli* has managed to develop resistance towards Trimethoprim by being dependent on an external source of thymine for DNA biosynthesis (King et al., 1983), and **e) reduction of outer membrane permeability.** For example. Mutations in the porin Por of *Neisseria gonorrhoeae* exerts enhanced resistance to penicillin and tetracyclines (Gill et al., 1998). **f) increased expulsion of antibiotics by the efflux pumps embedded in the bacterial membrane** (Image modified from Coates et al., 2002).

1.3 Bacterial multidrug resistance transporters

Efflux transporters are embedded within the bacterial membrane. In context to multidrug efflux, transporters in the inner membrane (IM) expel cytotoxic molecules from the cytoplasm to the periplasmic space and large protein complexes form a continuous channel from the IM to the outer membrane to release the substrates to the extracellular space from the periplasm (Zgurskaya, 2009). With the growing concern of multidrug resistance since the 1970s, antibiotic resistance mediated by efflux transporters was first observed with a single-

INTRODUCTION

drug efflux pump extruding tetracycline (Levy and McMurry, 1974, Mitchell, 1977, Levy and McMurry, 1978). Since then many multidrug efflux transporters have been identified from resistant clinical isolates (Piddock, 2006b, Sun et al., 2014). Many of the MDR transporters have overlapping substrate profiles to compensate for the functional loss of one another (Keogh et al., 2016). MDR efflux transporters are either chromosomally or plasmid encoded (Li and Nikaido, 2009) and they are regulated by transcriptional regulators which carry out constitutive or inducible expression (Sun et al., 2014, Piddock, 2006b, Ma et al., 1995). MDR efflux pumps also exhibit physiological roles such as bile tolerance, pathogenicity, biofilm formation, and quorum sensing (Piddock, 2006a, Sun et al., 2014). Efflux transporters besides antibiotic efflux and physiological roles also expel disinfectants, antiseptics, sterilants and preservatives that are routinely used in medical practice (Levy, 2002, Poole, 2007, Tumah, 2009, Hegstad et al., 2010).

MDR efflux transporters are classified based on their sequence similarities, energetic profiles, and substrate specificities. Phylogenetic approaches were also used to classify and interpret the function of novel transporters (Saier and Paulsen, 2001). Based on these analysis, seven superfamilies of MDR transporters were identified namely; i) the ABC (Adenosine triphosphate-binding cassette) superfamily (Higgins, 2001), ii) the MFS (Major facilitator superfamily), iii) the SMR (small multidrug resistance) superfamily (Paulsen et al., 1996), iv) the MATE (multidrug and toxic compound extrusion) family, all of which are widely distributed in both gram-positive and gram-negative organisms (Brown et al., 1999), V) the resistance-nodulation-division (RND) family found only in gram-negative organisms (Putman et al., 2000, Piddock, 2006b, Poole, 2007), and two more recently discovered superfamilies are VI) the AbgT family (Delmar and Yu, 2016) and the PACE (Proteobacterial antimicrobial compound efflux) family (Hassan et al., 2013, Hassan et al., 2015).

The seven families of transporters can be sub-classified into, “primary-active” and “secondary-active” transporters based on the energy source utilized for the extrusion of substrates (Fig. 2). ABC superfamily members are primary-active transporters which utilize the energy of ATP for drug export. The other six families are secondary-active transporters that use the electrochemical gradient (H^+ or ions) as the driving force for substrate expulsion. MFS members are discussed in detail in a separate section 1.4 and the other six families are discussed here (Saier, 2000, Putman et al., 2000).

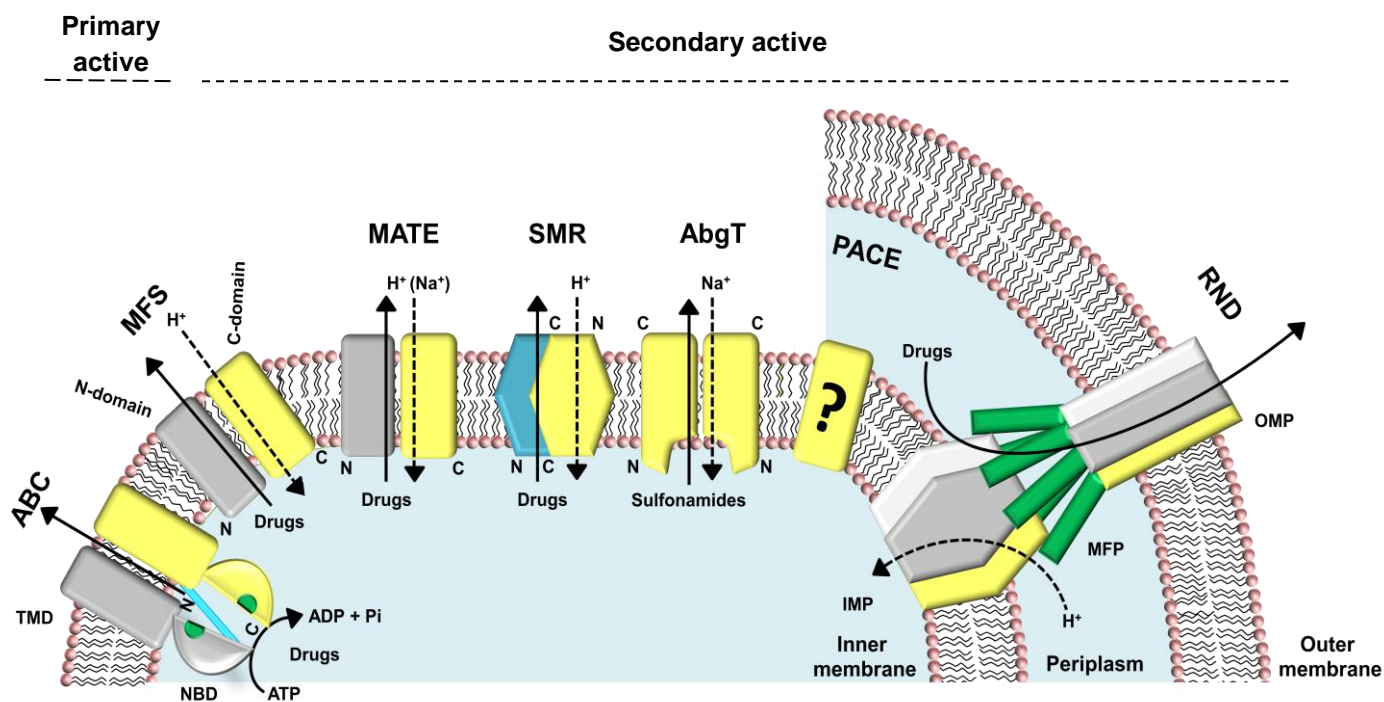


Fig 2. Bacterial multidrug resistant transporters: Primary active exporter: ABC transporters export drugs from the cytoplasm to the periplasm via the cavity sandwiched between the N- (grey) and C- (yellow) transmembrane domains (TMDs) in the membrane sequentially to the hydrolysis of ATP at the binding pockets (green) of the nucleotide binding domains (NBDs) in the periplasm. **Secondary active exporters:** Expulsion of antibiotic from the cytoplasm of bacteria is coupled to H⁺ or ions in secondary active transporters which are embedded in the inner membrane of gram-negative bacteria or span both the membranes in the case of RND-type tripartite efflux pumps. **MFS and MATE** antiporters consist of N- (grey) and C-terminal (yellow) domain of 6-TM helices orchestrating a central H⁺ or ion / substrate binding pocket which is also present in **SMR** antiporter but formed by the anti-parallel dimers (protomers as cyan and yellow). **AbgT** members function as homodimers (yellow) arranged parallel in the membrane with their N-terminus within the cytoplasm and the C-terminus on the periplasmic side. Homodimers enclose a water-filled cavity in the form of a bowl and the antiport activity of sulfonamides is achieved by proton motive force coupled with Na⁺. **PACE** family member awaits structural characterization given the small size of the molecule, it is expected that the transporter might function as oligomers in the membrane. **The RND-type tripartite complex** consists of trimeric inner membrane protein (inner membrane protein as white, grey, yellow highlighting each protomer) which interacts with hexameric membrane fusion protein (MFP, green). MFP, in turn, interacts with the trimeric outer membrane protein (OMP as white, grey and yellow protomer). The three components constitute the tripartite complex enclosing a continuous channel to intercept the substrates from the periplasm to be expelled to the exterior for the exchange of H⁺.

ABC transporters share similar architecture with two nucleotide binding domains (NBDs) in the cytoplasm which are able to bind and hydrolyse ATP at the dimer interface for expelling substrates via the substrate translocation pathway formed by the two transmembrane domains (TMDs) within the lipidic bilayer (Fig. 3). Crystal structures of ABC transporters and functional investigations support an “alternating access model” where the substrate translocation pathway is either exposed to the exterior or to the interior of the bacterial cell membrane when switching between the outward-facing and inward-facing conformational states (Theodoulou and Kerr, 2015).

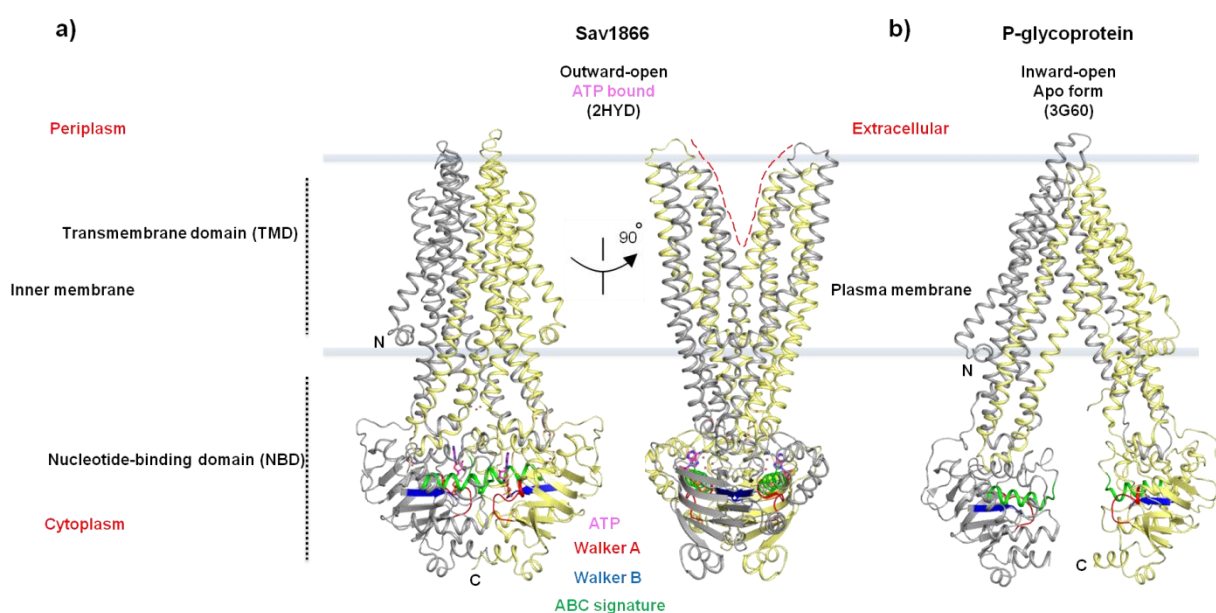


Fig 3. Crystal structures of ABC transporters captured in different conformational states: a) Sav1866, a bacterial multidrug exporter captured in an outward-open reveal that the NBDs within the cytoplasm are in close contact bound with two molecules of ATP (pink). View from the left figure of (a) rotated 90° about a vertical axis show the binding cavity (red dashed lines) is open to the periplasm formed by the TMDs [N-(grey) and C-terminal domain (yellow)] (Dawson and Locher, 2006). Recent studies show how the ATP energy harnessed in the NBDs is coupled to drug extrusion by rearrangement of the TMDs described in a two-stroke cycle. ATP binding and hydrolysis in one of the NBD results in intracellular closure of the transporter (dimerization of the NBDs) leading to an occluded state. The opening of the TMD binding site to the extracellular side requires the hydrolysis of the second ATP to release the substrate to the exterior (Verhalen et al., 2017). **b) P-glycoprotein (P-gp)**, a mammalian multidrug exporter captured in the inward-open state reveal the binding cavity is open to the cytoplasm competent for substrate binding where the NBDs are separated after ATP hydrolysis and release of the substrate. NBDs located in the cytoplasm consists of the highly conserved Walker A (red), Walker B (blue) and ABC signature conserved motifs (green) responsible for nucleotide binding and hydrolysis (Jin et al., 2012). The two conformational states illustrated here endorse the “Alternating access” mechanism.

MATE family of transporters transport cationic, lipophilic substances and xenobiotics (Tanaka et al., 2013). In contrast to the ABC transporters, MATE members use Na^+ or H^+ electrochemical gradient to transport substrates. Members of this family do not possess conserved motifs but show 40% sequence similarity (Du et al., 2015). MATE transporters

consist of 12 transmembrane helices (TM) which can be divided into two lobes as N-domain (TM1-TM6) and C-domain (TM7-TM12). The two domains enclose a binding pocket with acidic and hydrophobic residues which enable Na^+ or H^+ / substrate coupling (Lu, 2016). This topology is different to MFS transporters. Structural studies of MATE transporters has resulted in crystal structures of MATE transporters (NorM, DinF, PfMATE) captured in different conformational states (Tanaka et al., 2013, Lu et al., 2013a, Lu et al., 2013b, He et al., 2010). The structures reveal for the first time how polyaromatic cationic substrates interact within the binding pocket (Fig. 4).

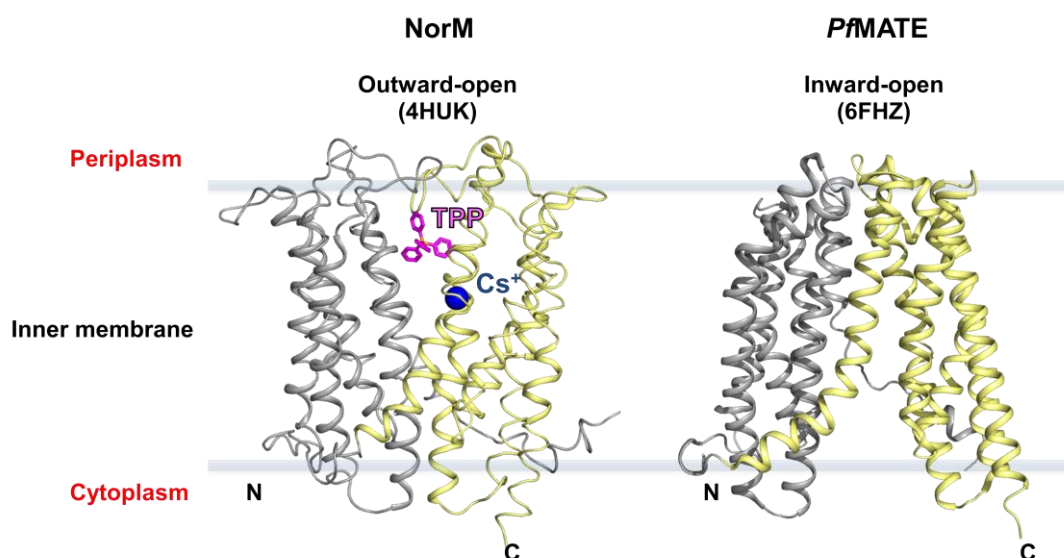


Fig 4. Crystal structures of MATE transporters captured in different conformational states: NorM from *Neisseria gonorrhoeae* consists of the N- (grey) and C-terminal domain (yellow) which encloses a binding cavity bound with monovalent cationic compound tetraphenylphosphonium (TPP^+ , pink). The cavity is open to the periplasm (outward-facing) and as a representation of the Na^+ binding site. It is highlighted with caesium ion (Cs^+) overlaid from the crystal structure PDBID: 4HUL, which is bound between the TM7 and TM8. Indirect allosteric binding of Na^+ from the periplasm to the binding site in the C-domain in the outward-open substrate bound state triggers rearrangement of TM helices 7 and 8 to weaken the interaction with the substrate to be released into the periplasm (Lu et al., 2013a). Crystal structure of PfMATE transporter from *Pyrococcus furiosus* reveal that the substrate binding site is open to the cytoplasm (Zakrzewska et al., 2019).

SMR family members belong to the drug/metabolite transporter (DMT) family (Jack et al., 2001) with four TM helices (Bay et al., 2008). SMR member, EmrE from *E.coli* is a well characterized H^+ /drug antiporter. EmrE expels cationic substrates and also antibiotics (Yerushalmi et al., 1995, Paulsen et al., 1996). Crystal structure of EmrE bound to cationic substrate tetraphenylphosphonium (TPP^+) (Fig. 5a) and investigations by electron cryomicroscopy of 2D crystals reveal an asymmetric, antiparallel homodimer consisting of eight helices enclosing a binding pocket formed by TM1-TM3 from each monomer and TM4 mediates interaction within the homodimer (Ubarretxena-Belandia et al., 2003, Chen et al.,

2007). A single-site alternating access model suggests that the antiporter switches between the outward- and inward-open conformation exposing the binding site to the exterior and to the interior of the cell to bind H^+ and substrates respectively (Dutta et al., 2014).

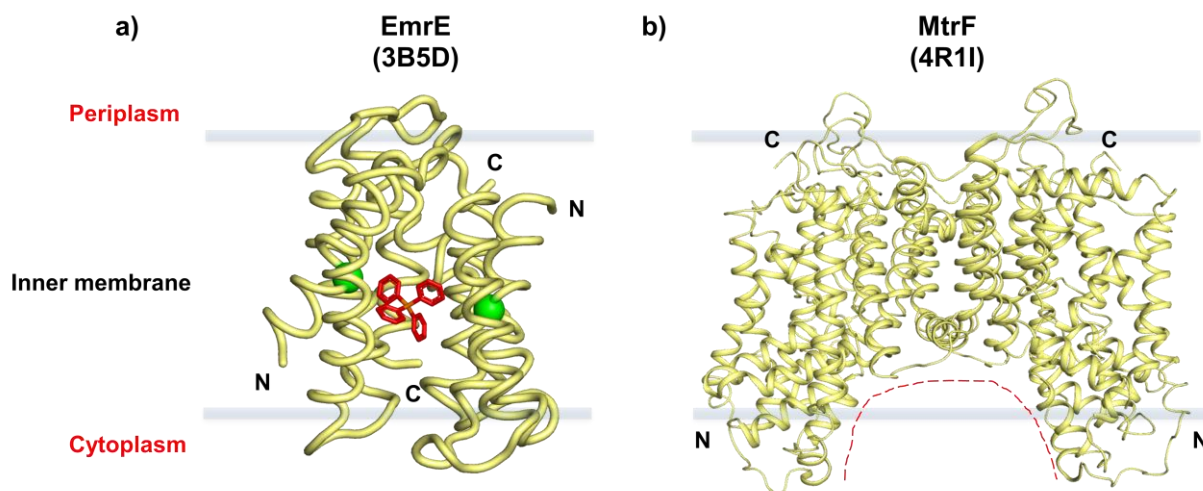


Fig 5. Crystal structures of SMR and AbgT family transporters: a) SMR member **EmrE** from *E.coli* nests within the lipidic bilayer as an antiparallel dimer (yellow protomers). The dimer binds tetraphenylphosphonium (red), a polyaromatic cation at its interface and the negatively charged residue Glu14^{TM1} (green spheres) on TM1 of each monomer protrudes towards the binding pocket to couple H^+ for the antiport of the substrate (Chen et al., 2007). b) AbgT member **MtrF** from *N. gonorrhoeae* functions as a homodimer in the cell membrane enclosing a bowl-shaped cavity (red dashed lines) extending from the cytoplasm to the middle of the membrane. Each of the protomers consists of a binding site and a channel which extends from the basin of the bowl-shaped cavity in the middle of the membrane to the periplasmic space. The channel is lined with highly conserved residues important for function (Su et al., 2015).

Functional characterization of **AbgT family** of transporters YdaH (*A. borkumensis*), MtrF (*N. gonorrhoeae*) revealed that these efflux pumps were able to actively extrude para-aminobenzoic acid (PABA), a precursor of folic acid. Based on this function, it was hypothesized that YdaH and MtrF may protect bacterial cells by exporting structurally similar drugs like PABA, i.e., sulfonamide antimetabolites. Transport assays confirmed that these pumps were able to actively extrude sulfonamide antimetabolites mediating antimicrobial resistance (Delmar and Yu, 2016). Crystal structures of YdaH, MtrF showed that the functional active unit in the membrane is a homodimer where each of the protomer is arranged parallelly in the plane of the lipidic bilayer (Bolla et al., 2015, Su et al., 2015). Each protomer consists of nine alpha helices and two alpha helical hairpins that enclose a solvent-filled bowl-shaped binding cavity formed by the homodimeric arrangement of TMDs in the membrane (Fig. 5b). The aqueous bowl-shaped binding cavity extends from the cytoplasm to the middle of the

membrane. AbgT family members utilize proton motive force (PMF) for extrusion of substrates (Prakash et al., 2003).

PACE family (Proteobacterial antimicrobial compound efflux) of transporters are widespread in many of the major gram-negative pathogens. Antiporters belonging to this family are able to confer resistance to biocides, antiseptics and disinfectants (Hassan et al., 2018, Hassan et al., 2013). So far no structural information is available but sequence alignment of AceI from *Acinetobacter baumannii* and its homologues suggest that the members are 4 TM helical proteins consisting of highly conserved residues that are important for substrate recognition and transport (Hassan et al., 2015). Transporters of this family are expected to function as oligomers in the lipidic bilayer given the small size of the molecule. Many aspects of this family of transporters such as energy utilization and coupling mechanism, structural information and substrate transport mechanism require further investigation, as these transporters represent a new class claiming their importance in mediating antimicrobial resistance.

Tripartite-RND transporter complexes present only in gram-negative bacteria efficiently pump the substrates directly from the periplasm to the exterior of the cell (Putman et al., 2000). One of the most well-studied RND-type tripartite complex is AcrAB-TolC from *E.coli* (stoichiometry of AcrA:AcrB:TolC - 6:3:3) (Li and Nikaido, 2009). Tripartite assembly consists of the RND-type transporter, periplasmic adaptor protein, AcrA and the outer membrane protein, TolC. Cryo-EM structure of the tripartite assembly reveals that AcrA interacts with AcrB embedded in the inner membrane and TolC nested in the outer membrane to form a continuous channel which runs from AcrB to end in the β -barrel domain of TolC (Du et al., 2014) (Fig. 6).

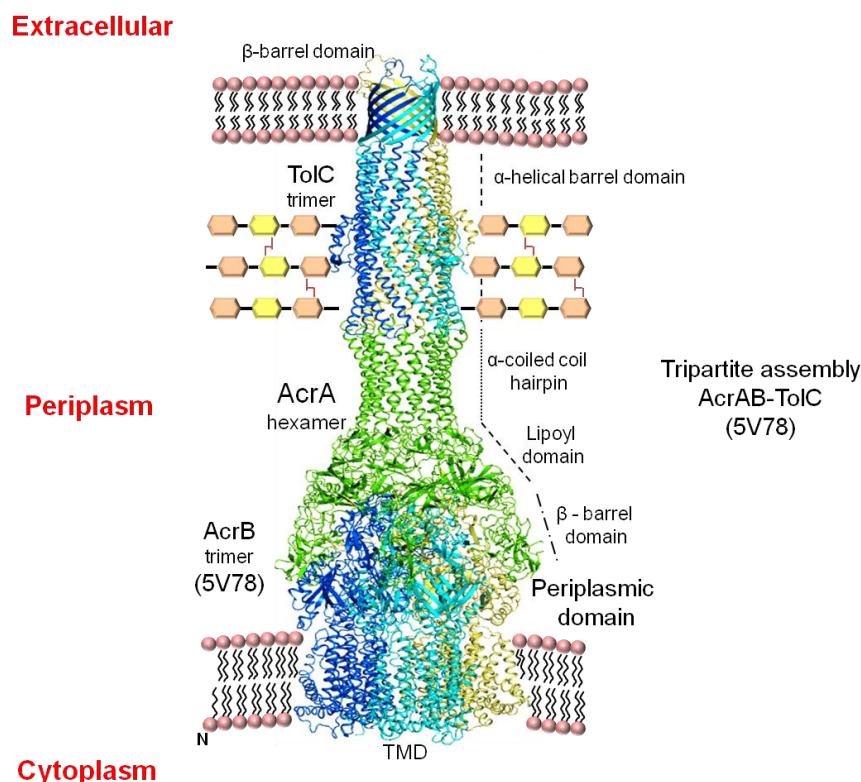


Fig 6. Cryo-EM structure of the RND-type tripartite complex: AcrAB-ToIC from *E. coli* stretches from the inner membrane to the outer membrane forming a continuous channel. The complex consists of the homotrimer AcrB (cyan, blue, yellow for each protomer) whose transmembrane domain (TMD) is nested within the lipid bilayer and the periplasmic domain protrudes into the periplasm. Pore from AcrB opens into the hexameric AcrA (green) lipoyl domain and further extends along the AcrA α -coiled coil hairpin domain to open into the TolC α -helical barrel domain (cyan, blue, yellow for each protomer) finally opening to the exterior to release the substrate out to the extracellular side of the bacterial outer membrane (Du et al., 2014).

AcrB is a paradigm of the RND transporters. It confers resistance to numerous antimicrobial compounds and substrates such as isoflavonoids, fatty acids, bile salts and steroids (Zgurskaya and Nikaido, 2000, Poole, 2004, Nishino et al., 2009). AcrB is a homotrimer. Crystal structure of AcrB reveals that each of the protomers consists of a 12 TM helical domain and a periplasmic domain which can be segmented into a porter and funnel domain (Murakami et al., 2002) (Fig. 7a). The porter domain consists of two substrate-binding pockets, i) a membrane proximal pocket for the access of substrates from the inner membrane (Pos, 2009) and ii) a distal (deep binding) pocket which opens into the funnel domain of AcrB (Fig. 7a, b).

AcrB being an H^+ dependent antiporter, the mechanism of drug extrusion involves proton binding which results in conformational changes within the TM domain (Eicher et al., 2014, Du et al., 2015). The structural rearrangements in the TM domain brings about closure of the binding pocket (portal domain) of the periplasmic domain and opens up an exit tunnel

towards the funnel domain in a peristaltic fashion to squeeze out the drug through the funnel domain (Vargiu et al., 2011) (Fig. 7e,f). AcrB displays a highly cooperative drug transport behaviour where at any instance each of the protomer binding pocket adopts distinct conformation as substrate access or Loose (L), substrate binding or Tight (T) and substrate extrusion or Open (O) in the transport cycle indicating a sequential rotation drug extrusion behaviour (Seeger, 2006, Murakami et al., 2006, Nagano and Nikaido, 2009).

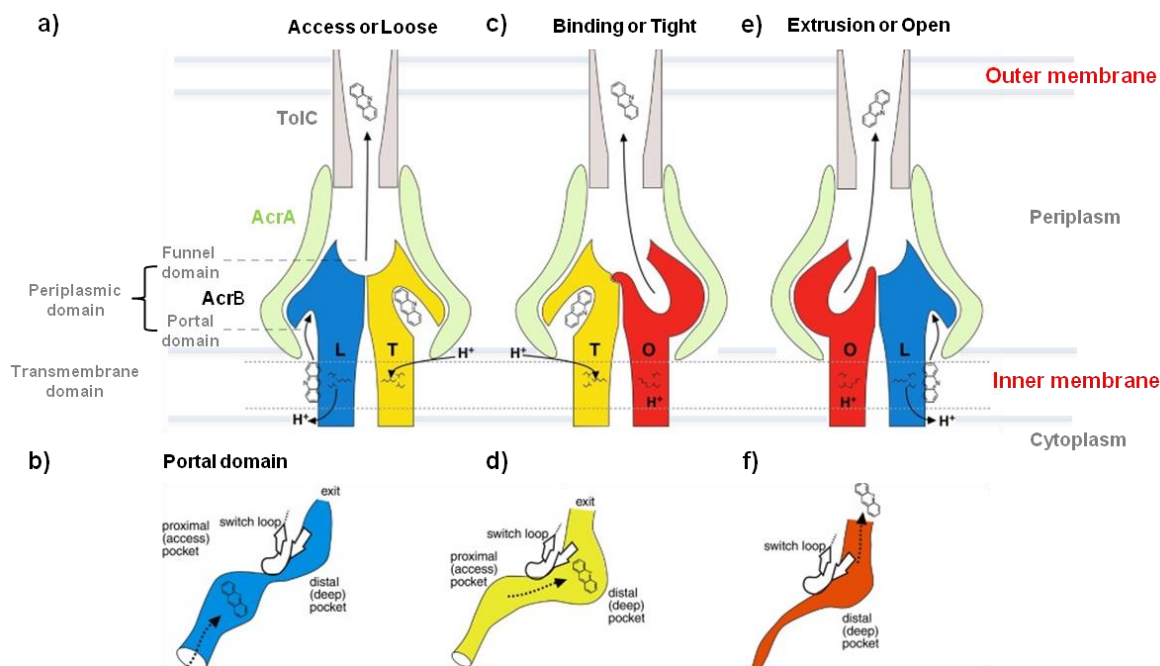


Fig 7. Peristaltic extrusion mechanism of AcrAB-ToIC complex: **a)** Periplasmic adaptor protein AcrA (light green) is coupled to TolC (grey) and AcrB (blue, yellow, red for each protomers) forming a continuous channel which opens to the cell exterior. AcrB consists of the transmembrane domain and the periplasmic domain which opens into AcrA hexamer. Periplasmic domain is segmented into funnel domain and portal domain. **b)** Portal domain consists of two substrate binding pockets segmented as proximal (substrate access pocket) and distal pocket (substrate exit pocket) connected to the funnel domain. **c,d)** Proton binding to a protomer (T) brings about structural changes (switch loop) in the transmembrane domain which allows the substrate to pass from the proximal pocket to the distal pocket. **e,f)** Deprotonation of the protomer (O) results in closure of the periplasmic side of the distal pocket and opens a exit tunnel connected to the funnel domain to squeeze out the substrate in a peristaltic fashion. AcrB protomers at any instance adopt three distinct conformations as substrate access or loose “L”, substrate binding or tight “T” and substrate extrusion or open “O” conformations indicating sequential rotation drug extrusion behaviour (Image modified from Du et al., 2015).

Sequential rotation mechanism of AcrB renders each of its protomers to be in an extrusion state at any time point to release the drug into the funnel domain to be channelled into the AcrA hexamer and further into TolC to be extruded to the exterior which keeps the TolC exit duct in an open state throughout the substrate translocation process. It is highly likely that the solitary transporters of the inner membrane cooperate with the RND-type tripartite

transporters delivering substrates to the periplasm from the cytoplasm and expelled from the periplasm by the RND-tripartite efflux pump (Tal and Schuldiner, 2009).

1.4 The Major Facilitator Superfamily

1.4.1 General Overview of MFS transporters

Major Facilitator Superfamily (MFS) transporters are ubiquitously present in all living organisms. MFS consists of several subfamilies of secondary active transporters which can be classified as uniporters, symporters, and antiporters by their mechanism of transport (Saier et al., 1999). Uniporters transport a single substrate, symporters transport a substrate in association with a coupling ion in the same direction and antiporters transport a substrate and an ion in opposite directions in consecutive steps (Marger and Saier, 1993, Quistgaard et al., 2016). MFS transporters are able to shuttle solutes such as sugars, polyols, drugs, neurotransmitters, amino acids, peptides, and inorganic anions (Saier et al., 1999, Saier and Paulsen, 2001). Most of them are substrate-specific and some of the transporters which non-specifically bind to dissimilar substrates are categorized within multiple subfamilies (Saier and Paulsen 2001, Li and Nikaido, 2009).

MFS transporters consists of either 12TM or 14TM helices (Law, 2008). Crystal structures of the 12TM and 14TM MFS transporters determined until date show a similar architecture as MATE transporters. MFS transporters consist of two pseudo-symmetrical bundles of 6TM helices connected together by an amphipathic loop or an α -helix (Fig. 8b, Table. 1). The N- and C-terminal bundles orchestrate a binding pocket which intercepts the substrates from the periplasm/extracellular or cytoplasm/intracellular depending on the transport directionality and releases the substrate on the other side. MFS transporters are therefore proposed to operate by a general mechanism proposed 51 years ago (Jardetzky, 1966), which is now termed as the, “Alternating access mechanism” in which the binding pocket is accessible from either side of the lipidic bilayer (Fig. 8a). To complete a transport cycle, the transporter must switch between two extreme conformational states, the outward-open (O_o) and inward-open state (I_o). The 6TM N- and C- terminal bundles rotate as rigid bodies about an axis parallel to the membrane to achieve these conformational states. Intermediate states of MFS transporters in substrate-bound or unbound forms have also been determined structurally as O_o -partially occluded, I_o -partially occluded and occluded

conformations which are the other conformational states in the transport cycle (Quistgaard et al., 2016) (Fig. 8b).

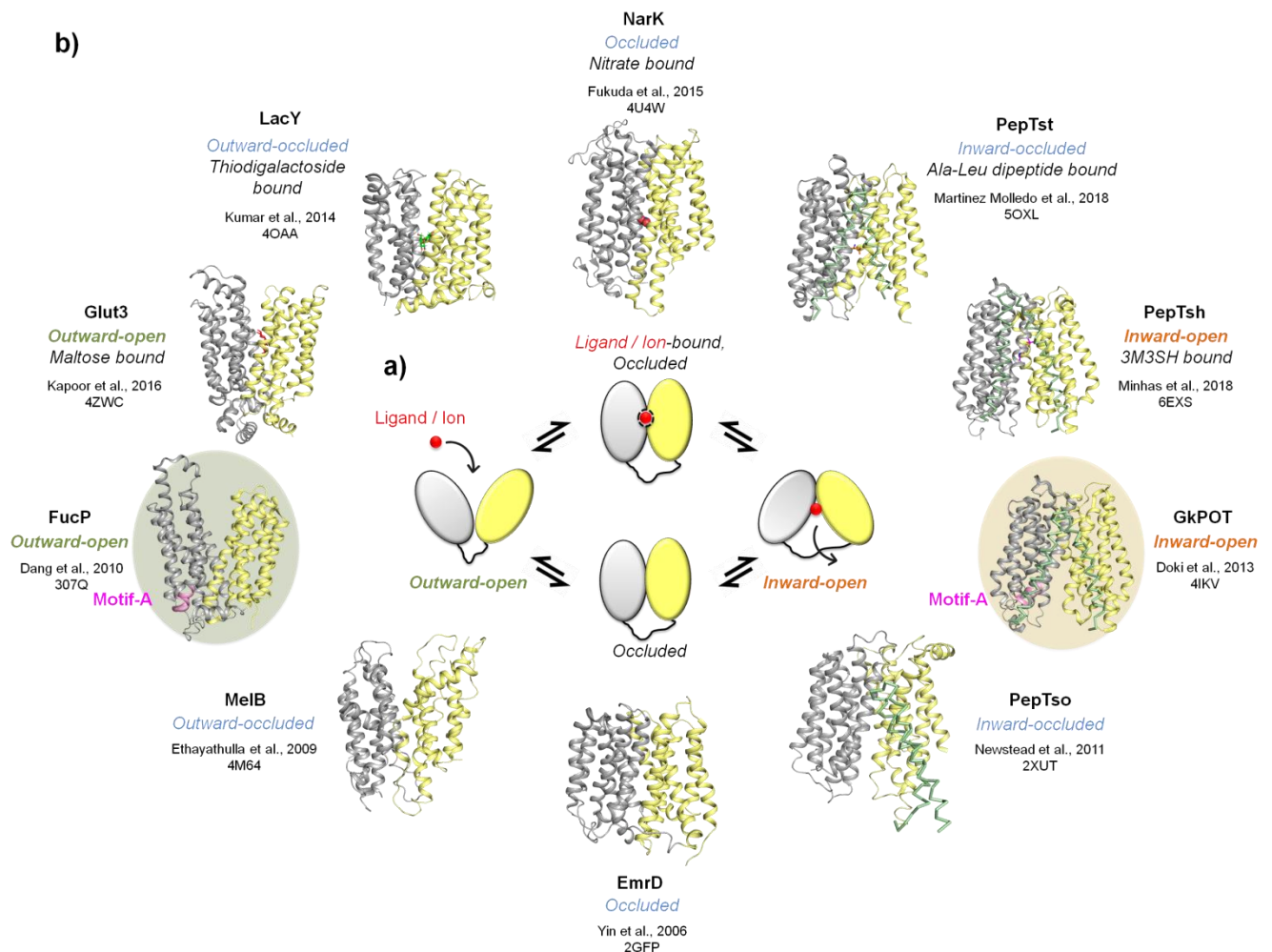


Fig 8. Conformational states of MFS transporters: **a) Alternating access mechanism in MFS transporters:** In the case of uniporters and symporters, ligand or ion (red) binding to the cavity formed by the 6 TM N- (grey) and C-terminal domain (yellow) induces conformational switching from outward-open (O_o) to ligand or ion bound occluded state where the transporter in the inward-open (I_o) state releases the bound ligand or ion. Apo-form of the transporter in the I_o state switches back to the O_o state via the occluded state. In the case of antiporters, ligand is released in the O_o state and bound in the I_o state state. **b) Conformational states of MFS transporters** - intermediary occluded states (blue) bound with ligand or apo-form traversing between O_o state (green background) and I_o state (orange background) are illustrated here with examples with their PDBID. The position of Motif-A (pink) in MFS transporters is highlighted in the crystal structures of O_o -FucP and I_o -GkPOT. Glut3 is a uniporter, EmrD, NarK are antiporters and the other MFS transporters presented here are symporters. MFS transporters highlighted with helices in green are 14TM-symporters (Image modified from Yan., 2015).

MFS pumps are energized by the proton motive force (PMF) existing across the lipidic bilayer and the uphill transport of substrates is driven mostly by coupling of H^+ , Na^+ or other ions in the case of symporters and antiporters. Acidic residues within the binding pocket play an important role in coupling ions which triggers the transport process (Masureel et al., 2013, Liu et al., 2015). For example, the most well-studied symporter *E.coli* LacY consists of two

proton titratable pair His332^{TM10} and Glu325^{TM10} within the central cavity which is conserved in many sugar porters upon protonation creates significant structural rearrangements initiating the symport process (Andersson et al., 2012), Acidic residues also play a role in interacting with the substrate together with a specific set of conserved residues in the case of substrate-specific transporters and the binding of the substrate is non-specific in the case of multidrug drug transporters (Alegre et al., 2016).

Conformational switching between different conformations is achieved and orchestrated not only by ion/substrate binding within the pocket but also by formation and breaking of gating interactions during the transport cycle (Quistgaard et al., 2016). Gating interactions (salt bridges) are mediated by the residues facing the binding pocket from the N- and C-terminal domain of the transporters. Initially, the formation of extracellular and intracellular gates was considered to play a crucial role in the transport cycle in all MFS transporters but later it became clear from the crystal structures of MFS transporters that this is not a general trend observed within the family (Law et al., 2008, Solcan et al., 2012). For example., LacY, XylE, Glut1, and BbFPN lack conserved gating residues on the extracellular side. However, it is clear that those transporters which have the residues involved in salt bridge formation have shown to play a fundamental role in transport. Mutation of these interacting residues results in arresting the function of the transporter claiming its importance. Gating residues from the highly conserved Motif-A, “GX3-(D/E)-(R/K)-X-G-X-(R/K)-(R/K)” (where “X” indicates any amino acid) are found between TM2-TM3 and/or also found less conserved between TM8-TM9 (Yamaguchi et al., 1991, Marshall., 1995) (Fig. 8b, 9). Motif-A is a hallmark of the MFS transporters but not conserved in all of them. Motif-A of TM2-TM3 is shown to form capping electrostatic interactions with the TM11 and TM8-TM9 interacts with TM5 when the N- and C-domains approach each other on the cytoplasmic side to stabilize the outward-open state. Structural and biochemical studies of uniporters and symporters have lead to understand the transport mechanism better comparatively to the multiple substrate binding behaviour of MFS MDR transporters (Yan., 2015, Lewinson et al., 2006). Nevertheless, the last two decades of research of the MFS-type MDR has provided a basic understanding at the structural and biochemical level, which is summarized below.

1.4.2 MFS-type MDR transporters

Physiological roles of MFS-MDR transporters:

Bacterial genomes harbour MFS-MDR transporter genes which possess altered physiological function other than MDR (Neyfakh, 1997). a) Knocking out the gene of Blt in *E.coli*, a putative gram-positive bacterial MDR transporter does not show any altered drug resistance profile but it affects the second function of acetylation of cellular polyamines (Woolridge et al., 1997). b) Eukaryotic vesicular monoamine MFS transporter (VMAT), a typical neurotransmitter is shown to transport organic cations which are normally transported by MDR transporters (Yelin and Schuldiner, 1995). c) *E.coli* expressing MdtM, a H⁺/Drug antiporter and a close homologue of MdfA is shown to tolerate high alkaline pH of 10 and is able to exchange Na⁺/ K⁺ in exchange for a H⁺ to maintain the internal proton concentration under external alkalization conditions (Holdsworth and Law, 2013). The alternative functions of MFS transporters probably were present before MDR which may have been an adaptation to selection pressure.

Contribution to drug resistance in bacteria:

12-TM Drug/H⁺ antiporter 1 family (DHA1) and 14-TM Drug/H⁺ antiporter 2 family (DHA2) are the two most prevalent groups of MFS-MDR transporters in bacteria (Paulsen., 1993). MFS-MDR transporters contribute to drug resistance significantly in gram-positive bacteria compared to gram-negative species. Gram-negative RND-type tripartite complex overexpressed in clinical strains mask the endogenous resistance of the non-RND transporters. Disrupting the genes of the MFS transporters (knockout strains) in gram-negative bacteria do not show any difference in drug resistance in the presence of RND transporters (Fluman and Bibi, 2009). However, in gram-positive bacteria, MDR transporter resistant genes intrinsically encoded in the genome (NorA) or acquired through plasmid transfer have high relevance in the drug resistance profile of the bacteria both clinically and physiologically (Schindler and Kaatz, 2016). For example, a) Plasmid-mediated elevated expression levels of pumps such as 14-TM QacA and QacB show high drug resistance profile in the clinically relevant isolates of *Staphylococcus aureus* (Paulsen et al., 1996).

Molecular basis of multiple substrate recognition:

Substrates of the MFS-MDR are structurally dissimilar but the physical nature of the substrates are predominantly hydrophobic. Transporters of this family have overlapping substrate profile and it is anticipated that they should adhere to similar transport principles (Fluman et al., 2009, Fluman and Bibi., 2009). MFS antiporters consists of a large hydrophobic

binding pocket and are lined with hydrophobic, negatively charged residues generating electrostatic and non-specific hydrophobic interactions which broaden the spectrum of substrate recognition (Putman et al., 2000). Mutating the substrate binding residues is likely to change the drug resistance profile drastically. Multiple substrate recognition behaviour can be exemplified with the QacA/QacB 14TM putative antiporters. QacB is a closely related homolog of QacA and differs from QacA by seven nucleotide substitutions. QacA is known to confer resistance towards divalent cations but in contrast, QacB lacking an acidic residue, Asp323^{TM10} does not confer resistance to divalent cationic compounds which can be restored by introducing the residue Aspartate at position 323 in TM10 (Paulsen et al., 1996).

Conserved motifs in MFS-MDR transporters:

MFS-type MDR consists of three conserved motifs – motif-A/B/C in the N-terminal domain involved in regulating the antiport activity but not present in all of them (Putman et al., 2000, Zhang et al., 2015). Motif-A and motif-B are conserved in symporters and antiporters and motif-C is specific only to antiporters (Jesus et al., 2005). Motif-A is already described under the section 1.4.1.

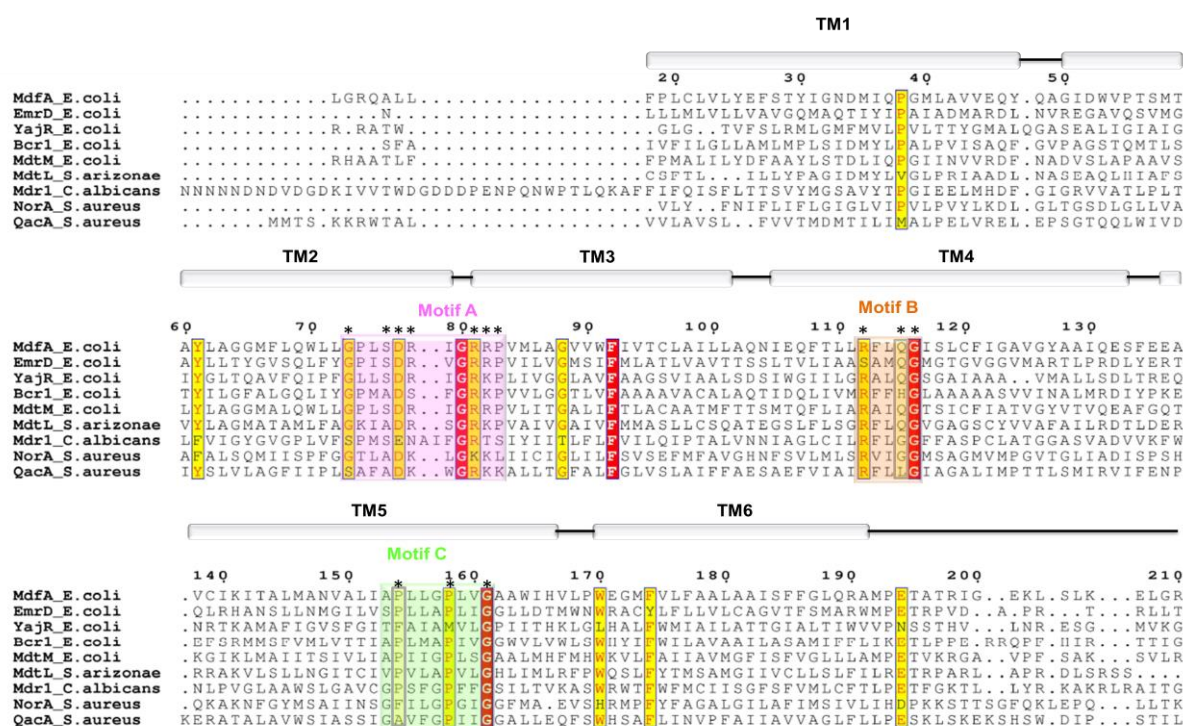


Fig 9. Sequence alignment of MFS-MDR antiporters: Clinically relevant isolates harbouring 12TM and 14TM MFS antiporter NorA and QacA from *Staphylococcus aureus* and 12TM MFS MDR antiporters from other bacteria were aligned using T-coffee alignment program. Sequence alignment highlights the highly conserved motifs A (pink), B (orange) and motif-C (green) present in the N-terminal domain of MFS-MDR transporters. Predicted secondary structure (α -helices – grey bars) for the aligned sequences of other antiporters were based on MdfA-I_F structure as the template (PDBID: 4ZP0) (Heng et al., 2015).

Motif-B, “RXXXG” present on TM4 consists of the evolutionarily conserved Arginine present in many of the MFS transporters located on the periplasmic side of TM4 (Fluman and Bibi, 2009) (Fig. 9, 10b). Biochemical data suggest that a positive charge is absolutely required at this position, His or Lys mutations are tolerated at this position in MdfA with partial loss of transport function (Sigal et al., 2005). It is hypothesized that the Arginine guanidium moiety can also be important for salt bridge formation to maintain the structural integrity (Law et al., 2008) or involves itself in proton translocation (Neutze et al., 2002).

Motif-C, “XPXXXP” sequence is also known as the “antiporter motif” and it extends along the helix of TM5 (Paulsen et al., 1993) (Fig. 9, 10). As this motif is only present in antiporters, it is expected to have a peculiar role in antiport activity. Previous studies suggest that the motif-C act as a molecular hinge for the two 6TM bundles to rotate against each other to achieve the conformational changes required for translocation of substrates (Jesus et al., 2005, Yaffe et al., 2013). Crystal structure of MFS-MDR antiporter EmrD (occluded state) reveal an alpha-helical conformation of motif-C (Yin et al., 2006) (Fig. 10a) which is not biochemically well characterized and YajR (outward-open) does not possess motif-C but only motif-B and motif-A (Jiang et al., 2013) (Fig. 10b). The functional role of motif-B and motif-C in MDR transport awaits further understanding which can be appreciated possibly from the structures and biochemical characterization of these motifs in MFS-MDR antiporters.

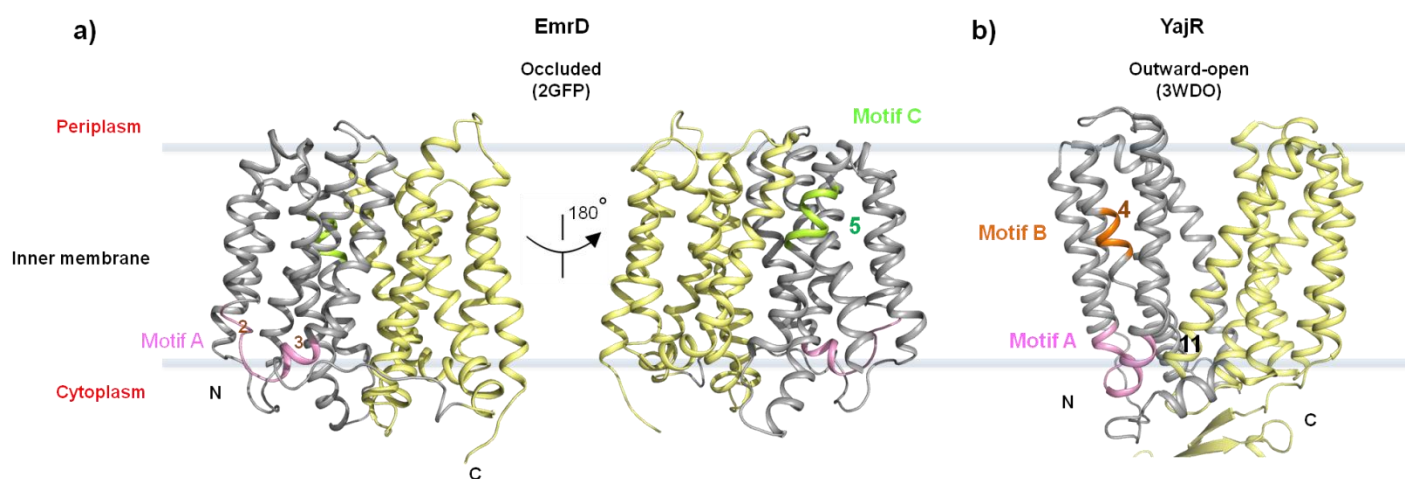


Fig 10. Crystal structures of MFS-MDR antiporter EmrD and YajR from *E.coli*: a,b) EmrD (occluded state) and YajR (outward-open state) highlight the conserved motif-A (pink) which spans between TM1 and TM2 (pink). Motif-A in YajR interacts with N-terminal part of TM11 to lock the transporter in an O_o state whereas in EmrD because of the occluded conformation the gating interaction between motif-A and TM11 are disrupted. View from the left figure of (a) rotated 180° about a vertical axis show motif-C (green) present on TM5 in EmrD adapts an α -helical conformation which is absent in YajR. b) Motif-B (orange) is located on TM4 in YajR buried within the N-terminal domain (grey) which is absent in EmrD.

Energy utilization in MFS-MDR transporters:

H⁺/Drug antiporters are driven by the proton motive force (PMF), also known as proton electrochemical gradient ($\Delta\mu_{H^+}$). The transport can be driven by the proton gradient existing across the inner membrane (ΔpH , inside alkaline) and/or by the membrane potential ($\Delta\psi$, negative inside).

Depending on the proton/substrate transport stoichiometry and the charge on the substrate, the transport can be defined as “electrogenic”, if there is a net movement of electric charge or as “electroneutral” when there is no net movement of electric charge. Electrogenic transport is driven by both the components ($\Delta\psi$, ΔpH) of the proton electrochemical gradient ($\Delta\mu_{H^+}$) whereas for electroneutral transport, ΔpH is the primary driving force (Lewinson et al., 2003). These characteristics explain the versatility of efflux pumps in handling cationic and neutral substrates for transport.

The focus of interest of this thesis is on the MFS-type MDR antiporter, MdfA from *E.coli* which is summarized under the section 2.3.

2 PURPOSE OF THIS THESIS

2.1 Aim of this thesis

MdfA is a paradigm for the major facilitator superfamily antiporter class. MdfA holds conserved motifs, molecular architecture and multiple substrate recognition patterns similar to other MFS-MDR antiporters. It is anticipated that deciphering the antiport mechanism of MdfA, as a model character will help in understanding the efflux principles of other MFS-MDR antiporters from pathogenic organisms.

The main aim of this thesis was to determine the high-resolution 3D structure of MdfA by X-ray crystallography and characterize the functional aspects of the antiporter in order to better understand the efflux mechanism. Owing to the obstacles in obtaining high resolution diffracting membrane protein crystals, the strategy that was followed was to use different membrane protein crystallization techniques to crystallize the wild type MdfA alone or in complex with an antibody fragment (Fab) appreciating its advantages.

2.2 Membrane protein production and crystallization

Structural information of membrane proteins help to understand how they work and are also helpful for the development of drugs to modulate their function. Structure determination of IMPs has tremendously increased since 2005 (<https://blanco.biomol.uci.edu/mpstruc/>) which were accelerated by the development of new technologies described below.

Overexpression of Membrane proteins:

Overexpression of membrane proteins in mg amounts is the first bottle neck in the process of membrane protein crystallization. In the case of bacterial expression system, homologous or heterologous membrane protein overexpression was made possible with the development of *E.coli* strains which cope up with the toxicity of membrane protein overexpression (Kwon et al., 2015). Bacterial expression culture conditions and expression regimes were also routinely screened to obtain optimal expression. Strategies like using strains other than *E.coli* for overexpression, protein engineering or selection of highly expressing homologues of the membrane protein under study, *E.coli* based cell-free expression systems are alternative ways of obtaining high yields of bacterial membrane protein expression (Schlegel et al., 2010). Eukaryotic membrane proteins have been routinely expressed with the baculovirus system using *Sf9* insect cells and also with the yeast strains *Saccharomyces cerevisiae*, *Pischia pastoris* and few of them have been expressed in *Lactococcus lactis*, mammalian cells (He et al., 2014).

Monitoring membrane protein overexpression is a critical step to assess whether the protein is properly inserted in the membrane. Cells expressing the membrane protein of interest are lysed and membranes are fractionated for assessing the membrane protein by western blot which can be laborious when multiple homologues or expression conditions are screened. The introduction of a fluorescent reporter system has enabled fast-tracking the entire screening process. GFP, a fluorescent reporter when C-terminally tagged to a membrane protein can be used as an indicator which fluoresces only when the protein is properly folded in the membrane and helps also to monitor the expression level (Drew et al., 2008).

Solubilisation, purification and stability of Membrane proteins:

Once sufficient level of membrane protein expression is reached, it is necessary to extract the membrane protein from the membranes with a suitable detergent. Concentration of the detergent used in the extraction process should be several fold above the critical micellar concentration (CMC) for efficient extraction of the membrane protein provided the protein is stable in the detergent used. For this purpose and to assess a suitable detergent for purification of the protein, fluorescence-detection size-exclusion chromatography (FSEC) method using GFP as an indicator was introduced to filter a detergent that aids in keeping the membrane protein of interest in a stable form in solution (Kawate and Gouaux, 2006). Detergents found harsh to the membrane protein lead to the formation of aggregates eluting in the void volume. However, this method does not explain if the protein is functional. The ultimate success of obtaining membrane protein crystals may partly depend on the choice of the detergent used in the purification process. For many of the MFS-type membrane protein structures determined to date (Table. 1), solubilisation of the membrane protein and purification was performed with a longer alkyl chain detergent. Just before crystallization setup, the purified protein was exchanged into smaller alkyl chain detergent because of the smaller size of the micelle which exposes the protein surface for crystal-crystal contacts (Deng et al., 2014, Dang et al., 2010, Sun et al., 2012). However, the use of smaller chain detergents can be harsh where its use is a balance between the stability of the protein and micelle size.

Thermostability of a membrane protein has also been correlated to the crystallization success. Apparent T_m (melting temperature) of a membrane protein can be determined using methods like CPM assay (Alexandrov et al., 2008) or nano-DSF (Boland et al., 2018) which monitors change in fluorescence as the protein unfolds by increase in temperature. Several variables like detergent, substrates, additives, protein variants (homologues, mutants) can be screened for thermostabilization of the membrane protein which have shown to influence on the outcome of crystallization trials (Sonoda et al., 2011). Many of the MFS-type proteins

crystallised either as mutants or in complex with a ligand correlate with the increase in stability or reduced conformational flexibility (Table. 1). Thermostability of membrane proteins can also be enhanced by complexing with crystallization chaperones like Fab fragments, single-chain variable fragments (scFv) or nanobody (Lieberman et al., 2011). Crystallization chaperones in complex with a membrane protein also provides significant advantageous by increasing the hydrophilic surface for crystal-crystal contacts and may also reduce conformational flexibility of the protein (Table. 1) which are critical for obtaining well-ordered crystals.

Table 1. Structures of MFS transporters

Transporter	Function	Conformational state	Resolution	PDB ID	Crystallized form	Crystallized method	Source	Published year
Uniporters								
Glut1	D-Glucose facilitator	Inward-open	3.17 Å, 3 Å, 2.9 Å, 2.99 Å	4PYP, 5EQI, 5EQG, 5EQH	Mutant, Apo form Inhibitor bound	Vapour diffusion	<i>Homo sapiens</i>	<i>Deng et al., 2014</i> <i>Kapoor et al., 2016</i>
Glut3	D-Glucose facilitator	Outward-occluded Outward-open Outward-occluded	1.5 Å 2.6 Å 2.4 Å	4ZW9 4ZWC, 4ZWB	Ligand bound Inhibitor bound	Lipidic cubic phase	<i>Homo sapiens</i>	<i>Deng et al., 2015</i>
Glut5	Fructose transporter	Inward-open Outward-open	3.2 Å 3.27 Å	4YB9, 4YBQ	Apo form	Vapour diffusion	<i>Bos Taurus</i> <i>Rattus norvegicus</i>	<i>Nomura et al., 2015</i>
Symporters								
LacY	Lactose:H ⁺	Inward-open Outward-occluded Partially outward-open Partially outward-open Outward-occluded	3.6 Å 3.5 Å 2.95 Å, 3.3 Å 3.6 Å 3.4 Å 3.5 Å 3.31 Å 3.3 Å 3 Å	1PV7, 1PV6 2CFQ, 2CFP 2V8N 2Y5Y 4OAA 4ZYR 5GXB 6C9W	Mutant, Ligand bound Mutant, Apo form Mutant, Apo form Ligand bound Ligand bound Mutant, Ligand bound Mutant, Ligand bound Mutant, Nb bound Mutant, Ligand / Nb bound	Vapour diffusion Lipidic cubic phase Vapour diffusion	<i>Escherichia coli</i>	<i>Abramson et al., 2003</i> <i>Mirza et al., 2006</i> <i>Guan et al., 2007</i> <i>Chaptal et al., 2011</i> <i>Kumar et al., 2014</i> <i>Kumar et al., 2015</i> <i>X. Jiang et al., 2016</i> <i>Kumar et al., 2018</i>
FucP	L-Fucose: H ⁺	Outward-open	3.1 Å 3.2 Å	3O7Q 3O7P	Detergent bound Mutant, Detergent bound	Vapour diffusion	<i>Escherichia coli</i>	<i>Dang et al., 2010</i>
MelB	Melibiose:Na ⁺ or Li ⁺ or H ⁺	Outward-partly occluded Outward inactive	3.35 Å	4M64	Apo form	Vapour diffusion	<i>Salmonella typhirium</i>	<i>Ethayathulla et al., 2014</i>
XylE	D-Xylose:H ⁺	Outward-facing, ligand-bound partly occluded Partly-occluded inward-facing Inward-open Inward-open	2.81 Å 2.89 Å 2.6 Å 3.8 Å 4.2 Å 3.51 Å	4GBY, 4GBZ, 4GC0, 4JA3, 4JA4 4QIQ	Ligand bound Apo form Apo form	Vapour diffusion	<i>Escherichia coli</i>	<i>L. Sun et al., 2012</i> <i>Quistgaard et al., 2013</i> <i>Wisedchaisri et al., 2014</i>
GlcP	D-Glucose:H ⁺	Inward-facing	3.2 Å	4LDS	Apo form	Vapour diffusion	<i>Staphylococcus epidermidis</i>	<i>Iancu et al., 2013</i>

PepT _{So}	Peptide:H ⁺	Inward-facing occluded	3.6 Å	2XUT	Apo form	Vapour diffusion	<i>Shewanella oneidensis</i>	<i>Newstead et al., 2011</i> <i>Guettou et al., 2014</i>
PepT _{So2}		Inward-facing	3.15 Å 3.91 Å 3.2 Å 3 Å	4PTH, 4TPG, 4TPJ, 4UVM	Ligand-bound	Vapour diffusion		
		Inward-open	4.13 Å	6J11	Apo form	Lipidic cubic phase		<i>Fowler et al., 2015</i> <i>Nagamura et al., 2019</i>
		Inward-open	3.9 Å 3.5 Å	6JKD, 6JKC	Apo form	Cryo-EM Lipidic cubic phase		
PepT _{St}	Peptide:H ⁺	Inward-open	3.3 Å	4APS	Apo form	Vapour diffusion	<i>Streptococcus thermophilus</i>	<i>Solcan et al., 2012</i> <i>Huang et al., 2015</i> <i>Martinez Molledo et al., 2018</i>
		Inward-open	2.3 Å	4XNJ, 4XNI	Apo form	Lipidic cubic phase		
		Inward-facing partly occluded	2.8 Å 2.38 Å	5OXL, 5OXX,	Ligand-bound	Lipidic cubic phase		
		Inward-open	2.30 Å 2.20 Å 2 Å 2.2 Å 2.2 Å 2.37 Å 1.95 Å	5OXM, 5OXN, 6EIA, 5OXQ, 5OXP, 5OXO	Ligand-bound HEPES, PO ₄ ²⁻ bound HEPES, PO ₄ ²⁻ bound PEG, PO ₄ ²⁻ bound Apo form			
GkPOT	Peptide:H ⁺	Inward-open	1.9 Å 2 Å 2.3 Å 2.1 Å 2.4 Å	4IKV 4IKW 4IKX 4IKY 4IKZ	Apo form SO ₄ ²⁻ bound Mutant, Apo form Mutant, SO ₄ ²⁻ bound Mutant, Ligand-bound	Lipidic cubic phase	<i>Geobacillus kaustrophilus</i>	<i>Doki et al., 2013</i>
YbgH	Peptide:H ⁺	Inward-facing	3.4 Å	4Q65	Apo form	Vapour diffusion	<i>Escherichia coli</i>	<i>Zhao et al., 2014</i>
PepT _{Ve}	Peptide:H ⁺	Inward-open	3.02 Å	4W6V	Apo form	Vapour diffusion	<i>Yersinia enterocolitica</i>	<i>Boggavarapu et al., 2015</i>
PepT _{Xc}	Peptide:H ⁺	Inward-facing	2.1 Å	6EI3	Apo form	Lipidic cubic phase	<i>Xanthomonas campestris</i>	<i>Parker et al., 2017</i>
PepT _{Sh}	Peptide:H ⁺	Inward-open	2.5 Å	6EXS	Ligand bound	Lipidic cubic phase	<i>Staphylococcus omissis</i>	<i>Minhas et al., 2018</i>
PipT	Phosphate:H ⁺	Inward-facing occluded	2.9 Å	4J05	PO ₄ ²⁻ bound	Vapour diffusion	<i>Piriformospora indica</i>	<i>Pedersen et al., 2013</i>
NRT1.1	Nitrate:H ⁺	Inward-facing	3.7 Å	5A2N,	Apo form	Vapour diffusion	<i>Arabidopsis thaliana</i>	<i>Parker et al., 2014</i> <i>Sun et al., 2014</i>
			3.71 Å	5A2O	NO ₃ ⁻ bound			
			3.25 Å	4OH3	NO ₃ ⁻ bound			

Sugar transport protein 10	Sugar:H ⁺	Outward-occluded	2.4 Å	6H7D	Ligand-bound	Lipidic cubic phase	<i>Arabidopsis thaliana</i>	<i>Paulsen et al., 2019</i>
----------------------------	----------------------	------------------	-------	------	--------------	---------------------	-----------------------------	-----------------------------

Antiporters

NarU	Nitrate:nitrite	Partially inward open Occluded	3.01 Å 3.11 Å	4IU9 4IU8	Nitrate bound	Vapour diffusion	<i>Escherichia coli</i>	<i>Yan et al., 2013</i>
NarK	Nitrate:nitrite	Inward-facing	2.6 Å 2.8 Å	4JR9 4JRE	Fab bound, Apo form Fab bound, Ligand bound	Vapour diffusion	<i>Escherichia coli</i>	<i>Zheng et al., 2013</i>
		Inward-open	2.35 Å 2.4 Å	4U4V 4U4T	Apo form NO ₃ ⁻ bound	Lipidic cubic phase		<i>Fukuda et al., 2015</i>
		Occluded	2.4 Å	4U4W	NO ₃ ⁻ bound			
GlpT	Glycerol-3-phosphate:Pi	Inward-open	3.3 Å	1PW4	Apo form	Vapour diffusion	<i>Escherichia coli</i>	<i>Huang et al., 2003</i>
EmrD	Drug:H ⁺	Occluded	3.5 Å	2GFP	Apo form	Vapour diffusion	<i>Escherichia coli</i>	<i>Yin et al., 2006</i>
YajR	Drug:H ⁺	Outward-open	3.15 Å	3WDO	Apo form	Vapour diffusion	<i>Escherichia coli</i>	<i>Jiang et al., 2013</i>
MdfA	Drug:H ⁺	Inward-facing	2 Å 2.45 Å	4ZP0, 4ZOW, 4ZP2, 6GV1	Mutant, Detergent-bound Mutant, Ligand-bound Mutant, Detergent-bound Fab bound, Apo form	Vapour diffusion Lipidic cubic phase	<i>Escherichia coli</i>	<i>Heng et al., 2015</i>
			Outward-open Inward-facing					
		2.2 Å 2.2 Å		6EUQ 6OOM	Mutant, Ligand-bound Mutant, Detergent-bound	Vapour diffusion Vapour diffusion		<i>Nagarathinam et al., 2018</i> <i>Zomot et al., 2018</i> <i>Wu et al., 2019</i>
		Outward-open	2.2 Å	5AYN	Apo form	Lipidic cubic phase		
Inward-open	3 Å 3 Å		5AYM 5AYO	Ion-bound Apo-form				

[Table updated and modified from Quistgaard et al., 2016, Yan., 2015]

Crystallization of membrane proteins:

Membrane proteins can be crystallized using three different techniques, a) bicelle-based, b) vapour diffusion or by the c) lipidic cubic phase method of which the latter two are quite prominent (Caffrey, 2003). Vapour diffusion technique involves mixing of the precipitant with the membrane protein-detergent complex (PDC) and the PDC molecules nucleate at supersaturation conditions to grow into crystals in the metastable zone. By vapour diffusion technique, many of the MFS-type proteins have been crystallized either as a mutant or in complex with a ligand or in complex with crystallization chaperones or in the presence of smaller alkyl chain detergents (7 to 11 alkyl chain) for their advantageous mentioned earlier. Some of the uniporters like GLUT1, GLUT3 and symporters like PepT_{so}, NRT1.1 have been crystallized at 4°C to decrease crystal growth kinetics for obtaining well-ordered crystals. All the strategies mentioned may be trialed for each membrane protein to grow well-ordered crystals to obtain high-resolution data for structure determination which have also been applied exhaustively for structure determination of many MFS transporters (Deng et al., 2014, Dang et al., 2010, Sun et al., 2012).

The Lipidic cubic phase (LCP) consists of highly curved non-interpenetrating bi-continuous layers of a lipid bilayer and a aqueous channel where the membrane protein of interest to be crystallized is present in the lipidic bilayer (Caffrey, 2015). By adding a precipitant to the lipidic cubic phase, local alteration in the LCP occurs forming a continuous lamellar phase where the protein molecules diffuse to nucleate and grow into a crystal by the continuous supply of the proteins from the LCP (Fig. 11a). How is the lipidic cubic phase formed? Mixing of a lipid such as monoolein (monoacylglycerol - MAG), an unsaturated 18 alkyl chain lipid together with the protein at a ratio of 3:2 results in the spontaneous formation of the lipidic cubic phase. Crystals can also be formed in the lipidic sponge phase (LSP). LCP is highly viscous in nature where by the addition of a precipitant decreases the curvature of lipid bilayer turning the viscous material into a spongified state called the lipidic sponge phase (LSP). The difference between the two phases is the size of the aqueous channel which is wider in the LSP to accommodate ectodomains of membrane protein or crystallization chaperones (Wadsten et al., 2006). Lipids of varied chain length are available for formation of the lipidic cubic phase. The choice of the lipid length influences on the thickness of the lipidic bilayer which in turn dictates the size of the aqueous channel enabling to accommodate the hydrophilic domain of the membrane protein or bound crystallization chaperones to mediate crystal-crystal contacts (Caffrey, 2015).

LCP method results in the growth of crystals of Type I packing where the interactions observed are hydrophobic and polar formed by lipid-protein and protein-protein interactions respectively (Fig. 11b). Type II packing is observed with crystals grown by vapour diffusion technique where the interactions are predominantly hydrophilic mediated by exposed surface of the protein covered by the detergent micelle (Birch et al., 2018)

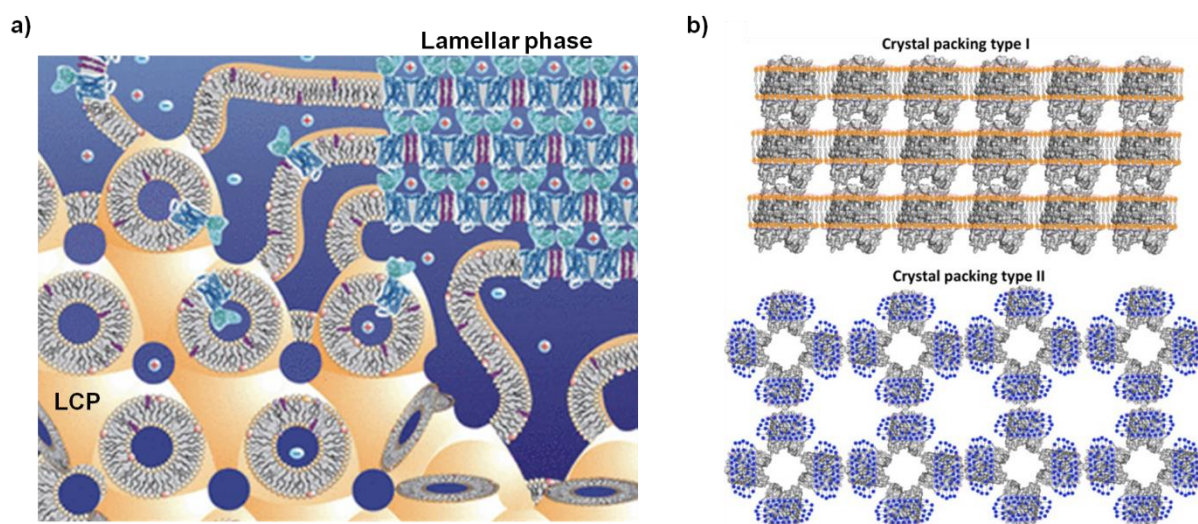


Fig 11. Lipidic cubic phase and types of packing of membrane protein crystals: **a)** Lipidic cubic phase is proposed to be made of bicontinuous layers of lipid bilayer (light brown) and an aqueous channel (blue). Precipitant addition perturbs the three dimensional LCP to transform to a lamellar phase in which membrane protein molecules diffuse to nucleate and grow into a 3D-crystal by the continuous supply of membrane protein from the LCP or LSP (Image from Caffrey, 2011). **b)** Membrane protein crystals grown by the LCP results in Type I packing where the interactions are mediated by lipid (grey line) - protein (grey surface) and protein-protein molecules. Extensive interactions are observed between the hydrophobic and hydrophilic surface of the membrane protein molecules embedded with lipidic bilayer (orange lines). In contrast, Type II packing is observed with crystals grown by the VD technique where the interaction is mediated only by exposed part of the protein (grey) covered with detergent micelle (blue dots) (Image from Birch et al., 2018).

2.3 Multidrug facilitator Assembly, MdfA:

MdfA from *E.coli* is an interesting model for studying MFS multidrug resistance transport mechanism as it encompasses all the bona fide structural, mechanistic and biochemical properties of MDR (Bibi et al., 2001, Sigal et al., 2006). Orthologs of MdfA are found in several pathogenic bacteria (Sigal et al., 2006) and overexpression of MdfA has been observed in clinical isolates of *E.coli* (Wang et al., 2013). Last two decades of research has revealed interesting aspects of proton/multidrug recognition determinants, transport modes and physiological role of MdfA.

MdfA is a 410 amino acid secondary-active monomeric antiporter (Edgar and Bibi, 1997, Sigal et al., 2007). It is encoded by the *cmr* gene and was initially thought to be a chloramphenicol-specific transporter (Bohn and Bouloc, 1998). Biochemical studies later showed that *E.coli* expressing multicopy plasmid of MdfA exhibit resistance to a diverse group of clinical substrates such as neutral drugs, zwitterionic compounds, monovalent cations, and divalent cations with long linkers (Edgar and Bibi, 1997, Fluman et al., 2014). MdfA can transport its substrates in an electrogenic (neutral substrates) or electroneutral mode (cationic substrates) and the H⁺/Drug stoichiometry has been found to be 1 (Lewinson et al., 2003, Tirosh et al., 2012, Fluman et al., 2012). Transport experiments have shown that apart from H⁺/drug exchange activity, it can also function as a (Na⁺)(K⁺)/ H⁺ antiporter (Lewinson et al., 2004). As a result, cells expressing this antiporter can tolerate high alkaline external pH which is likely to be a physiological role of the antiporter.

MdfA consists of a hydrophobic pocket with negatively charged residues which can bind a single substrate or simultaneously bind two substrates (Lewinson and Bibi, 2001). Several transport assays and binding experiments have shown that Glu26^{TM1} and Asp34^{TM1} are important for the active transport of cationic substrates, but for neutral substrates, they may compensate for each other deficiencies (Sigal et al., 2005, Sigal et al., 2009) (Fig. 12). Probing dicyclohexylcarbodiimide (DCCD) reagent reactivity (a powerful reagent for probing protonated acidic residues in a hydrophobic environment), radiolabeled [³H]-TPP binding assay and peptide mass spectrometry experiments allowed Fluman et al., 2012 to address the H⁺/Drug coupling mechanism. They suggested that the Glu26^{TM1} is the main substrate binding site and Asp34^{TM1} is the major proton binding site and also came up with an antiport mechanism for MdfA (Fluman et al., 2012). Furthermore, it was also demonstrated that the essential negatively charged residue Glu26^{TM1} can be delocalized within the binding pocket and the substrates may reorient in the binding cavity and can be still actively transported (Fluman

et al., 2009). Spontaneous mutations Ala150Glu (TM5) and Val335Glu (TM10) rescued the transport of their respective inactive mutants Glu26Thr/Asp34Met (TM1) and Glu26Thr (TM1) endorsing the promiscuous substrate recognition nature of the binding pocket (Adler and Bibi, 2005, Sigal et al., 2009). This property can also be exemplified by the ability of MdfA to transport divalent cations which had been made possible by manipulating the drug binding pocket by inserting a third acidic residue in the binding pocket (Met358Glu^{TM11}) (Tirosh et al., 2012). Although many interesting features of MdfA such as proton/substrate binding determinants, H⁺/Drug stoichiometry, multiple substrate recognition were experimentally determined. Many questions relevant to the MdfA antiport mechanism are still unanswered: a) What is the mechanism of H⁺/Drug coupling, b) Are the H⁺ and substrate relayed through the acidic residues Glu26^{TM1} and Asp34^{TM1}?, c) How are the conformational changes in MdfA achieved? d) What are the functional role of conserved motifs, motif-B and motif-C in MdfA antiport mechanism, e) What are the differences in the recognition of multiple substrates within the binding pocket of MdfA, f) What is the entry port for the substrates, and g) How are divalent cationic substrates with long linkers transported?

Inward-facing (I_F) structures of MdfA:

Recently the high-resolution crystal structures of MdfA-Q131R mutant complexed to chloramphenicol (2.4 Å, pH 5.8), deoxycholate (2.0 Å, pH 5.8) and LDAO detergent molecule (2.2 Å, pH 8.5) were all determined in the inward-facing (I_F) state (Heng et al., 2015) (Fig. 12 a,b, Fig. 13). The captured conformational state of MdfA is termed as “inward-facing (I_F)” because the binding pocket is only partially open to the cytoplasm where the periplasmic side is closed by gating of residues from TM 1, 2, 5, 7 and 8 (Fig. 12c, d). I_F structures of MdfA confirms the canonical 12TM MFS fold which can be divided into pseudosymmetrical 6TM N- and C-terminal bundles (Fig. 12a). 12TM helices can also be grouped as three-helix repeats with the 1st helix of each repeat (TM 1, 4, 7, 10) termed as cavity helices that constitute the binding pocket, 2nd helix of each repeat (TM 2, 5, 8, 11) is termed as rocker helix, and 3rd helix of each repeat (TM 3, 6, 9, 12) is located at the periphery of the antiporter and extensively interact with the lipidic bilayer and is denoted as support helix (Fig. 12c). I_F structure exhibits a large hydrophobic pocket and the ligands interact with a specific set of residues in each structure and are also hydrogen bonded to Asp34^{TM1} in all the three structures (Fig. 12a, b, d, Fig. 13). Mutation of the twelve residues interacting with chloramphenicol to alanine individually abolishes the transport activity of MdfA.

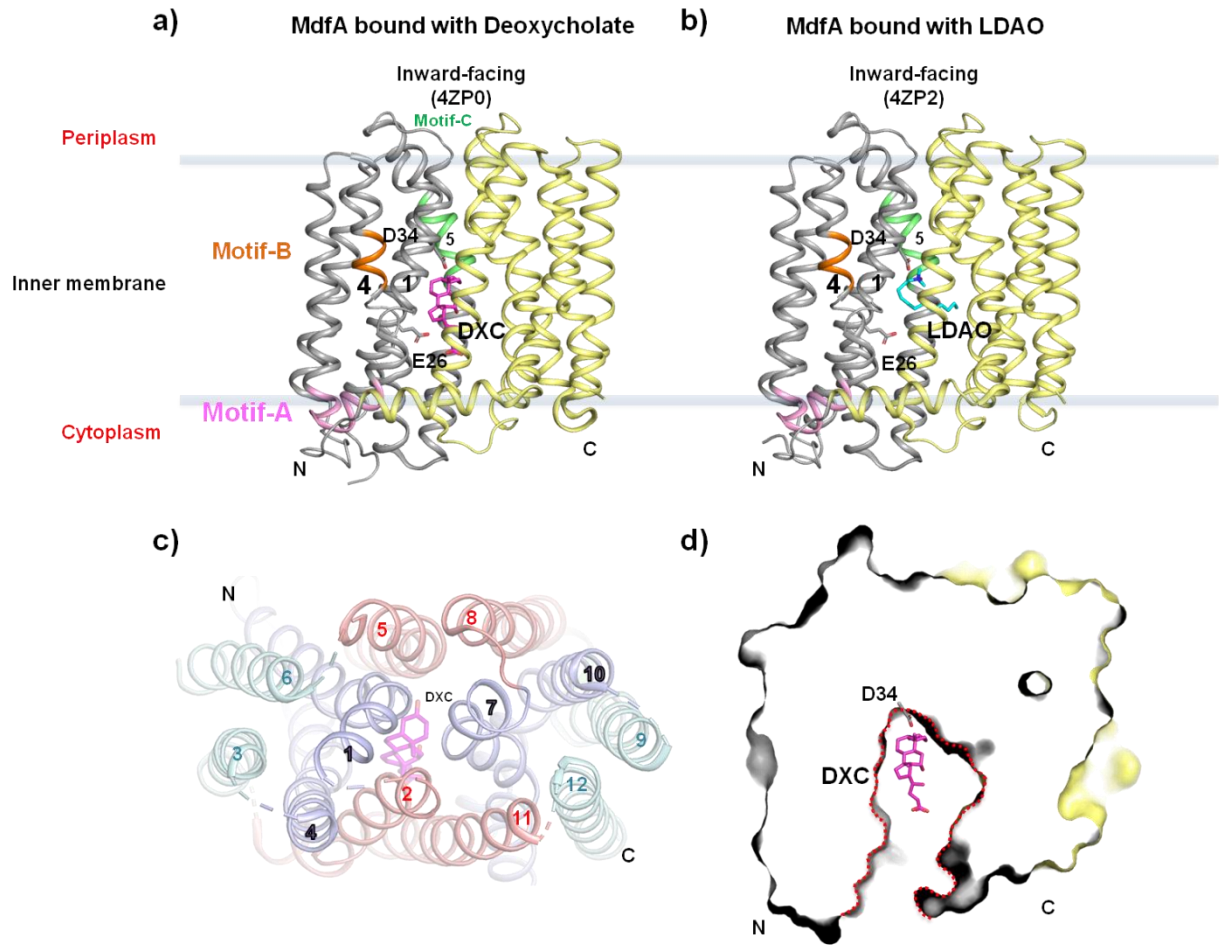


Fig 12. Inward-facing (IF) structures of MdfA bound with deoxycholate (DXC) and lauryldimethylamine-N-Oxide (LDAO): The N- (grey) and C-terminal (yellow) domains approach close to each other on the periplasmic side of the transporter to enclose a substrate binding pocket partially open to the cytoplasm but closed to the periplasm. **a)** Deoxycholate (DXC, pink stick) is bound to the negatively charged residue Asp34^{TM1} (grey stick) within the binding pocket. The highly conserved motifs A (pink), B (orange) and C (green) are localized to the N-terminal domain. **b)** LDAO detergent molecule (cyan stick) is bound to the negatively charged residue Asp34^{TM1} (grey stick). **c)** Periplasmic view of DXC bound (pink stick) I_F structure of MdfA highlighted with the cavity helices (TM 1, 4, 7, 10 as salmon), rocker helices (TM 2, 5, 8, 11 as light purple) and support helices (TM 3, 6, 9, 12 as cyan). MdfA binding pocket is closed to the periplasm by gating of the residues from helices TM 1, 2, 5, 7 and 8. **d)** Sliced surface representation of DXC bound (pink stick) structure of MdfA revealing a large binding pocket (indicated as red-dashed lines) partially open to the cytoplasm (Heng et al., 2015).

Conserved motif of MdfA, motif-B, “R112^{TM4}XXXG116^{TM4}” is buried within the periplasmic side of the N-terminal domain. Arg112^{TM4} forms a hydrogen bond network connecting Asp34^{TM1} which is bridged by a water molecule and also Arg112^{TM4} is surrounded by a number of hydrophobic residues (Fig. 13b). The motif-B hints to be an integral part of the antiport mechanism but the biochemical data do not lend any clue about its involvement in the

transport mechanism. Motif-C, “AP154^{TM5}XXGP158^{TM5}” extends as an ideal α -helix in the I_F structure (Fig. 13b).

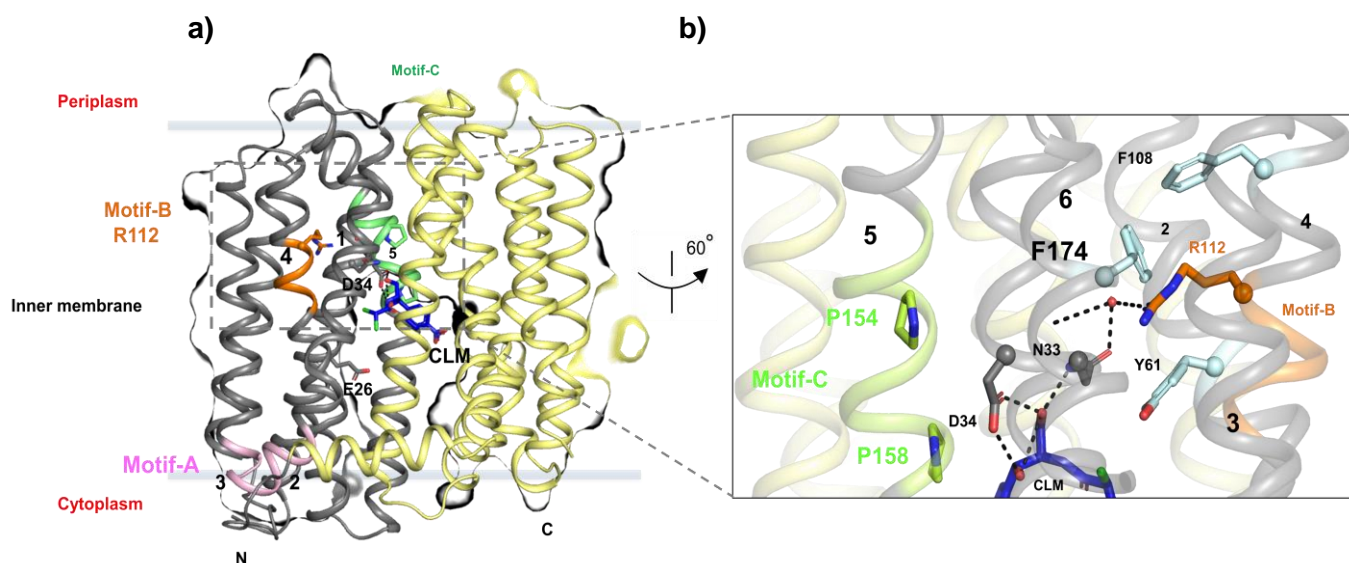


Fig 13. Chloramphenicol bound Inward-facing (I_F) structure of MdfA: a) N- (grey) and C-terminal domain (yellow) enclose a cavity partially open to the cytoplasm in which chloramphenicol (blue sticks) is bound to the negatively charged residue, Asp34^{TM1} and also interacts with other residues in the binding pocket. The conserved motifs are located on the N-terminal domain; motif-A (pink, TM2-TM3), motif-B (orange, TM4) buried within the N-terminal domain and motif-C (green, TM5) adopts an α -helical conformation. b) Chloramphenicol bound to Asp34^{TM1} communicates to the highly conserved motif-B Arg112^{TM4} (orange sticks) via a hydrogen bond network Asp34^{TM1}-Asn33^{TM1}-H₂O-Arg112^{TM4} (grey sticks, water molecule as red sphere). The motif-B Arg112^{TM4} is surrounded by hydrophobic residues (cyan sticks) and the architecture is to be preserved for the antiport activity of MdfA. View from figure (a) rotated 60° about a vertical axis (Heng et al., 2015).

From the ligand complexed - I_F structures [chloramphenicol (Cm) (Fig. 13a), dexoxycholate (DXC) (Fig. 12a) and lauryldimethylamine-N-Oxide (LDAO) (Fig. 12b)], it is apparent that Asp34^{TM1} is the main substrate binding site and it is also shown to be involved in proton binding. The binding cavity in the I_F state is open to the cytoplasm which allows the substrate to bind to Asp34^{TM1}. Although, the inward-facing structure of MdfA is determined in complex with substrates and non-substrates providing a molecular understanding of substrate recognition in the binding pocket. The dearth of structures of other conformational states has very much hampered the understanding of the transport mechanism of MdfA with the proposed models making it much more complex to understand (Fluman et al., 2012, Heng et al., 2015).

3 SUMMARY OF THE RESULTS AND DISCUSSION

The main results and discussion of each manuscript are summarized here. For a detailed description kindly refer to the respective manuscript.

3.1 Manuscript I

Generation of conformation-specific antibody fragments for crystallization of the multidrug resistance transporter MdfA.

Jaenecke F*, Nakada-Nakura Y*, Nagarathinam K., Ogasawara S, Liu K, Hotta Y, Iwata S, Nomura N, Tanabe M.

Bacterial Multidrug Exporters. *Methods in Molecular Biology*, vol 1700, 2018. Humana Press, New York, NY

Membrane proteins are notoriously difficult to crystallize. The major problem in obtaining high-resolution diffracting crystals of a membrane protein is the conformational flexibility of the membrane protein and the limitations in purifying substantial quantity of functional membrane protein amenable for crystallization trials. Moreover, membrane proteins are routinely purified in detergents which often affect the stability and also mask the surface of the molecules diminishing the crystal-crystal contacts. These bottlenecks can be circumvented by crystallizing the membrane protein of interest together with a Fab fragment that can recognize the conformational epitope of MdfA, as it provides beneficial effects by arresting the antiporter to a particular conformational state and also extends the hydrophilic surface for mediating crystal-crystal contacts (Hino et al., 2013). We anticipated that the binding of the Fab fragment may also increase the thermostability of MdfA, as higher the stability of a membrane protein is usually correlated with crystallization success.

MdfA was overexpressed with a C-terminal GFP-octahistidine tag and purified in two steps of Ni²⁺ affinity chromatography. Pure MdfA was reconstituted in liposomes and assessed for functionality by the substrate TPP-induced fluorescence quenching assay as shown by Fluman et al., 2009. Quenching of MdfA fluorescence was observed with increasing concentration of TPP indicating that MdfA reconstituted in liposomes is functional which were further used for mice immunization to raise antibodies against them. Fab fragments recognizing conformational epitopes were positively selected (liposome ELISA) against fragments that bound to linear epitopes (negative selection / denatured MdfA-targeted ELISA). In this fashion, four Fab fragments YN1006, YN1010, YN1074, YN1082 were positively selected. Each Fab formed a stable complex with MdfA and was purified by size exclusion

SUMMARY OF THE RESULTS AND DISCUSSION

chromatography. We, characterized the thermostability of MdfA-Fab complexes and MdfA-WT at pH 7 by N-[4-(7-diethylamino-4-methyl-3-coumarinyl)phenyl] maleimide (CPM) thermostability assay. We identified that the MdfA-YN1074 Fab complex (71 °C) showed enhanced stability of about 8 to 12 °C compared to other MdfA-Fab complexes (62.5 to 63.6 °C) and MdfA alone (58 °C). Crystallization of the highly thermostable Fab complex MdfA-YN1074 with the lipidic cubic phase (LCP) method resulted in crystals diffracting to 3.5 Å which is explained in detail in the manuscript II. These results relate to the advantages of using antibody fragment (Fab) mediated crystallization of the multidrug resistance antiporter, MdfA where the protocol can also be extended to other difficult to crystallize MFS transporters or membrane proteins in general that alter between different conformational states to achieve transport.

3.2 Manuscript II

The multidrug-resistance transporter MdfA from *Escherichia coli*: crystallization and X-ray diffraction analysis.

Nagarathinam K*, Jaenecke F, Nakada-Nakura Y*, Liu K, Hotta Y, Iwata S, Stubbs M.T., Nomura N., Tanabe M.

Acta Crystallogr F Struct Biol Commun. 2017 Jul 1;73(Pt 7):423-430

The manuscript I describes the protocol to generate conformation-specific antibodies towards the multidrug resistance antiporter, MdfA. We identified through systematic screening that the Fab YN1074 used as a crystallization chaperone stabilized the antiporter effectively (CPM assay) and improved the crystallization properties. In manuscript II, we probed the stability of MdfA and the MdfA-YN1074 Fab complex as a function of pH and also investigated the effects of different crystallization methods on the diffraction quality of the crystals of MdfA wild type and MdfA-Fab complex.

We identified that the stability of the MdfA-YN1074 Fab complex was independent of the pH with high stability (71 °C) compared to MdfA which showed a decrease in stability (66 °C to 58 °C) on increasing pH from 5.5 to 7. This demonstrates that the Fab-YN1074 stabilizes the low pH form of the antiporter in comparing with the MdfA stability at pH 5.5 and the complex was suitable for crystallization screening in a wide range of pH conditions.

Vapour diffusion method:

Crystallization of MdfA alone with the vapour diffusion (VD) method resulted in hexagonal crystals diffracting to a lower resolution of 7 Å and the crystals belonged to the hexagonal space group P6_{1/5}22 with unit cell parameters a = b = 94.5, c = 663.1 Å. Crystallization of MdfA-YN1006 and MdfA-YN1082 Fab complexes resulted in crystals diffracting poorly to 30 Å, whereas for MdfA-YN1010 Fab complex no crystals were obtained. In contrast, crystals of the MdfA-YN1074-VD diffracted to a maximal resolution of 6 to 7 Å. MdfA-YN1074-VD crystals belonged to the orthorhombic space group P2₁2₁2₁ with unit cell parameters a = 76.6, b = 141.6, c = 296.6 Å.

Lipidic cubic phase method:

The limitations in obtaining high-resolution diffracting quality crystals with the vapour diffusion method prompted us to explore the lipidic cubic phase (LCP) method which is an alternative for membrane protein crystallization. Initial LCP setups, in general, were performed with 9.9 MAG (18-C) as the host lipid (Caffrey, 2015). Crystallization of the MdfA and MdfA-YN1082 Fab complex in 9.9 MAG resulted in crystals diffracting to 30 Å needle-shaped

SUMMARY OF THE RESULTS AND DISCUSSION

crystals of MdfA-YN1074 Fab complex which showed weak diffraction to 8 Å belonging to the hexagonal space group $P6_{1/5}22$ with unit cell parameters $a = b = 73.3$, $c = 950.1$ Å. The restriction in obtaining high-resolution with 9.9 MAG drew our attention to reduce the alkyl chain length for further screening. Host lipids were selected based on reported membrane protein structures crystallized by the LCP method (Caffrey, 2015). The rationale behind screening with reduced alkyl chain length is to improve partitioning of MdfA within the lipidic bilayer for crystal-crystal contacts and to increase the aqueous channel size to accommodate the Fab fragment and also to augment the lateral diffusion of MdfA molecules by influencing the curvature of the bicontinuous lipidic bilayer. Screening with 7.7 MAG (14-C), 7.8 MAG (15-C) and 7.9 MAG (16-C) led to the growth of crystals not more than 50 µm with poor diffraction. Screening with 8.8 MAG (16-C) resulted in hexagonal crystals which grew to full size (100 µm) over 5 – 7 weeks and diffracted best to 3 Å. Due to the presence of very long c-axis, the crystals were mounted perpendicular to the beam with a slight tilt to best resolve the diffraction spots. Anisotropy of the diffraction data restricted the resolution of the data set to 3.4 Å. These crystals belonged to the hexagonal space group with unit cell parameters $a = b = 73.3$, $c = 927.9$ Å.

Crystal packing analysis:

Molecular replacement was performed to analyze the crystal packing in each of the crystal forms of MdfA-VD, MdfA-YN1074 Fab complex-VD and MdfA-YN1074 Fab complex-LCP. Two molecules of MdfA (solvent content 74.5%) or MdfA-YN1074 Fab complex (solvent content 70%) was located in their respective asymmetric unit (ASU) of the crystals grown by vapour diffusion method. On the other hand, only one complex of MdfA-YN1074 Fab complex was found in the ASU of the LCP crystals. In all the three crystal forms, adjacent monomers of MdfA in the crystal lattice orient themselves in the opposite directions (anti-parallel).

Crystal packing of the molecules in MdfA-VD crystal reveal that the lateral contacts are mediated by the hydrophobic TM helices and the interlayer contacts are mediated by residues from the periplasmic and cytoplasmic hydrophilic surfaces of the antiporter resulting in only feeble interactions (Fig. 14a). MdfA molecules arrange themselves to form superhelical “chains” with the helical axis parallel to the crystallographic six-fold screw axis. The presence of large spaces between the chains presumably occupied by detergent micellar structures yield weak interactions, in turn leading to lower resolution diffraction (Fig.14a).

MdfA-YN1074-VD crystal packing reveal that the Fab bound to the cytoplasmic side of the antiporter, extending Fab-Fab interactions between the MdfA monomers of the adjacent

SUMMARY OF THE RESULTS AND DISCUSSION

layers within the ASU. Lateral contacts are formed between antiparallel MdfA monomers and interactions are also formed between the periplasmic hydrophilic portion of MdfA molecules which are less extensive compared to the lateral contacts. The MdfA-YN1074 Fab complexes are arranged as rippled stacks where the interlayer spaces are presumably occupied by disordered detergent micelles resulting in weak diffraction behaviour (Fig. 14b).

Membrane protein crystal packing types are explained under section 2.2. In contrast to Type II packing observed with MdfA-YN1074 Fab complex-VD crystals, Type I packing is observed in the crystals of MdfA-YN1074 Fab complex-LCP which is typical for crystals obtained from the LCP (Caffrey, 2015). Two sets of extensive hydrophobic lateral contacts are formed by each monomer to the adjacent MdfA molecules. Lateral hydrophobic contacts observed in the 2D arrangement of the MdfA-YN1074 Fab complex here have been maximized, as the MdfA molecules are partitioned in the lipidic bilayer and laterally diffuse to effectively pack with the neighbouring monomers. Fab fragment bound to the cytoplasmic side of the antiporter extend interactions to one another and they occupy the aqueous channel space sandwiched between the MdfA monomers embedded in the adjacent lipidic bilayer. High solvent content is not typical for LCP crystals but the spaces observed between the Fab molecules contribute to this high value (68.1% solvent content) (Fig 14. d,e).

These results disclose the fact that the weak interaction between the molecules of MdfA-VD or MdfA-YN1074 Fab complex-VD within the crystal lattice has lead to weak diffraction behaviour. The weak diffraction is also augmented by the presence of disordered detergent micelles that surrounds each MdfA monomer which prevents 2D arrangements as observed for LCP crystals.

The superior diffraction quality observed with MdfA-YN1074 Fab complex-LCP crystals is due to the favourable partitioning of intramembrane (MdfA) and hydrophilic contacts (Fab YN1074) observed in the packing of these crystals. Although in this case, the choice of the crystallization method i.e. the lipidic cubic phase method is important for achieving superior diffraction quality of the crystals, host lipid screening is also seemingly an important parameter to be explored for this method. We noticed that the morphology of the crystals had changed remarkably to the MAGs used and the c-axis unit cell length is 22 Å shorter with crystals grown from 8.8 MAG (16-C) compared to the use of 9.9 MAG (18-C) for crystallization. The use of different MAGs might influence on the 2D packing of the membrane protein layers or the orientation of MdfA in the bilayer itself which in turn influences the positioning of the Fab and this impacts on the packing and diffraction quality of the crystals.

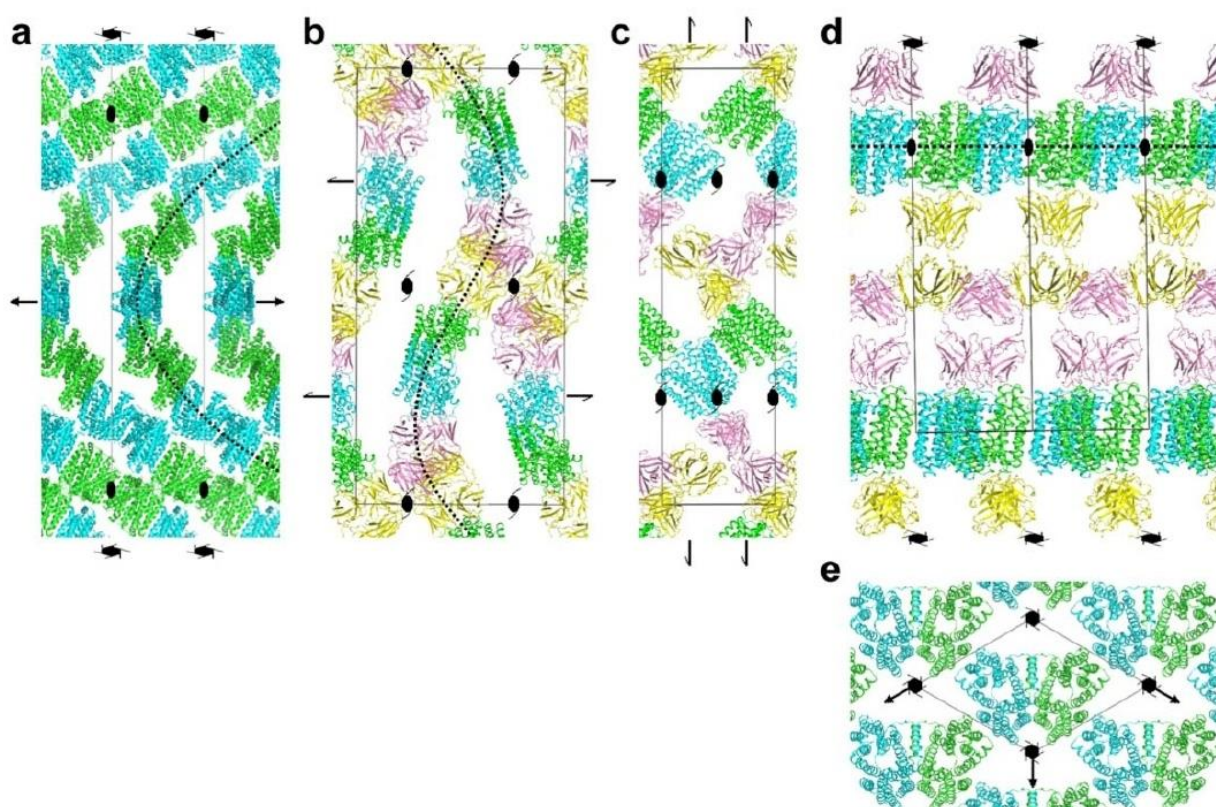


Fig 14. Crystal packing in MdfA crystals: Packing arrangements of (a) the transporter (**MdfA-VD**) and (b, c) the MdfA-YN1074 complex within vapour diffusion grown (**MdfA-YN1074-VD**) crystals, and (d, e) the MdfA-YN1074 membrane protein complex within lipidic cubic phase grown crystals (**MdfA-YN1074-LCP**). Selected symmetry element symbols are shown for orientation. (a) The two MdfA monomers (green, cyan) within the asymmetric unit of **MdfA-VD** align to form infinite superhelical chains (dotted line) that are stabilized by lateral hydrophobic contacts. Individual chains contact each other via a small number of hydrophilic contacts. View parallel to the crystallographic a-axis. (b) Crystal contacts in **MdfA-YN1074-VD** are dominated by interactions between the Fabs (yellow, pink) from symmetry-related molecules. Within the lattice, the molecules are arranged in rippled layers (dotted line), with major contacts between the layers provided by the Fabs. View parallel to the crystallographic a-axis. (c) One layer from (b), viewed parallel to the crystallographic b-axis. (d) In the **MdfA-YN1074-LCP** crystals, MdfA (green; for clarity, two-fold symmetry related molecules are shown in cyan, although these are crystallographically equivalent) is found in a two-dimensional membrane-like array. MdfA layers sandwich those of the Fab YN1074 (yellow; pink), resulting in favorable segregation of hydrophobic and hydrophilic crystal contacts. View parallel to crystallographic a-axis. (e) The MdfA layer from (d), viewed parallel to the crystallographic c-axis (Image and legend reproduced from manuscript II).

3.3 Manuscript III

Outward open conformation of a Major Facilitator Superfamily multidrug/H⁺ antiporter provides insights into switching mechanism.

Nagarathinam K*, Nakada-Nakura Y*, Parthier C, Terada T, Juge N, Jaenecke F, Liu K, Hotta Y, Miyaji T, Omote H, Iwata S, Nomura N, Stubbs M.T., Tanabe M. Nature Communications 9, Article number: 4005 (2018)

The manuscript describes the structural differences between the outward-open state (O_o) and the already published inward-facing state (I_F) of MdfA. Based on the observed structural differences, biochemical and molecular dynamics simulation data of MdfA, a conformational-switching mechanism from outward-open to the inward-facing state has been proposed. MdfA being the first antiporter for which more than one conformational state is available, we anticipate that the proposed conformational-switching mechanism of MdfA will serve as a model system for understanding the switching mechanism of other MFS-MDR antiporters.

Phases were determined by molecular replacement with PHASER MR using the separate N- and C-lobes of MdfA of the inward-facing conformation (PDBID: 4ZP0) and a Fab fragment (PDBID: 1IBG) as individual search models. The model was rebuilt manually using COOT and refined using PHENIX. Detailed information on structure determination can be found under the methods section of the manuscript.

Structure of MdfA in the outward-open (O_o) state:

The crystal structure of the MdfA-Fab complex reveals that the Fab fragment is bound to the cytoplasmic side of the antiporter stabilizing the outward-open state (O_o), where this conformation was also observed with the crystals of wildtype MdfA grown by the VD technique (manuscript II). Molecular dynamics simulations of the O_o structure without the Fab fragment remained stable in a solvated membrane environment indicating that the binding of the Fab fragment on the cytoplasmic side does not induce any changes to the captured conformational state of MdfA.

MdfA consists of two 6TM bundles of N-terminal and C-terminal domain connected by a loop and an amphipathic helix. The two bundles approach each other to form a “V-shaped” structure with the cavity closed to the cytoplasmic side but exposed to the periplasm adapting the O_o state. The cytoplasmic side is sealed by a number of hydrophobic residues from cytoplasmic halves of TM2, TM5 of the N-terminal domain and TM8, TM10, TM11 of the C-terminal domain (Fig. 15a). The cytoplasmic closure is also mediated by interdomain

SUMMARY OF THE RESULTS AND DISCUSSION

electrostatic interactions from the highly conserved motif-A, Asp77 from the TM2 C-terminus interacting with N-terminus of TM11 and also by Arg336 from the C-terminus of TM10 interacting with the C α -backbone atoms extending between TM4-TM5. In comparison with the ligand bound inward-facing state, the two TM bundles have undergone a global rotation by 33.5° in a plane parallel to the lipidic bilayer endorsing the “alternating access mechanism” by which the cavity becomes partially open to the cytoplasm. The electrostatic and hydrophobic interactions observed on the cytoplasmic side of MdfA in the O_o state are replaced predominantly by hydrophobic contacts between the periplasmic halves of TM 1, 2 and 5 of the N-terminal domain and TMs 7, 8 and 11 of the C-terminal domain in the I_F state on the periplasmic side (Fig. 15b).

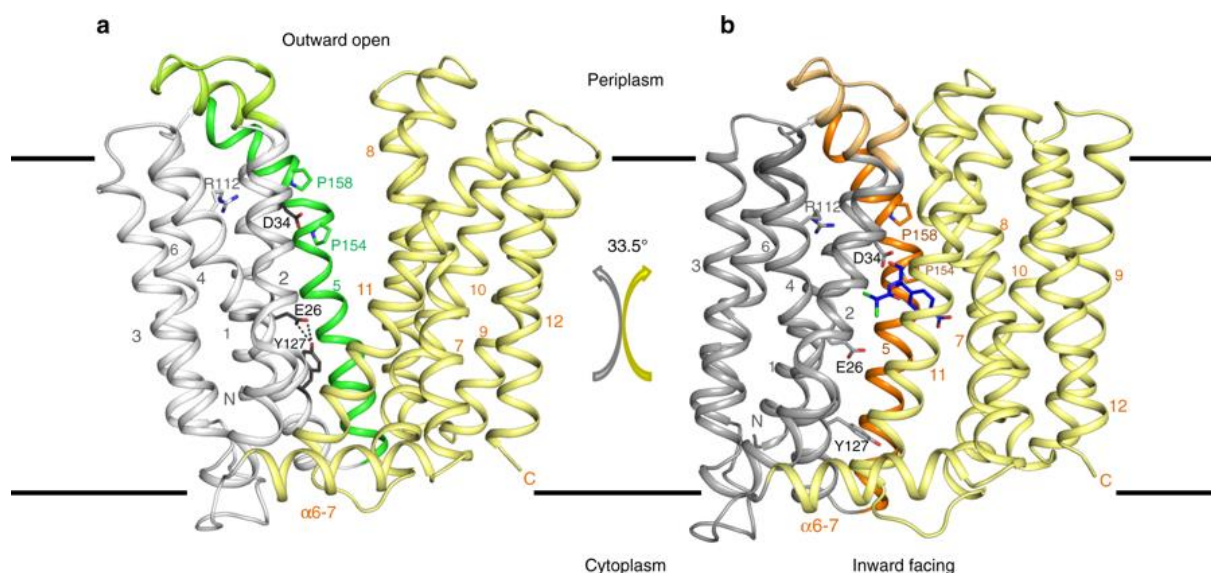


Fig 15. Structure of MdfA in the outward open (O_o) and inward facing (I_F) states: a) The transporter in the O_o conformation (this work); b) MdfA in the ligand-bound I_F state (Heng et al., 2015). The N- (white/grey) and C-terminal (yellow) six transmembrane helical domains are shown in ribbon representation, with transmembrane helices (TMs) numbered. Note the difference in the relative orientation of the two domains by 33.5°. TM5, whose conformation differs between the two states, is shown in green (O_o) or orange (I_F); the TM1–TM2 termini are in corresponding light colours. The position of chloramphenicol bound in the I_F state is depicted using blue sticks (Image and legend reproduced from manuscript III).

Overlaying the N- and C-terminal bundles of the O_o and previously published I_F structure (PDBID: 4ZOW) separately, strikingly reveals three statistically significant structural deviations in the O_o state. The largest deviation is observed in TM5 (residues 136 to 153), which ends in the antiporter motif-C “AP¹⁵⁴XXGP¹⁵⁸” that is absent in symporters and uniporters (Varela et al., 1995). Residues 136 to 153 of the TM5 in the O_o state exhibit a profound 10° kink, accompanied by a ca. 45° clockwise twist parallel to the helix axis. In the I_F structure, TM5 adapts an ideal α -helical conformation (Fig. 16 a,b). In the O_o state, the

SUMMARY OF THE RESULTS AND DISCUSSION

maximum deviation in TM5 is found at residue Met146^{TM5}, which is in close proximity to the side chain Tyr127^{TM4}. Further, the Tyr127^{TM4} is found hydrogen bonded to Glu26^{TM1} at a distance of 2.5 Å. In the I_F state the space occupied by Tyr127^{TM4} is replaced by Met146^{TM5} (Fig. 16c).

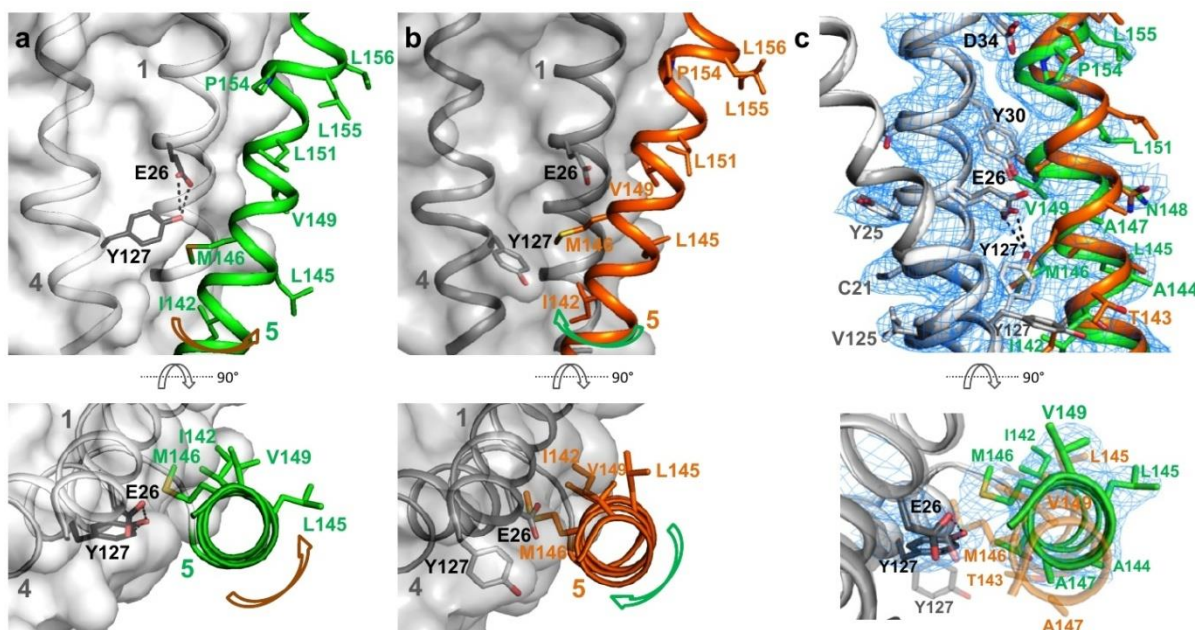


Fig 16. The O_o and I_F conformations differ by local twisting of TM5. a) In the O_o state, TM5 (green) is partially distorted, resulting in C α displacements compared to the I_F state of up to 2.9 Å (Met146^{TM5}). The side chain of Met146^{TM5} rests against the phenolic side chain of Tyr127^{TM4}, whose hydroxyl moiety is ca. 2.5 Å from the side chain carboxylate group of Glu26^{TM1}, suggesting the presence of a charge-assisted hydrogen bond. b) TM5 adopts an ideal α -helical conformation in the I_F state through the displacement of the Tyr127^{TM4} side chain by that of Met146^{TM5}. TM5 straightens, rotating around its axis such that its hydrophobic side chains can engage/disengage the C-terminal domain. c) Electron density for TM5 in the O_o conformation, superimposed with coordinates of the final (green) and initial (orange) models (Image and legend reproduced from manuscript III).

The second structural difference between the O_o state and ligand bound-I_F state is a significant expansion of an array of hydrophobic residues (hydrophobic core) found around the highly conserved Arg112^{TM4} (motif-B) which is buried within the N-terminal domain on the periplasmic side of MdfA (Fig. 17). Although the structural difference between the two states in this region appears to be small, note that this observation may be absolutely different on comparing to an apo-I_o state of the transporter. The third structural difference is found on the cytoplasmic side of the transporter localized to TM8 Arg281-Val284. When comparing this segment between the ligand bound I_F structures show inherent structural variability implying that this region may not play a major role in the antiport activity of MdfA.

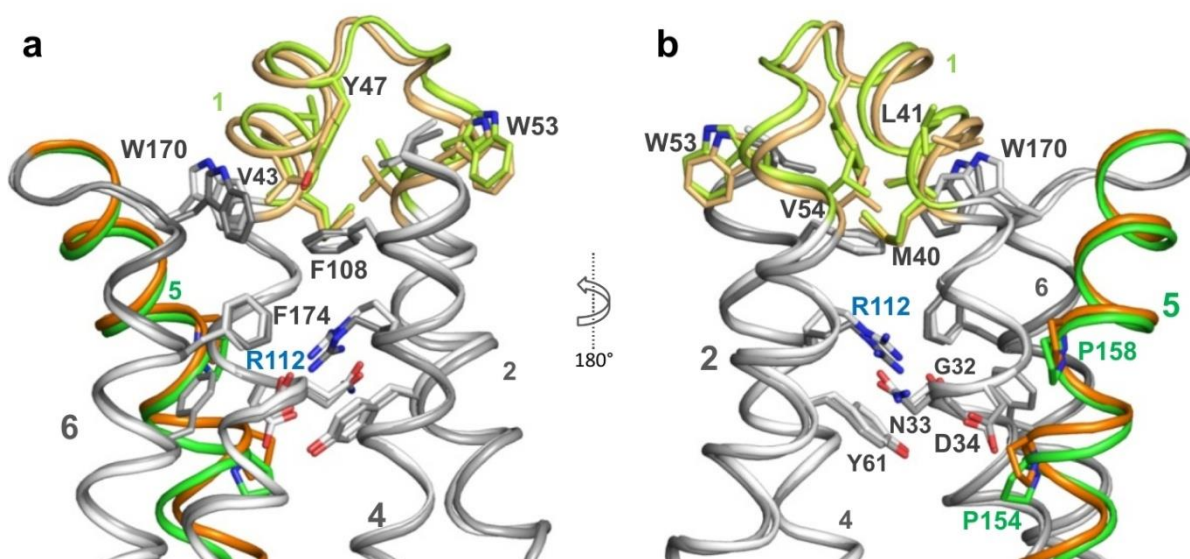


Fig 17. Small but significant differences are observed in the hydrophobic core near the periplasmic face of the N-terminal domain. The core is in contact with the buried guanidiny moiety of conserved Arg112^{TM4} (motif B), which in turn is connected to Asn33^{TM1}-Asp34^{TM1} by a hydrogen bond network (not shown). Views (a) from the “left” of Figure 7 rotated 180° about a vertical axis. Image and legend reproduced from manuscript III.

Selected residues were assessed for their importance in MdfA antiport activity (performed by Mikio Tanabe and collaborators). MdfA WT and mutants were reconstituted into liposomes to assess for the transport of chloramphenicol. Mutants Tyr127^{TM4}Phe, Met146^{TM5}Ala and Trp170^{TM6}Ala showed reduced transport activity compared to wildtype indicating their involvement in MdfA function. Variant Glu26^{TM1}Gln did not drastically affect the transport indicating that this residue is not important for chloramphenicol transport as suggested by previous studies (Sigal et al., 2009), although this may well differ for cationic substrates recognition and transport.

Combinations of different protonation states of the two critical acidic residues Asp34^{TM1} and Glu26^{TM1} involved in transport were assessed by MD simulations (performed by Tohru Terada). Conformational changes were monitored by the change in distances between helices TM5 and TM8 on the periplasmic and cytoplasmic halves of the transporter. Starting from the O_o state, protonation of Asp34^{TM1} [O_o(E26⁻/D34^P), O_o(E26^P/D34^P)] resulted in an occluded form of MdfA (Fig. 18). In the occluded form, the TM5 remains kinked and the Glu26^{TM1}-Tyr127^{TM4} hydrogen bond remained stable. Simulations were performed on the I_F structure of MdfA (Arg131 mutated to Gln) after removing the ligand [I_F(E26⁻/D34^P)] which resulted in the cytoplasmic closure leading also to an occluded state with the kinking of TM5

helix (Fig. 18). The occluded cavity achieved within the binding pocket from the O_o state resembles the cavity formed from the I_F state.

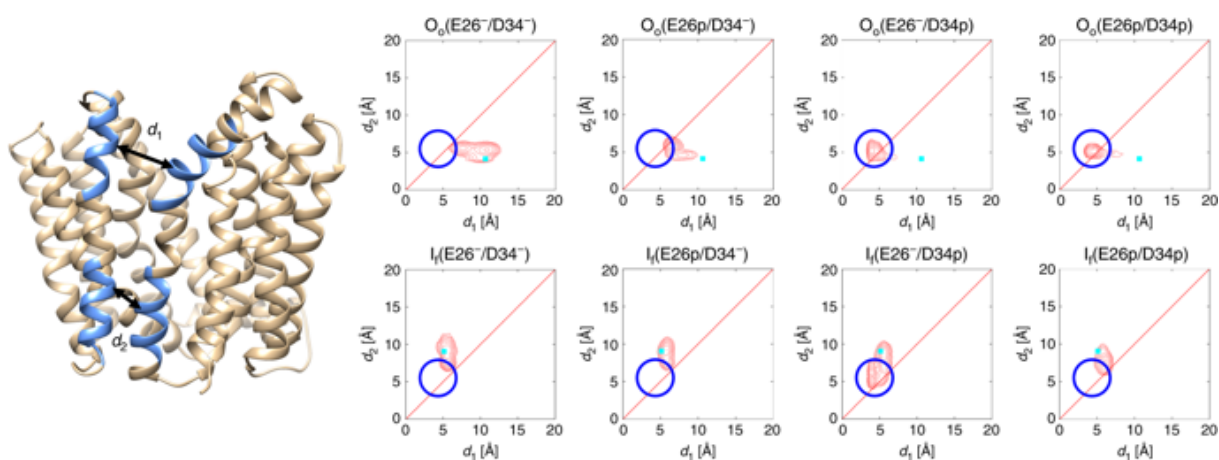


Fig 18. Molecular dynamics studies of MdfA: Conformational distributions of MdfA obtained following MD simulations. Starting from each initial conformation (O_o vs. I_F) and Glu26/Asp34 protonation state, the conformational distributions of the MD simulations were calculated as a function of d_1 and d_2 (d_1 : minimum distance between C α atoms of residues 156–165 (TM5) and those of residues 253–262 (TM8); d_2 : minimum distance between C α atoms of residues 139–148 (TM5) and those of residues 270–279 (TM8)). Cyan squares indicate the corresponding distances in the initial conformations (O_o : this study; I_F PDB 4ZOW), and the blue circles indicate the position of the peak in the plot for O_o (E26⁻/D34^p) (Image and legend reproduced from manuscript III).

Discussion:

The structural observations comparing the outward-open and the previously published inward-facing structure show three variable regions within the N- and the C-terminal domains: the hydrophobic core surrounding the TM4 motif-B and around the TM5 motif-C are believed to play an important role in the conformational switching process. TM5 motif-C is observed in a kinked form in the O_o conformation and is prevented to relax to a straight conformation by Tyr127^{TM4} which is on the opposite facet of Met146^{TM5}. While in the I_F state the space occupied by Tyr127^{TM4} is replaced by Met146^{TM5} by untwisting of TM5. Chloramphenicol transport assays demonstrate the significance of these two residues in transport where their respective mutants show no transport.

Molecular dynamics simulation studies were performed on the two critical acidic residues for transport (Glu26^{TM1} and Asp34^{TM1}) on both the conformational states of the transporter as the starting trajectory. Protonation of Asp34^{TM1} in the O_o conformation leads to an occluded state of MdfA with the hydrogen bond preserved between Glu26^{TM1}-Tyr127^{TM4} and TM5 remaining kinked. MD simulations on the I_F state (Arg131 mutated to Gln) without the ligand also leads to an occluded state and a kinked TM5. This implies that the protonation of Asp34^{TM1} in the O_o and apo- I_F state leads to an occluded conformation where the occluded cavity achieved from the both the states are similar. Further, conformational switching from the

SUMMARY OF THE RESULTS AND DISCUSSION

occluded state to the I_F state, may result in the untwisting of the kinked TM5 to a relaxed straight form which may also be achieved by the ligand binding to the I_F state inferred from the ligand bound I_F crystal structures in which the TM5 adapts a straight α -helical conformation.

The absence of structures of ligand bound outward-open, apo inward-open and occluded conformational states precludes from proposing a complete transport cycle for MdfA. The observed structural differences between the O_o state (this study) and the ligand bound I_F state (previously published), molecular dynamics simulations and transport assays lend themselves in proposing a conformational switching mechanism from O_o to the I_F state.

Exposure of the binding cavity of MdfA to low periplasmic pH in the O_o state is likely to protonate Asp34^{TM1}. Changes in the chemical environment around Asp34^{TM1} by protonation or by ligand binding present at the proximity of buried guanidinium moiety Arg112^{TM4} motif-B may reorganize the hydrophobic cluster. Structural rearrangements in the hydrophobic cluster can be associated to the weakening of the charged hydrogen bond between Glu26^{TM1} and Tyr127^{TM4}, where Tyr127^{TM4} is found to be on the same helix TM4 of Arg112^{TM4}. The displacement of Tyr127^{TM4} may allow Met146^{TM5} to occupy its space by the untwisting of kinked TM5 which adopts a straight α -helical conformation in the I_F state. The motif-C present on helix TM5 achieves different conformations (kinked or straight form) which are associated in dictating the conformational states either as O_o or I_F state respectively. The highly conserved TM5 motif-C appears to play a central role in the relative orientations of the two domains and the conformational switching mechanism proposed here may apply to 12 TM helical MFS type-MDR antiporters harbouring the conserved motifs as MdfA.

4 CONCLUSIONS AND FUTURE PERSPECTIVES

This research work reports the strategy undertaken to obtain high-resolution diffracting crystals of wild type MdfA, structural characterization of MdfA and a proposal for the conformational switching mechanism. Selected Fab fragments were complexed with MdfA for their advantages. MdfA and MdfA-Fab complexes were assessed by CPM thermostability assay to identify thermostable variants for crystallization trials. Multiple strategies were employed to crystallize highly stable MdfA variants and optimize their diffraction properties. Fab fragment mediated crystallization of MdfA using the lipidic cubic phase method combined with host lipid screening resulted in crystals with superior diffraction quality. The protocol and results presented in manuscripts I and II may guide in crystallizing other MFS-MDR antiporters and integral membrane proteins in general. Structure determination revealed the antiporter, MdfA to be crystallized in an O_o state with the Fab fragment bound to the cytoplasmic side of the transporter. Comparing the O_o crystal structure with the I_F structure (Heng et al., 2015) allowed to identify the structural differences. The differences show that in the O_o structure that the transmembrane helix (TM) 5 was kinked around motif-C, “APXXGP”, observed only in antiporters and a slight significant expansion of the hydrophobic cluster was observed surrounding Arg112^{TM4} of conserved motif-B, “RXXQG”. Chloramphenicol transport assays were performed by mutating selected residues to demonstrate their involvement in MdfA transport and all of them showed reduce transport activity compared to wildtype indicating their involvement in MdfA function. Molecular dynamics simulations were performed to assess the conformational changes in MdfA by protonating in different combinations of the two critical acidic residues Asp34^{TM1} and Glu26^{TM1} involved in transport. Both the wildtype MdfA (R131Q) apo- I_F structure and O_o conformational state used as starting models in MD simulations showed changed in conformation to an occluded state with TM5 in a kinked form. Our observations from the structural differences, transport assays and molecular simulation data led to propose a proton-activated conformational switching mechanism with the TM5 motif-C playing a key role between the two conformational states.

As many more interesting aspects of MFS-MDR need to be addressed, the immediate questions that arise relevant to the proposed mechanism are mentioned here. MdfA is currently the only MFS-MDR antiporter for which more than one conformational state. It would therefore be important to determine further ligand bound and unbound structures of occluded and inward-open states which might capture the structural variations of TM5 and the N-

CONCLUSIONS AND FUTURE PERSPECTIVES

terminal domain hydrophobic cluster around motif-B respectively. Molecular insights may acknowledge our conclusions and also support in updating the transport cycle of MdfA.

Further, in order to support the proposed mechanism of MdfA with evidence, EPR spectroscopy or smFRET can be probed to calculate spatial separation of the two 6TM bundles by mimicking the acidic residues in MdfA in a protonated state (Asp34^{TM1}Asn, Glu26^{TM1}Gln) or performing the studies in the presence of ligand (Masureel et al., 2013). These studies can be performed by reconstituting MdfA into liposomes in the presence of a pH gradient. EPR or smFRET studies may also be extended to assess the spatial separation of the two bundles in the inward-open conformation, as we suspect that the current ligand bound inward-facing structures binding cavity is not completely open to the periplasm as seen in LacY (Abramson et al., 2003). Inhibitor screening can be performed to identify candidates that abolish transport and MdfA structures solved in complex with inhibitor provide insights into the mechanism of inhibition. This might be crucial for dissecting the differences in substrate and inhibitor recognition pattern of the promiscuous multidrug binding pocket.

These studies on the structure of MdfA in an outward-open conformation have allowed hypothesizing a conformational mechanism in comparison to the inward-facing ligand bound structure. The efflux mechanism described for the MFS-type MDR antiporter MdfA may also be extended to other MFS type-MDR antiporters having similar characteristics to understand their efflux principles.

5 REFERENCES

- Abraham, E. P., & Chain, E. (1940). An enzyme from bacteria able to destroy penicillin. 1940. *Reviews of Infectious Diseases*, 10(4), 677–678.
- Abramson, J., Smirnova, I., Kasho, V., Verner, G., Kaback, H. R., & Iwata, S. (2003). Structure and mechanism of the lactose permease of *Escherichia coli*. *Science*, 301(5633), 610–615.
- Adler, J., & Bibi, E. (2005). Promiscuity in the geometry of electrostatic interactions between the *Escherichia coli* multidrug resistance transporter MdfA and cationic substrates. *Journal of Biological Chemistry*, 280(4), 2721–2729.
- Alegre, K. O., Paul, S., Labarbuta, P., & Law, C. J. (2016). Insight into determinants of substrate binding and transport in a multidrug efflux protein. *Scientific Reports*, 6, 22833.
- Alexandrov, A. I., Mileni, M., Chien, E. Y. T., Hanson, M. A., & Stevens, R. C. (2008). Microscale fluorescent thermal stability assay for membrane proteins. *Structure*, 16(3), 351–359.
- Andersson, M., Bondar, A. N., Freitas, J. A., Tobias, D. J., Kaback, H. R., & White, S. H. (2012). Proton-coupled dynamics in lactose permease. *Structure*, 20(11), 1893–1904.
- Bay, D. C., Rommens, K. L., & Turner, R. J. (2008). Small multidrug resistance proteins: A multidrug transporter family that continues to grow. *Biochimica et Biophysica Acta - Biomembranes*, 1778(9), 1814–1838.
- Bennett, P. M. (2009). Plasmid encoded antibiotic resistance: acquisition and transfer of antibiotic resistance genes in bacteria. *British Journal of Pharmacology*, 153(S1), 347–357.
- Bibi, E., Adler, J., Lewinson, O., & Edgar, R. (2001). MdfA, an interesting model protein for studying multidrug transport. *Journal of Molecular Microbiology and Biotechnology*, 3(2), 171–177.
- Birch, J., Axford, D., Foadi, J., Meyer, A., Eckhardt, A., Thielmann, Y., & Moraes, I. (2018). The fine art of integral membrane protein crystallisation. *Methods*, 147, 150–162.
- Boggavarapu, R., Jeckelmann, J.-M., Harder, D., Ucurum, Z., & Fotiadis, D. (2015). Role of electrostatic interactions for ligand recognition and specificity of peptide transporters. *BMC Biology*, 13(1), 58.
- Bohn, C., & Boulloc, P. (1998). The *Escherichia coli* cmlA gene encodes the multidrug efflux pump Cmr/MdfA and is responsible for isopropyl- β -D-thiogalactopyranoside exclusion and spectinomycin sensitivity. *Journal of Bacteriology*, 180(22), 6072–6075.
- Boland, C., Olatunji, S., Bailey, J., Howe, N., Weichert, D., Fetics, S. K., ... Caffrey, M. (2018). Membrane (and Soluble) Protein Stability and Binding Measurements in the Lipid Cubic Phase Using Label-Free Differential Scanning Fluorimetry. *Analytical Chemistry*, 90(20), 12152–12160.
- Bolla, J. R., Su, C. C., Delmar, J. A., Radhakrishnan, A., Kumar, N., Chou, T. H., ... Yu, E. W. (2015). Crystal structure of the *Alcanivorax borkumensis* YdaH transporter reveals an unusual topology. *Nature Communications*, 6(1), 6874.
- Brown, M. H., Paulsen, I. T., & Skurray, R. A. (1999). The multidrug efflux protein NorM is a prototype of a new family of transporters. *Molecular Microbiology*, 31(1), 394–395.
- Caffrey, M. (2003). Membrane protein crystallization. *Journal of Structural Biology*, 142(1), 108–32.
- Caffrey, M. (2011). Biochemical Society Annual Symposium No . 78 Crystallizing membrane proteins for structure – function studies using lipidic mesophases. *Society*, 725–732.

- Caffrey, M. (2015). A comprehensive review of the lipid cubic phase or in meso method for crystallizing membrane and soluble proteins and complexes. *Acta Crystallographica Section F: Structural Biology Communications*, 71(1), 3–18.
- Chaptal, V., Kwon, S., Sawaya, M. R., Guan, L., Kaback, H. R., & Abramson, J. (2011). Crystal structure of lactose permease in complex with an affinity inactivator yields unique insight into sugar recognition. *Proceedings of the National Academy of Sciences*, 108(23), 9361–9366.
- Chen, Y.-J., Pornillos, O., Lieu, S., Ma, C., Chen, A. P., & Chang, G. (2007). X-ray structure of EmrE supports dual topology model. *Proceedings of the National Academy of Sciences of the United States of America*, 104(48), 18999–9004.
- Coates, A., Hu, Y., Bax, R., & Page, C. (2002). The future challenges facing the development of new antimicrobial drugs. *Nature Reviews Drug Discovery*, 1(11), 895–910.
- Cox, G., & Wright, G. D. (2013). Intrinsic antibiotic resistance: Mechanisms, origins, challenges and solutions. *International Journal of Medical Microbiology*, 303(6–7), 287–292.
- D'Costa, V. M., King, C. E., Kalan, L., Morar, M., Sung, W. W. L., Schwarz, C., ... Wright, G. D. (2011). Antibiotic resistance is ancient. *Nature*, 477(7365), 457–461.
- Dang, S., Sun, L., Huang, Y., Lu, F., Liu, Y., Gong, H., ... Yan, N. (2010). Structure of a fucose transporter in an outward-open conformation. *Nature*, 467(7316), 734–738.
- Davies, J. (1994). Inactivation of antibiotics and the dissemination of resistance genes. *Science*, 264(5157), 375–382.
- Davies, J. (2006). Where have all the antibiotics gone? *Canadian Journal of Infectious Diseases and Medical Microbiology*, 17(5), 287–290.
- Dawson, R. J. P., & Locher, K. P. (2006). Structure of a bacterial multidrug ABC transporter. *Nature*, 443(7108), 180–185.
- De Jesus, M., Jin, J., Guffanti, A. A., & Krulwich, T. A. (2005). Importance of the GP dipeptide of the antiporter motif and other membrane-embedded proline and glycine residues in tetracycline efflux protein Tet(L). *Biochemistry*, 44(38), 12896–12904.
- de Lima Procópio, R. E., da Silva, I. R., Martins, M. K., de Azevedo, J. L., & de Araújo, J. M. (2012). Antibiotics produced by *Streptomyces*. *Brazilian Journal of Infectious Diseases*, 16(5), 466–471.
- Delcour, A. H. (2009). Outer membrane permeability and antibiotic resistance. *Biochimica et Biophysica Acta (BBA) - Proteins and Proteomics*, 1794(5), 808–816.
- Delmar, J. A., & Yu, E. W. (2016). The AbgT family: A novel class of antimetabolite transporters. *Protein Science*, 25(2), 322–337.
- Deng, D., Sun, P., Yan, C., Ke, M., Jiang, X., Xiong, L., ... Yan, N. (2015). Molecular basis of ligand recognition and transport by glucose transporters. *Nature*, 526(7573), 391–396.
- Deng, D., Xu, C., Sun, P., Wu, J., Yan, C., Hu, M., & Yan, N. (2014). Crystal structure of the human glucose transporter GLUT1. *Nature*, 510(7503), 121–125.
- Doki, S., Kato, H. E., Solcan, N., Iwaki, M., Koyama, M., Hattori, M., ... Nureki, O. (2013). Structural basis for dynamic mechanism of proton-coupled symport by the peptide transporter POT. *Proceedings of the National Academy of Sciences of the United States of America*, 110(28), 11343–8.
- Drew, D., Newstead, S., Sonoda, Y., Kim, H., von Heijne, G., & Iwata, S. (2008). GFP-based

- optimization scheme for the overexpression and purification of eukaryotic membrane proteins in *Saccharomyces cerevisiae*. *Nature Protocols*, 3(5), 784–798.
- Drlica, K., Malik, M., Kerns, R. J., & Zhao, X. (2008). Quinolone-mediated bacterial death. *Antimicrobial Agents and Chemotherapy*, 52(2), 385–392.
- Du, D., van Veen, H. W., Murakami, S., Pos, K. M., & Luisi, B. F. (2015). Structure, mechanism and cooperation of bacterial multidrug transporters. *Current Opinion in Structural Biology*, 33, 76–91.
- Du, D., Wang, Z., James, N. R., Voss, J. E., Klimont, E., Ohene-Agyei, T., ... Luisi, B. F. (2014). Structure of the AcrAB–TolC multidrug efflux pump. *Nature*, 509(7501), 512–515.
- Dutta, S., Morrison, E. A., & Henzler-Wildman, K. A. (2014). Blocking dynamics of the SMR transporter EmrE impairs efflux activity. *Biophysical Journal*, 107(3), 613–620.
- Edgar, R., & Bibi, E. (1997). MdfA, an *Escherichia coli* multidrug resistance protein with an extraordinarily broad spectrum of drug recognition. *Journal of Bacteriology*, 179(7), 2274–2280.
- Eicher, T., Seeger, M. A., Anselmi, C., Zhou, W., Brandstätter, L., Verrey, F., ... Pos, K. M. (2014). Coupling of remote alternating-access transport mechanisms for protons and substrates in the multidrug efflux pump AcrB. *ELife*, 3, 22–25.
- Ethayathulla, A. S., Yousef, M. S., Amin, A., Leblanc, G., Kaback, H. R., & Guan, L. (2014). Structure-based mechanism for Na⁺/melibiose symport by MelB. *Nature Communications*, 5(1), 3009.
- Fernandes, P. (2006). Antibacterial discovery and development—the failure of success? *Nature Biotechnology*, 24(12), 1497–1503.
- Fernández, L., Breidenstein, E. B. M., & Hancock, R. E. W. (2011). Creeping baselines and adaptive resistance to antibiotics. *Drug Resistance Updates*, 14(1), 1–21.
- Fleming, A. (1929). On the antibacterial action of cultures of a penicillium, with special reference to their use in the isolation of *B. influenzae*. *British Journal of Experimental Pathology*, 10(3), 226–236.
- Fluman, N., Adler, J., Rotenberg, S. A., Brown, M. H., & Bibi, E. (2014). Export of a single drug molecule in two transport cycles by a multidrug efflux pump. *Nature Communications*, 5, 4615.
- Fluman, N., & Bibi, E. (2009). Bacterial multidrug transport through the lens of the major facilitator superfamily. *Biochimica et Biophysica Acta - Proteins and Proteomics*, 1794(5), 738–747.
- Fluman, N., Cohen-Karni, D., Weiss, T., & Bibi, E. (2009). A promiscuous conformational switch in the secondary multidrug transporter MdfA. *Journal of Biological Chemistry*, 284(47), 32296–32304.
- Fluman, N., Ryan, C. M., Whitelegge, J. P., & Bibi, E. (2012). Dissection of Mechanistic Principles of a Secondary Multidrug Efflux Protein. *Molecular Cell*, 47(5), 777–787.
- Fowler, P. W., Orwick-Rydmark, M., Radestock, S., Solcan, N., Dijkman, P. M., Lyons, J. A., ... Newstead, S. (2015). Gating topology of the proton-coupled oligopeptide symporters. *Structure*, 23(2), 290–301.
- French, G. L. (2010). The continuing crisis in antibiotic resistance. *International Journal of Antimicrobial Agents*, 36(3), 3–7.
- Fukuda, M., Takeda, H., Kato, H. E., Doki, S., Ito, K., Maturana, A. D., ... Nureki, O. (2015). Structural basis for dynamic mechanism of nitrate/nitrite antiport by NarK. *Nature*

Communications, 6(1), 7097.

- Giedraitienė, A., Vitkauskienė, A., Naginienė, R., & Pavilonis, A. (2011). Antibiotic resistance mechanisms of clinically important bacteria. *Medicina (Kaunas, Lithuania)*, 47(3), 137–46.
- Gill, M. J., Simjee, S., Al-Hattawi, K., Robertson, B. D., Easmon, C. S. F., & Ison, C. A. (1998). Gonococcal resistance to beta-lactams and tetracycline involves mutation in loop 3 of the porin encoded at the penB locus. *Antimicrobial Agents and Chemotherapy*, 42(11), 2799–2803.
- Guan, L., Mirza, O., Verner, G., Iwata, S., & Kaback, H. R. (2007). Structural determination of wild-type lactose permease. *Proceedings of the National Academy of Sciences of the United States of America*, 104(39), 15294–15298.
- Guettou, F., Quistgaard, E. M., Raba, M., Moberg, P., Löw, C., & Nordlund, P. (2014). Selectivity mechanism of a bacterial homolog of the human drug-peptide transporters PepT1 and PepT2. *Nature Structural & Molecular Biology*, 21(8), 728–731.
- Hancock, R. E W, & Bell, A. (1988). Antibiotic uptake into gram-negative bacteria. *European Journal of Clinical Microbiology & Infectious Diseases*, 7(6), 713–720.
- Hancock, Robert E W. (1997). The bacterial outer membrane as a drug barrier. *Trends in Microbiology*, 5(1), 37–42.
- Hassan, K. A., Jackson, S. M., Penesyan, A., Patching, S. G., Tetu, S. G., Eijkelkamp, B. A., ... Paulsen, I. T. (2013). Transcriptomic and biochemical analyses identify a family of chlorhexidine efflux proteins. *Proceedings of the National Academy of Sciences*, 110(50), 20254–20259.
- Hassan, K. A., Liu, Q., Elbourne, L. D. H., Ahmad, I., Sharples, D., Naidu, V., ... Paulsen, I. T. (2018). Pacing across the membrane: the novel PACE family of efflux pumps is widespread in Gram-negative pathogens. *Research in Microbiology*, 169(7–8), 450–454.
- Hassan, K. A., Liu, Q., Henderson, P. J. F., & Paulsen, I. T. (2015). Homologs of the *Acinetobacter baumannii* acei transporter represent a new family of bacterial multidrug efflux systems. *MBio*, 6(1), 1–5.
- He, X., Szewczyk, P., Karyakin, A., Evin, M., Hong, W. X., Zhang, Q., & Chang, G. (2010). Structure of a cation-bound multidrug and toxic compound extrusion transporter. *Nature*, 467(7318), 991–994.
- He, Y., Wang, K., & Yan, N. (2014). The recombinant expression systems for structure determination of eukaryotic membrane proteins. *Protein & Cell*, 5(9), 658–672.
- Hegstad, K., Langsrud, S., Lunestad, B. T., Scheie, A. A., Sunde, M., & Yazdankhah, S. P. (2010). Does the Wide Use of Quaternary Ammonium Compounds Enhance the Selection and Spread of Antimicrobial Resistance and Thus Threaten Our Health? *Microbial Drug Resistance*, 16(2), 91–104.
- Heng, J., Zhao, Y., Liu, M., Liu, Y., Fan, J., Wang, X., ... Zhang, X. C. (2015). Substrate-bound structure of the *E. coli* multidrug resistance transporter MdfA. *Cell Research*, 25(9), 1060–1073.
- Higgins, C. F. (2001). ABC transporters: Physiology, structure and mechanism - An overview. *Research in Microbiology*, 152(3–4), 205–210.
- Hino, T., Iwata, S., & Murata, T. (2013). Generation of functional antibodies for mammalian membrane protein crystallography. *Current Opinion in Structural Biology*, 23(4), 563–568.
- Holdsworth, S. R., & Law, C. J. (2013). Multidrug resistance protein MdtM adds to the repertoire of antiporters involved in alkaline pH homeostasis in *Escherichia coli*. *BMC Microbiology*, 13, 113.

- Huang, C.-Y., Olieric, V., Ma, P., Panepucci, E., Diederichs, K., Wang, M., ... IUCr. (2015). *In meso in situ* serial X-ray crystallography of soluble and membrane proteins. *Acta Crystallographica Section D Biological Crystallography*, 71(6), 1238–1256.
- Huang, Y., Lemieux, M. J., Song, J., Auer, M., & Wang, D.-N. (2003). Structure and Mechanism of the Glycerol-3-Phosphate Transporter from *Escherichia coli*. *Science*, 301(5633), 616–620.
- Iancu, C. V., Zmoon, J., Sang, B. W., Aleshin, A., & Choe, J. Y. (2013). Crystal structure of a glucose/H⁺ symporter and its mechanism of action. *Proceedings of the National Academy of Sciences of the United States of America*, 110(44), 17862–17867.
- Jack, D. L., Yang, N. M., & Saier, M. H. (2001). The drug/metabolite transporter superfamily. *European Journal of Biochemistry*, 268(13), 3620–3639.
- Jacob, F. (1977). Evolution and Tinkering. *Science*, 196, 1161–1166.
- Jardetzky, O. (1966). Simple Allosteric Model for Membrane Pumps. *Nature*, 211(5052), 969–970.
- Jessen-Marshall, A. E., Paul, N. J., & Brooker, R. J. (1995). The conserved motif, GXXX(D/E)(R/K)XG[X](R/K)(R/K), in hydrophilic loop 2/3 of the lactose permease. *Journal of Biological Chemistry*, 270(27), 16251–16257.
- Jiang, D., Zhao, Y., Wang, X., Fan, J., Heng, J., Liu, X., ... Zhang, X. C. (2013). Structure of the YajR transporter suggests a transport mechanism based on the conserved motif A. *Proceedings of the National Academy of Sciences*, 110(36), 14664–14669.
- Jiang, X., Smirnova, I., Kasho, V., Wu, J., Hirata, K., Ke, M., ... Kaback, H. R. (2016). Crystal structure of a LacY–nanobody complex in a periplasmic-open conformation. *Proceedings of the National Academy of Sciences*, 113(44), 12420–12425.
- Jin, M. S., Oldham, M. L., Zhang, Q., & Chen, J. (2012). Crystal structure of the multidrug transporter P-glycoprotein from *Caenorhabditis elegans*. *Nature*, 490(7421), 566–569.
- Kapoor, K., Finer-Moore, J. S., Pedersen, B. P., Caboni, L., Waight, A., Hillig, R. C., ... Stroud, R. M. (2016). Mechanism of inhibition of human glucose transporter GLUT1 is conserved between cytochalasin B and phenylalanine amides. *Proceedings of the National Academy of Sciences of the United States of America*, 113(17), 4711–6.
- Kawate, T., & Gouaux, E. (2006). Fluorescence-Detection Size-Exclusion Chromatography for Precrystallization Screening of Integral Membrane Proteins. *Structure*, 14(4), 673–681.
- Keogh, J. P., Hagenbuch, B., Rynn, C., Stieger, B., & Nicholls, G. (2016). Chapter 1 Membrane Transporters: Fundamentals, Function and Their Role in ADME. *Drug Transporters: Volume 1: Role and Importance in ADME and Drug Development*, 1, 3–56.
- King, C. H., Shlaes, D. M., & Dul, M. J. (1983). Infection caused by thymidine-requiring, trimethoprim-resistant bacteria. *Journal of Clinical Microbiology*, 18(1), 79–83.
- Kohanski, M. A., Dwyer, D. J., & Collins, J. J. (2010). How antibiotics kill bacteria: from targets to networks. *Nature Reviews Microbiology*, 8(6), 423–435.
- Kumar, H., Finer-Moore, J. S., Jiang, X., Smirnova, I., Kasho, V., Pardon, E., ... Stroud, R. M. (2018). Crystal Structure of a ligand-bound LacY–Nanobody Complex. *Proceedings of the National Academy of Sciences*, 115(35), 8769–8774.
- Kumar, H., Finer-Moore, J. S., Kaback, H. R., & Stroud, R. M. (2015). Structure of LacY with an α -substituted galactoside: Connecting the binding site to the protonation site. *Proceedings of the National Academy of Sciences*, 112(29), 9004–9009.

- Kumar, H., Kasho, V., Smirnova, I., Finer-Moore, J. S., Kaback, H. R., & Stroud, R. M. (2014). Structure of sugar-bound LacY. *Proceedings of the National Academy of Sciences of the United States of America*, *111*(5), 1784–1788.
- Kwon, S. K., Kim, S. K., Lee, D. H., & Kim, J. F. (2015). Comparative genomics and experimental evolution of *Escherichia coli* BL21(DE3) strains reveal the landscape of toxicity escape from membrane protein overproduction. *Scientific Reports*, *5*, 16076.
- Law, C. J., Maloney, P. C., & Wang, D.-N. (2008). Ins and Outs of Major Facilitator Superfamily Antiporters. *Annual Review of Microbiology*, *62*(1), 289–305.
- Levy, S. B. (2002). Active efflux, a common mechanism for biocide and antibiotic resistance. *Symposium Series (Society for Applied Microbiology)*, (31), 65–71.
- Levy, S. B. (2005). Antibiotic resistance - The problem intensifies. *Advanced Drug Delivery Reviews*, *57*(10), 1446–1450.
- Levy, S. B., & McMurry, L. (1974). Detection of an inducible membrane protein associated with R-factor-mediated tetracycline resistance. *Biochemical and Biophysical Research Communications*, *56*(4), 1060–1068.
- Levy, S. B., & McMurry, L. (1978). Plasmid-determined tetracycline resistance involves new transport systems for tetracycline. *Nature*, *276*(5683), 90–92.
- Lewinson, O., & Bibi, E. (2001). Evidence for simultaneous binding of dissimilar substrates by the *Escherichia coli* multidrug transporter MdfA. *Biochemistry*, *40*(42), 12612–12618.
- Lewinson, O., Adler, J., Poelarends, G. J., Mazurkiewicz, P., Driessen, A. J. M., & Bibi, E. (2003). The *Escherichia coli* multidrug transporter MdfA catalyzes both electrogenic and electroneutral transport reactions. *Proceedings of the National Academy of Sciences of the United States of America*, *100*(4), 1667–72.
- Lewinson, O., Adler, J., Sigal, N., & Bibi, E. (2006). Promiscuity in multidrug recognition and transport: The bacterial MFS Mdr transporters. *Molecular Microbiology*, *61*(2), 277–284.
- Lewinson, O., Padan, E., & Bibi, E. (2004). Alkalitolerance: a biological function for a multidrug transporter in pH homeostasis. *Proceedings of the National Academy of Sciences of the United States of America*, *101*(39), 14073–8.
- Li, X. Z., & Nikaido, H. (2009). Efflux-mediated drug resistance in bacteria: An update. *Drugs*, *69*(12), 1555–1623.
- Lieberman, R. L., Culver, J. A., Entzminger, K. C., Pai, J. C., & Maynard, J. A. (2011). Crystallization chaperone strategies for membrane proteins. *Methods*, *55*(4), 293–302.
- Liu, Y., Ke, M., & Gong, H. (2015). Protonation of Glu¹³⁵ Facilitates the Outward-to-Inward Structural Transition of Fucose Transporter. *Biophysical Journal*, *109*(3), 542–551.
- Livermore, D. M. (1988). Permeation of beta-lactam antibiotics into *Escherichia coli*, *Pseudomonas aeruginosa*, and other gram-negative bacteria. *Reviews of Infectious Diseases*, *10*(4), 691–8.
- Lu, M., Symersky, J., Radchenko, M., Koide, A., Guo, Y., Nie, R., & Koide, S. (2013a). Structures of a Na⁺-coupled, substrate-bound MATE multidrug transporter. *Proceedings of the National Academy of Sciences*, *110*(6), 2099–2104.
- Lu, Min. (2016). Structures of multidrug and toxic compound extrusion transporters and their mechanistic implications. *Channels*, *10*(2), 88–100.

- Lu, Min, Radchenko, M., Symersky, J., Nie, R., & Guo, Y. (2013b). Structural insights into H⁺-coupled multidrug extrusion by a MATE transporter. *Nature Structural & Molecular Biology*, 20(11), 1310–1317.
- Ma, D., Cook, D. N., Alberti, M., Pon, N. G., Nikaido, H., & Hearst, J. E. (1995). Genes *acrA* and *acrB* encode a stress-induced efflux system of *Escherichia coli*. *Molecular Microbiology*, 16(1), 45–55.
- Marger, M. D., & Saier, M. H. (1993). A major superfamily of transmembrane facilitators that catalyze uniport, symport and antiport. *Trends in Biochemical Sciences*, 18(1), 13–20.
- Martínez, J. L., Baquero, F., & Andersson, D. I. (2007). Predicting antibiotic resistance. *Nature Reviews Microbiology*, 5(12), 958–965.
- Martinez Molledo, M., Quistgaard, E. M., Flayhan, A., Pieprzyk, J., & Löw, C. (2018). Multispecific Substrate Recognition in a Proton-Dependent Oligopeptide Transporter. *Structure*, 26(3), 467–476.e4.
- Masureel, M., Martens, C., Stein, R. A., Mishra, S., Ruyschaert, J.-M., Mchaourab, H. S., & Govaerts, C. (2013). Protonation drives the conformational switch in the multidrug transporter LmrP. *Nature Chemical Biology*, 10(2), 149–155.
- Minhas, G. S., Bawdon, D., Herman, R., Rudden, M., Stone, A. P., James, A. G., ... Newstead, S. (2018). Structural basis of malodour precursor transport in the human axilla. *ELife*, 7, 34995.
- Mirza, O., Guan, L., Verner, G., Iwata, S., & Kaback, H. R. (2006). Structural evidence for induced fit and a mechanism for sugar/H⁺ symport in LacY. *The EMBO Journal*, 25(6), 1177–1183.
- Mitchell, P. (1977). Vectorial chemiosmotic processes. *Annual Review of Biochemistry*, 46(1), 996–1005.
- Murakami, S., Nakashima, R., Yamashita, E., Matsumoto, T., & Yamaguchi, A. (2006). Crystal structures of a multidrug transporter reveal a functionally rotating mechanism. *Nature*, 443(7108), 173–179.
- Murakami, S., Nakashima, R., Yamashita, E., & Yamaguchi, A. (2002). Crystal structure of bacterial multidrug efflux transporter AcrB. *Nature*, 419(6907), 587–593.
- Nagamura, R., Fukuda, M., Kawamoto, A., Matoba, K., Dohmae, N., Ishitani, R., ... IUCr. (2019). Structural basis for oligomerization of the prokaryotic peptide transporter PepT. *Acta Crystallographica Section F Structural Biology Communications*, 75(5), 348–358.
- Nagano, K., & Nikaido, H. (2009). Kinetic behavior of the major multidrug efflux pump AcrB of *Escherichia coli*. *Proceedings of the National Academy of Sciences of the United States of America*, 106(14), 5854–5858.
- Nagarathinam, K., Nakada-Nakura, Y., Parthier, C., Terada, T., Juge, N., Jaenecke, F., ... Tanabe, M. (2018). Outward open conformation of a Major Facilitator Superfamily multidrug/H⁺ antiporter provides insights into switching mechanism. *Nature Communications*, 9(1).
- Neu, H. C. (1992). The Crisis in Antibiotic Resistance. *Science*, 257(5073), 1064–1073.
- Neutze, R., Pebay-Peyroula, E., Edman, K., Royant, A., Navarro, J., & Landau, E. M. (2002). Bacteriorhodopsin: A high-resolution structural view of vectorial proton transport. *Biochimica et Biophysica Acta - Biomembranes*, 1565(2), 144–167.
- Newstead, S., Drew, D., Cameron, A. D., Postis, V. L. G., Xia, X., Fowler, P. W., ... Iwata, S. (2011). Crystal structure of a prokaryotic homologue of the mammalian oligopeptide-proton symporters, PepT1 and PepT2. *The EMBO Journal*, 30(2), 417–426.

- Neyfakh, A. A. (1997). Natural functions of bacterial multidrug transporters. *Trends in Microbiology*, 5(8), 309–313.
- Nikaido, H. (1994). Prevention of drug access to bacterial targets: permeability barriers and active efflux. *Science*, 264(5157), 382–388.
- Nikaido, Hiroshi. (2009). Multidrug Resistance in Bacteria. *Annu Rev Biochem.*, (2), 119–146.
- Nishino, K., Nikaido, E., & Yamaguchi, A. (2009). Regulation and physiological function of multidrug efflux pumps in *Escherichia coli* and *Salmonella*. *Biochimica et Biophysica Acta (BBA) - Proteins and Proteomics*, 1794(5), 834–843.
- Nomura, N., Verdon, G., Kang, H. J., Shimamura, T., Nomura, Y., Sonoda, Y., ... Drew, D. (2015). Structure and mechanism of the mammalian fructose transporter GLUT5. *Nature*, 526(7573), 397–401.
- O' Neil, J. (2014). Review on Antibiotic resistance. Antimicrobial Resistance : Tackling a crisis for the health and wealth of nations. *Health and Wealth Nations*.
- Oeppen, J., & Vaupel, J. W. (2002). Demography: Broken limits to life expectancy. *Science*, 296(5570), 1029–1031.
- Parker, J. L., Li, C., Brinth, A., Wang, Z., Vogeley, L., Solcan, N., ... Newstead, S. (2017). Proton movement and coupling in the POT family of peptide transporters. *Proceedings of the National Academy of Sciences of the United States of America*, 114(50), 13182–13187.
- Parker, J. L., & Newstead, S. (2014). Molecular basis of nitrate uptake by the plant nitrate transporter NRT1.1. *Nature*, 507(7490), 68–72.
- Paulsen, I T, Brown, M. H., Littlejohn, T. G., Mitchell, B. A., & Skurray, R. A. (1996). Multidrug resistance proteins QacA and QacB from *Staphylococcus aureus*: membrane topology and identification of residues involved in substrate specificity. *Proceedings of the National Academy of Sciences of the United States of America*, 93(8), 3630–5.
- Paulsen, I T, Brown, M. H., & Skurray, R. A. (1996). Proton-dependent multidrug efflux systems. *Microbiological Reviews*, 60(4), 575–608.
- Paulsen, Ian T., & Skurray, R. A. (1993). Topology, structure and evolution of two families of proteins involved in antibiotic and antiseptic resistance in eukaryotes and prokaryotes - an analysis. *Gene*, 124(1), 1–11.
- Paulsen, Ian T., Skurray, R. A., Tam, R., Saier, M. H., Turner, R. J., Weiner, J. H., ... Grinius, L. L. (1996). The SMR family: A novel family of multidrug efflux proteins involved with the efflux of lipophilic drugs. *Molecular Microbiology*, 19(6), 1167–1175.
- Paulsen, P. A., Custódio, T. F., & Pedersen, B. P. (2019). Crystal structure of the plant symporter STP10 illuminates sugar uptake mechanism in monosaccharide transporter superfamily. *Nature Communications*, 10(1), 407.
- Pedersen, B. P., Kumar, H., Waight, A. B., Risenmay, A. J., Roe-Zurz, Z., Chau, B. H., ... Stroud, R. M. (2013). Crystal structure of a eukaryotic phosphate transporter. *Nature*, 496(7446), 533–536.
- Piddock, L. J. V. (2006a). Multidrug-resistance efflux pumps — not just for resistance. *Nature Reviews Microbiology*, 4(8), 629–636.
- Piddock, L. J. V. (2006b). Clinically Relevant Chromosomally Encoded Multidrug Resistance Efflux Pumps in Bacteria. *Clinical Infectious Diseases: An Official Publication of the Infectious Diseases Society of America*, 19(2), 382–402.

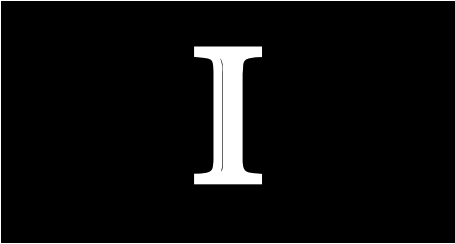
- Poole, K. (2004). Efflux-mediated multiresistance in Gram-negative bacteria. *Clinical Microbiology and Infection*, 10(1), 12–26.
- Poole, K. (2007). Efflux pumps as antimicrobial resistance mechanisms. *Annals of Medicine*, 39(3), 162–176.
- Pos, K. M. (2009). Drug transport mechanism of the AcrB efflux pump. *Biochimica et Biophysica Acta (BBA) - Proteins and Proteomics*, 1794(5), 782–793.
- Prakash, S., Cooper, G., Singhi, S., & Saier, M. H. (2003). The ion transporter superfamily. *Biochimica et Biophysica Acta (BBA) - Biomembranes*, 1618(1), 79–92.
- Putman, M., van Veen, H. W., & Konings, W. N. (2000). Molecular Properties of Bacterial Multidrug Transporters. *Microbiology and Molecular Biology Reviews*, 64(4), 672–693.
- Quistgaard, E. M., Löw, C., Guettou, F., & Nordlund, P. (2016). Understanding transport by the major facilitator superfamily (MFS): structures pave the way. *Nature Reviews Molecular Cell Biology*, 17(2), 123–132.
- Quistgaard, E. M., Löw, C., Moberg, P., Trésaugues, L., & Nordlund, P. (2013). Structural basis for substrate transport in the GLUT-homology family of monosaccharide transporters. *Nature Structural & Molecular Biology*, 20(6), 766–768.
- Saier, Jr, M. H., & Paulsen, I. T. (2001). Phylogeny of multidrug transporters. *Seminars in Cell & Developmental Biology*, 12(3), 205–213.
- Saier, M. H. (2000). A Functional-Phylogenetic Classification System for Transmembrane Solute Transporters. *Microbiology and Molecular Biology Reviews*, 64(2), 354–411.
- Saier, M. H., Beatty, J. T., Goffeau, A., Harley, K. T., Heijne, W. H., Huang, S.-C. C., ... Virk, P. S. (1999). The major facilitator superfamily. *Journal of Molecular Microbiology and Biotechnology*, 1(2), 257–279.
- Santajit, S., & Indrawattana, N. (2016). Mechanisms of Antimicrobial Resistance in ESKAPE Pathogens. *BioMed Research International*, 2016, 1–8.
- Schatz, A., Bugle, E., & Waksman, S. A. (1944). Streptomycin, a Substance Exhibiting Antibiotic Activity Against Gram-Positive and Gram-Negative Bacteria. *Experimental Biology and Medicine*, 55(1), 66–69.
- Schindler, B. D., & Kaatz, G. W. (2016). Multidrug efflux pumps of Gram-positive bacteria. *Drug Resistance Updates*, 27, 1–13.
- Schlegel, S., Klepsch, M., Gialama, D., Wickström, D., Slotboom, D. J., & De Gier, J. W. (2010). Revolutionizing membrane protein overexpression in bacteria. *Microbial Biotechnology*, 3(4), 403–411.
- Seeger, M. A. (2006). Structural Asymmetry of AcrB Trimer Suggests a Peristaltic Pump Mechanism. *Science*, 313(5791), 1295–1298.
- Sengupta, S., Chattopadhyay, M. K., & Grossart, H. P. (2013). The multifaceted roles of antibiotics and antibiotic resistance in nature. *Frontiers in Microbiology*, 4(47), 1–13.
- Sigal, N., Cohen-Karni, D., Siemion, S., & Bibi, E. (2006). MdfA from Escherichia coli, a model protein for studying secondary multidrug transport. *Journal of Molecular Microbiology and Biotechnology*, 11(6), 308–317.
- Sigal, N., Fluman, N., Siemion, S., & Bibi, E. (2009). The secondary multidrug/proton antiporter MdfA

- tolerates displacements of an essential negatively charged side chain. *Journal of Biological Chemistry*, 284(11), 6966–6971.
- Sigal, N., Lewinson, O., Wolf, S. G., & Bibi, E. (2007). E. coli multidrug transporter MdfA is a monomer. *Biochemistry*, 46(17), 5200–5208.
- Sigal, N., Vardy, E., Molshanski-Mor, S., Eitan, A., Pilpel, Y., Schuldiner, S., & Bibi, E. (2005). 3D model of the Escherichia coli multidrug transporter MdfA reveals an essential membrane-embedded positive charge. *Biochemistry*, 44(45), 14870–14880.
- Solcan, N., Kwok, J., Fowler, P. W., Cameron, A. D., Drew, D., Iwata, S., & Newstead, S. (2012). Alternating access mechanism in the POT family of oligopeptide transporters. *The EMBO Journal*, 31(16), 3411–3421.
- Sonoda, Y., Newstead, S., Hu, N. J., Alguel, Y., Nji, E., Beis, K., ... Drew, D. (2011). Benchmarking membrane protein detergent stability for improving throughput of high-resolution x-ray structures. *Structure*, 19(1), 17–25.
- Su, C.-C., Bolla, J. R., Kumar, N., Radhakrishnan, A., Long, F., Delmar, J. A., ... Yu, E. W. (2015). Structure and function of Neisseria gonorrhoeae MtrF illuminates a class of antimetabolite efflux pumps. *Cell Reports*, 11(1), 61–70.
- Sun, Ji, Bankston, J. R., Payandeh, J., Hinds, T. R., Zagotta, W. N., & Zheng, N. (2014). Crystal structure of the plant dual-affinity nitrate transporter NRT1.1. *Nature*, 507(7490), 73–77.
- Sun, Jingjing, Deng, Z., & Yan, A. (2014). Bacterial multidrug efflux pumps: Mechanisms, physiology and pharmacological exploitations. *Biochemical and Biophysical Research Communications*, 453(2), 254–267.
- Sun, L., Zeng, X., Yan, C., Sun, X., Gong, X., Rao, Y., & Yan, N. (2012). Crystal structure of a bacterial homologue of glucose transporters GLUT1–4. *Nature*, 490(7420), 361–366.
- Tal, N., & Schuldiner, S. (2009). A coordinated network of transporters with overlapping specificities provides a robust survival strategy. *Proceedings of the National Academy of Sciences*, 106(22), 9051–9056.
- Tanaka, Y., Hipolito, C. J., Maturana, A. D., Ito, K., Kuroda, T., Higuchi, T., ... Nureki, O. (2013). Structural basis for the drug extrusion mechanism by a MATE multidrug transporter. *Nature*, 496(7444), 247–251.
- Taniguchi, R., Kato, H. E., Font, J., Deshpande, C. N., Wada, M., Ito, K., ... Nureki, O. (2015). Outward- and inward-facing structures of a putative bacterial transition-metal transporter with homology to ferroportin. *Nature Communications*, 6, 8545.
- Tenover, F. C. (2006). Mechanisms of Antimicrobial Resistance in Bacteria. *American Journal of Medicine*, 119(6), 3–10.
- Theodoulou, F. L., & Kerr, I. D. (2015). ABC transporter research: going strong 40 years on. *Biochemical Society Transactions*, 43(5), 1033–1040.
- Tirosh, O., Sigal, N., Gelman, A., Sahar, N., Fluman, N., Siemion, S., & Bibi, E. (2012). Manipulating the drug/proton antiport stoichiometry of the secondary multidrug transporter MdfA. *Proceedings of the National Academy of Sciences*, 109(31), 12473–12478.
- Tommasi, R., Brown, D. G., Walkup, G. K., Manchester, J. I., & Miller, A. A. (2015). ESKAPEing the labyrinth of antibacterial discovery. *Nature Reviews Drug Discovery*, 14(9), 662–662.
- Tumah, H. N. (2009). Bacterial biocide resistance. *Journal of Chemotherapy*, 21(1), 5–15.

- Ubarretxena-Belandia, I., Baldwin, J. M., Schuldiner, S., & Tate, C. G. (2003). Three-dimensional structure of the bacterial multidrug transporter EmrE shows it is an asymmetric homodimer. *EMBO Journal*, 22(23), 6175–6181.
- Van Hoek, A. H. A. M., Mevius, D., Guerra, B., Mullany, P., Roberts, A. P., & Aarts, H. J. M. (2011). Acquired antibiotic resistance genes: An overview. *Frontiers in Microbiology*, 2(203), 1–27.
- Varela, M. F., Sansom, C. E., & Griffith, J. K. (1995). Mutational analysis and molecular modelling of an amino acid sequence motif conserved in antiporters but not in symporters in a transporter superfamily. *Molecular Membrane Biology*, 12(4), 313–319.
- Vargiu, A. V., Collu, F., Schulz, R., Pos, K. M., Zacharias, M., Kleinekathöfer, U., & Ruggerone, P. (2011). Effect of the F610A mutation on substrate extrusion in the AcrB transporter: Explanation and rationale by molecular dynamics simulations. *Journal of the American Chemical Society*, 133(28), 10704–10707.
- Verhalen, B., Dastvan, R., Thangapandian, S., Peskova, Y., Koteiche, H. A., Nakamoto, R. K., ... Mchaourab, H. S. (2017). Energy transduction and alternating access of the mammalian ABC transporter P-glycoprotein. *Nature*, 543(7647), 738–741.
- Wadsten, P., Wöhri, A. B., Snijder, A., Katona, G., Gardiner, A. T., Cogdell, R. J., ... Engström, S. (2006). Lipidic Sponge Phase Crystallization of Membrane Proteins. *Journal of Molecular Biology*, 364(1), 44–53.
- Wang, D., Hu, E., Chen, J., Tao, X., Gutierrez, K., & Qi, Y. (2013). Characterization of novel ybjG and dacC variants in Escherichia coli. *Journal of Medical Microbiology*, 62(11), 1728–1734.
- Wiedenbeck, J., & Cohan, F. M. (2011). Origins of bacterial diversity through horizontal genetic transfer and adaptation to new ecological niches. *FEMS Microbiology Reviews*, 35(5), 957–976.
- Wisedchaisri, G., Park, M.-S., Iadanza, M. G., Zheng, H., & Gonen, T. (2014). Proton-coupled sugar transport in the prototypical major facilitator superfamily protein XyleE. *Nature Communications*, 5(1), 4521.
- Woolridge, D. P., Vazquez-Laslop, N., Markham, P. N., Chevalier, M. S., Gerner, E. W., & Neyfakh, A. A. (1997). Efflux of the natural polyamine spermidine facilitated by the Bacillus subtilis multidrug transporter Blt. *Journal of Biological Chemistry*, 272(14), 8864–8866.
- Wu, H. H., Symersky, J., & Lu, M. (2019). Structure of an engineered multidrug transporter MdfA reveals the molecular basis for substrate recognition. *Communications Biology*, 2(210), 1–12.
- Yaffe, D., Radestock, S., Shuster, Y., Forrest, L. R., & Schuldiner, S. (2013). Identification of molecular hinge points mediating alternating access in the vesicular monoamine transporter VMAT2. *Proceedings of the National Academy of Sciences of the United States of America*, 110(15), 1332–1341.
- Yamaguchi, A., Adachi, K., Akasaka, T., Ono, N., & Sawai, T. (1991). Metal-tetracycline/H⁺ antiporter of Escherichia coli encoded by a transposon Tn10: Histidine 257 plays an essential role in H⁺ translocation. *Journal of Biological Chemistry*, 266(10), 6045–6051.
- Yan, H., Huang, W., Yan, C., Gong, X., Jiang, S., Zhao, Y., ... Shi, Y. (2013). Structure and Mechanism of a Nitrate Transporter. *Cell Reports*, 3(3), 716–723.
- Yan, N. (2015). Structural Biology of the Major Facilitator Superfamily Transporters. *Annual Review of Biophysics*, 44(1), 257–283.
- Yelin, R., & Schuldiner, S. (1995). The pharmacological profile of the vesicular monoamine transporter resembles that of multidrug transporters. *FEBS Letters*, 377(2), 201–207.

- Yerushalmi, H., Lebendiker, M., & Schuldiner, S. (1995). EmrE, an Escherichia coli 12-kDa multidrug transporter, exchanges toxic cations and H⁺ and is soluble in organic solvents. *Journal of Biological Chemistry*, 270(12), 6856–6863.
- Yin, Y. (2006). Structure of the Multidrug Transporter EmrD from Escherichia coli. *Science*, 312(5774), 741–744.
- Yu, E. W., Aires, J. R., & Nikaido, H. (2003). AcrB multidrug efflux pump of Escherichia coli: Composite substrate-binding cavity of exceptional flexibility generates its extremely wide substrate specificity. *Journal of Bacteriology*, 185(19), 5657–5664.
- Zakrzewska, S., Mehdipour, A. R., Malviya, V. N., Nonaka, T., Koepke, J., Muenke, C., ... Michel, H. (2019). Inward-facing conformation of a multidrug resistance MATE family transporter. *Proceedings of the National Academy of Sciences*, 116(25), 12275–12284.
- Zgurskaya, H. I. (2009). Multicomponent drug efflux complexes: architecture and mechanism of assembly. *Future Microbiology*, 4(7), 919–932.
- Zgurskaya, H. I., & Nikaido, H. (2000). Multidrug resistance mechanisms: Drug efflux across two membranes. *Molecular Microbiology*, 37(2), 219–225.
- Zhanel, G. G., Homenuik, K., Nichol, K., Noreddin, A., Vercaigne, L., Embil, J., ... Hoban, D. J. (2004). The Glycylcyclines: A Comparative Review with the Tetracyclines. *Drugs*, 64(1), 63–88.
- Zhang, X. C., Zhao, Y., Heng, J., & Jiang, D. (2015). Energy coupling mechanisms of MFS transporters. *Protein Science*, 24(10), 1560–1579.
- Zhao, Y., Mao, G., Liu, M., Zhang, L., Wang, X., & Zhang, X. C. (2014). Crystal Structure of the E. coli Peptide Transporter YbgH. *Structure*, 22(8), 1152–1160.
- Zheng, H., Wisedchaisri, G., & Gonen, T. (2013). Crystal structure of a nitrate/nitrite exchanger. *Nature*, 497(7451), 647–651.
- Zomot, E., Yardeni, E. H., Vargiu, A. V., Tam, H. K., Mallocci, G., Ramaswamy, V. K., ... Bibi, E. (2018). A New Critical Conformational Determinant of Multidrug Efflux by an MFS Transporter. *Journal of Molecular Biology*, 430(9), 1368–1385.

6 PUBLICATIONS



Generation of Conformation-Specific Antibody Fragments for crystallization of the Multidrug Resistance Transporter MdfA

Abstract

A major hurdle in membrane protein crystallography is generating crystals diffracting sufficiently for structure determination. This is often attributed not only to the difficulty of obtaining functionally active protein in mg amounts but also to the intrinsic flexibility of its multiple conformations. The cocrystallization of membrane proteins with antibody fragments has been reported as an effective approach to improve the diffraction quality of membrane protein crystals by limiting the intrinsic flexibility. Isolating suitable antibody fragments recognizing a single conformation of a native membrane protein is not a straightforward task. However, by a systematic screening approach, the time to obtain suitable antibody fragments and consequently the chance of obtaining diffracting crystals can be reduced. In this chapter, we describe a protocol for the generation of Fab fragments recognizing the native conformation of a major facilitator superfamily (MFS)-type MDR transporter MdfA from *Escherichia coli*. We confirmed that the use of Fab fragments was efficient for stabilization of MdfA and improvement of its crystallization properties

Link to the manuscript I:

<https://pubmed.ncbi.nlm.nih.gov/29177828/>

II



STRUCTURAL BIOLOGY
COMMUNICATIONS

ISSN 2053-230X

The multidrug-resistance transporter MdfA from *Escherichia coli*: crystallization and X-ray diffraction analysis

Kumar Nagarathinam,^{a,b} Frank Jaenecke,^a Yoshiko Nakada-Nakura,^c Yunhon Hotta,^c Kehong Liu,^c So Iwata,^{c,d,e} Milton T. Stubbs,^{a,b} Norimichi Nomura^{c,d} and Mikio Tanabe^{a*†}

Received 15 February 2017

Accepted 7 June 2017

Edited by A. Nakagawa, Osaka University, Japan

† Current and correspondence address: Structural Biology Research Center, Photon Factory, Institute of Materials Structure Science, High Energy Accelerator Research Organization (KEK), 1-1 Oho, Tsukuba, Ibaraki 305-0801, Japan.

Keywords: MFS transporter; multidrug resistance; membrane protein; crystallization; antibody fragment; lipidic cubic phase.

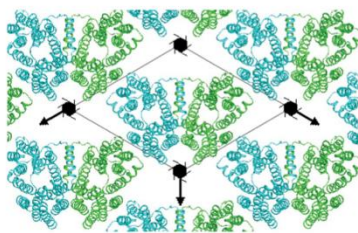
Supporting information: this article has supporting information at journals.iucr.org/f

^aZIK HALOmem, Martin-Luther-Universität Halle-Wittenberg, Kurt-Mothes Strasse 3, 06120 Halle (Saale), Germany, ^bInstitut für Biochemie und Biotechnologie, Martin-Luther-Universität Halle-Wittenberg, Kurt-Mothes Strasse 3, 06120 Halle (Saale), Germany, ^cDepartment of Cell Biology, Graduate School of Medicine, Kyoto University, Konoe-cho, Sakyo-ku, Kyoto 606-8501, Japan, ^dResearch Acceleration Program, Membrane Protein Crystallography Project, Japan Science and Technology Agency, Konoe-cho, Sakyo-ku, Kyoto 606-8501, Japan, and ^eSPring-8 Center, RIKEN, Sayo, Kohto 1-1-1, Hyogo 679-5148, Japan. *Correspondence e-mail: mikio.tanabe@kek.jp

The active efflux of antibiotics by multidrug-resistance (MDR) transporters is a major pathway of drug resistance and complicates the clinical treatment of bacterial infections. MdfA is a member of the major facilitator superfamily (MFS) from *Escherichia coli* and provides resistance to a wide variety of dissimilar toxic compounds, including neutral, cationic and zwitterionic substances. The 12-transmembrane-helix MdfA was expressed as a GFP-octahistidine fusion protein with a TEV protease cleavage site. Following tag removal, MdfA was purified using two chromatographic steps, complexed with a Fab fragment and further purified using size-exclusion chromatography. MdfA and MdfA–Fab complexes were subjected to both vapour-diffusion and lipidic cubic phase (LCP) crystallization techniques. Vapour-diffusion-grown crystals were of type II, with poor diffraction behaviour and weak crystal contacts. LCP lipid screening resulted in type I crystals that diffracted to 3.4 Å resolution and belonged to the hexagonal space group $P6_122$.

1. Introduction

Active efflux by multidrug-resistance (MDR) transporters is a major cause of bacterial resistance to many classes of antibiotics (Nikaido, 2009). MDR transporters can be classified into primary transporters [such as ATP-binding cassette (ABC) transporters] that utilize ATP hydrolysis as an energy source, and secondary transporters, which utilize the energy stored in the transmembrane electrochemical gradient. On the basis of similarities in their sequences, the secondary transporters are further categorized into at least four large superfamilies, including the major facilitator superfamily (MFS), the resistance–nodulation–division (RND) family, the multidrug and toxic compounds extrusion (MATE) family and the small multidrug-resistance (SMR) family (Putman *et al.*, 2000). Proteins belonging to the MFS play a major role in prokaryotic MDR, yet the mechanism of drug transport is not entirely clear. The current accepted paradigm is that MFS transporters utilize a ‘rocker-switch alternating access’ mechanism, whereby the N-terminal and C-terminal six-helix bundles rotate with respect to each other about an axis within the plane of the membrane that passes through the central substrate-binding site. This mechanism requires at least three states: inward open, outward open and a (potentially



© 2017 International Union of Crystallography

research communications

transient) occluded form that may be further divided into inward and outward occluded states (Yan, 2013; Quistgaard *et al.*, 2016).

Sequence analysis of *Escherichia coli* MdfA suggested the presence of 12 transmembrane (TM) helices, a hallmark of the MFS (Edgar & Bibi, 1997; Sigal *et al.*, 2006), which was confirmed by the recent crystal structures of ligand-bound forms of MdfA in the inward-facing state (Heng *et al.*, 2015; Liu *et al.*, 2016). MdfA is capable of coupling the efflux of a number of lipophilic cationic, zwitterionic and neutral substrates to the transmembrane proton (H^+) or ion chemical gradient, allowing it to translocate antibiotics such as chloramphenicol, erythromycin, ethidium, tetraphenylphosphonium and rhodamine (Edgar & Bibi, 1997). A second physiological function of MdfA is found in pH regulation owing to its activity as an $H^+/Na^+,K^+$ antiporter: knockout of MdfA results in bacterial growth restriction under strongly alkaline conditions (Lewinson *et al.*, 2004).

Although MdfA can transport many structurally unrelated compounds, it has been suggested that similar conformations of the transporter are induced by the different permeant substrates (Fluman *et al.*, 2009), implying a common transport mechanism within the framework of the rocker-switch model. Two negatively charged residues located in TM helix 1 (Glu26 and Asp34) have been identified as playing critical roles in substrate and proton transport (Edgar & Bibi, 1999; Fluman *et al.*, 2012). The postulated transport mechanism involves competition between proton and substrate binding at these two acidic residues in the binding cavity of MdfA. Specifically, Asp34 is proposed to be involved in both proton and substrate binding (supported by the chloramphenicol-bound structure; Heng *et al.*, 2015), while protonation of Glu26 is thought to shift the conformation of the transporter from the outward open state to the inward open state; interplay between these two sites is thought to drive transport (Fluman *et al.*, 2012).

For a complete understanding of substrate binding and the transport mechanism, it is essential to identify and visualize additional conformational states of MdfA. Key prerequisites for structural analysis include homogenous and stable MdfA, yet such preparations remain a challenge for membrane proteins, which often suffer from poor expression levels and loss of activity after extraction from their native membranes by detergents. In addition, the resulting detergent micelle surrounding the protein may hamper the protein crystallization process and impact on the diffraction quality of membrane-protein crystals. Co-crystallization of membrane proteins with antibody fragments has been reported to be an effective means of improving the diffraction quality of membrane-protein crystals by limiting intrinsic flexibility. In addition, antibody binding increases the surface area exposed from detergent micelles, which is often thought to be critical for producing crystal contacts (Hino *et al.*, 2013).

Prior to this study, we expressed and purified the MFS-type MDR transporter MdfA from *E. coli* to generate and isolate antibody Fab fragments against MdfA, with a view towards using these as potential crystallization chaperones (Hino *et al.*, 2013). In this way, we were able to identify Fab fragments that

stabilize MdfA as measured using the *N*-[4-(7-diethylamino-4-methyl-3-coumarinyl)phenyl]maleimide (CPM) thermostability assay (Jaenecke *et al.*, 2017). Here, we show that the Fab fragment YN1074 is also able to suppress pH-dependent stability changes in the transporter. The MdfA–YN1074 complex could be crystallized using both hanging-drop vapour-diffusion and lipidic cubic phase (LCP) methods, and we demonstrate that lipid screening has a significant effect on the quality of crystals grown using LCP. The best crystals grew in LCP using the lipid 1-(8*Z*-hexadecenoyl)-*rac*-glycerol (8.8 MAG) and diffracted to a maximum resolution of 3.4 Å.

2. Materials and methods

2.1. Macromolecule production

2.1.1. Materials. All general reagents and materials were purchased from Sigma–Aldrich and Carl Roth, unless otherwise specified. Ni^{2+} -NTA resin was purchased from Qiagen. The detergents *n*-dodecyl- β -*D*-maltopyranoside (DDM), *n*-decyl- β -*D*-maltopyranoside (DM), *n*-nonyl- β -*D*-maltopyranoside (NM) and lauryl maltose neopentyl glycol (LMNG) were obtained from Anatrace (Maumee, Ohio, USA). Monoolein was obtained from Nu-Chek Prep (Elysian, Minnesota, USA) and other MAGs were purchased from Avanti Polar lipids (Alabaster, Alabama, USA). Polyethylene glycols (PEGs) for crystallization were obtained from Molecular Dimensions, whereas other materials for crystallization were obtained from Jena Biosciences, Hampton Research and Rigaku Reagents.

2.1.2. Cloning of MdfA. The *mdfA* gene (NCBI GenBank accession No. AAC73929.1 for *E. coli* K-12 substrain MG1655) was amplified from *E. coli* Top10 cells and cloned upstream of the TEV cleavage-site sequence (TEVcs) of pWaldo-GFPe (Drew *et al.*, 2001) via the XhoI and KpnI restriction sites, allowing expression of the MdfA-(TEVcs)-GFP-His₈ fusion protein. Two nucleotides were introduced between the gene sequences of *mdfA* and the TEVcs by site-directed mutagenesis in order to ensure the correct reading frame, using the oligonucleotides 5'-TCGCACGAAGGGG-GTACCTATGGATCCGAAAACCTGTAC-3' and 5'-GTA-CAGGTTTTTCGGATCCATAGGTACCCCTTCGTGCGA-3'. *E. coli* C43 (DE3) cells were transformed with this plasmid and used for overexpression of the MdfA-(TEVcs)-GFP fusion protein.

2.1.3. MdfA expression and purification. A single colony was inoculated into LB medium containing kanamycin ($75 \mu\text{g ml}^{-1}$) at 37°C overnight. The overnight culture was diluted (1:100; an OD₆₀₀ of approximately ~0.05) in 2× YT medium supplemented with kanamycin and the cells were grown at 37°C to an optical density (OD₆₀₀) of ~0.4. The temperature was decreased to 28°C and expression of the protein was induced by the addition of 0.4 mM IPTG. Cells were harvested 6 h after induction by centrifugation at 5000g for 10 min at 4°C.

The cell pellets were resuspended in 20 mM Tris pH 7.5, 150 mM NaCl, 5 mM EDTA buffer supplemented with

10 $\mu\text{g ml}^{-1}$ DNaseI, 1 mM PMSF and then disrupted by high-pressure homogenization (APV homogenizers). Cell debris was removed by centrifugation at 10 000g for 15 min, and the membrane fraction was collected by ultracentrifugation at 100 000g for 90 min. Isolated membranes were flash-frozen in liquid nitrogen and stored at -80°C . The membrane fraction was solubilized in 150 ml solubilization buffer (25 mM Tris, 200 mM NaCl pH 7.3) containing 1% DDM; the detergents DM, NM and LMNG were also screened, but only DDM yielded a monodisperse peak in SEC. Insoluble material was removed by centrifugation at 100 000g for 1 h and the solubilized fraction was incubated with 10 ml Ni^{2+} beads (batch binding) equilibrated in buffer A (20 mM Tris, 150 mM NaCl, 0.02% DDM pH 7.5) for 2 h. MdfA-GFP was purified by immobilized Ni^{2+} -affinity chromatography, with 0.02% DDM added to all buffers. The resin was washed with five column volumes (CV) of buffer A containing 20 mM imidazole, followed by 12 CV of buffer A containing 50 mM imidazole. MdfA-GFP was eluted with buffer A containing 250 mM imidazole, and fractions were pooled and exchanged with buffer A to reduce the concentration of imidazole (to ~ 10 mM) before treatment with TEV protease.

MdfA-GFP in the presence of a half-molar ratio of hexahistidine (His_6)-tagged TEV protease (Drew *et al.*, 2008) was dialyzed overnight against buffer A supplemented with 1 mM β -mercaptoethanol at 4°C using a 3 kDa molecular-weight cutoff membrane. After dialysis, the sample was passed through 15 ml Ni^{2+} -NTA resin equilibrated in dialysis buffer to separate the resulting MdfA (flowthrough) from the C-terminally His_8 -tagged GFP and the His_6 -tagged TEV protease. The fraction containing MdfA was concentrated and applied onto a Superdex 200 10/300 GL size-exclusion chromatography (SEC) column equilibrated with buffer B (10 mM MES, 20 mM NaCl, 0.02% DDM pH 7.0).

2.1.4. Preparation of Fab fragments. Fab fragments were generated as described previously (Jaenecke *et al.*, 2017; Supplementary Fig. S1) according to established protocols (Day *et al.*, 2007). Briefly, a proteoliposome antigen was prepared by reconstituting purified, functional MdfA at high density into phospholipid vesicles that consisted of a 10:1 mixture of egg phosphatidylcholine (Avanti Polar Lipids) and the adjuvant lipid A (Sigma) to facilitate the immune response. BALB/c mice were immunized with the proteoliposome antigen using three injections at two-week intervals. Antibody-producing hybridoma cell lines were generated using a conventional fusion protocol (Köhler & Milstein, 1975; Pontecorvo, 1976). Hybridoma clones producing antibodies against MdfA were selected by an enzyme-linked immunosorbent assay on immobilized phospholipid vesicles containing purified MdfA (liposome ELISA), allowing positive selection of those antibodies recognizing the native conformation of MdfA. Additional screening for reduced antibody binding to SDS-denatured MdfA was used to select against linear epitope-recognizing antibodies (negative selection). Whole IgG molecules, collected from large-scale culture supernatant of monoclonal hybridomas and purified using protein G affinity chromatography, were digested with papain (Nacalai) and

Fab fragments were isolated using a Superdex 200 gel-filtration column followed by protein A affinity chromatography (Bio-Rad). This procedure resulted in the isolation of four MdfA-specific monoclonal antibodies (YN1006, YN1010, YN1074 and YN1082), the Fab fragments of each of which form a stable complex with the transporter that can be isolated using SEC (Jaenecke *et al.*, 2017).

2.1.5. Preparation of MdfA–Fab fragment YN1074 complexes. Purified MdfA was incubated with Fab fragment YN1074 in a molar ratio of 1:1.5 for 16 h in buffer B prior to SEC. Peak fractions containing MdfA–YN1074 complexes were concentrated to ~ 5 mg ml^{-1} and used for crystallization. In a second set of experiments, the pH of buffer B during both MdfA–Fab complex formation and subsequent SEC and CPM thermostability assays was modified in the range between pH 5.5 and 7.0.

2.1.6. Thermostability assays of MdfA and the MdfA–Fab complex. CPM thermostability analysis was performed as described by Alexandrov *et al.* (2008) with minor modifications. Briefly, 12 μl MdfA or MdfA–Fab complex (2 mg ml^{-1}) was mixed with 45.6 μl buffer B and 2.4 μl CPM dye (at 5 mg ml^{-1}). The reaction mixture was transferred to a clean PCR tube and heated from 25 to 90°C at a rate of $1^{\circ}\text{C min}^{-1}$ in a Rotor Gene Q cyclor (Qiagen). The fluorescence of the dye (excitation and emission wavelengths of 365 and 460 nm, respectively) was monitored during the heating process. Calculation of the first derivative of the melting curve (performed with the *Rotor Gene Q* software v2.1.0) indicates a maximum at the apparent transition temperature/melting temperature T_m of the protein.

2.2. Crystallization

MdfA and the MdfA–YN1074 complex were concentrated to 5 and 2.5 mg ml^{-1} , respectively, using a 100 kDa molecular-weight cutoff Amicon (Millipore) prior to crystallization screening. Crystallization trials using the vapour-diffusion method were performed in 96-well sitting-drop plates using a Cartesian MicroSys NQ crystallization robot (Zinsser Analytic) with commercially available screening matrices (MemPlus and MemGold2 from Molecular Dimensions as well as Wizard I, II, III and IV from Rigaku Reagents). Droplets containing equal volumes of reservoir solution (200 nl) and protein solution (200 nl) were incubated against 70 μl of each reservoir solution at 16°C .

Initial LCP crystallization setups were made by mixing MdfA or the MdfA–YN1074 complex at 2.5, 5 or 10 mg ml^{-1} with monoolein acyl-glycerol (9.9 MAG) in a 2:3 ratio using the two-syringe coupling method (Caffrey & Cherezov, 2009). Protein-containing LCP (100 nl) was dispensed over each well of the Laminex glass plate (Molecular Dimensions) using a LISSYII robot (Zinsser Analytic) and overlaid with 1 μl precipitant solution from commercially available screening matrices (MemGold, MemGold2, MemStart+MemSys and MemMeso from Molecular Dimensions, JBScreen Membrane and JBScreen Pentaerythritol from Jena Bioscience, Crystal Screen HT, MemFac HT and Index HT from Hampton

research communications

Table 1
MdfA production information.

Source organism	<i>E. coli</i>
DNA source	<i>E. coli</i> Top10
Forward primer	AGGAGACTCGAGATGCAAAATAAATTAGCT
Reverse primer	TTTCGGATCCATAGGTACCCCTTCGTGGCGAA
Expression vector	pWaldo-GFPe
Expression host	<i>E. coli</i> C43 (DE3)
Complete amino-acid sequence of the construct produced	MQNKLASGARLGRQALLFPLCLVLYEFSTYIGNN- MIQPGMLAVVEQYQAGIDWVPTSMAYLAGGM- FLQWLLGPLSDRIGRRPVMLAGVWVIVTCLA- ILLAQNIQFTLLRFLQGISLFCFVAVGYAAI- QESFEEAVCIKITALMANVALIAPLLGPLVGA- AWIHVLPWEGMFVLAALAAISFFGLQRAMPE- TATRIGEKLSLKELEGRDYKLVKNGRFVAGAL- ALGFVSLPLLAWIAQSPHIIITGEQLSSVEYG- LLQVPIFGALIAGNLLARLTSRRTVRSLLIIM- GGWPIMIGLLVAAAATVSSHAYLWMTAGLSI- YAFGIGLANAGLVRLTLFASDMSKGTVSAAMG- MLQMLIFTVGIETSKHAWLNGGNLFLNLFNLV- NGILWLSLMVIFLKDQKMGNSHEG

Research and Wizard 1 & 2 from Rigaku Reagents) for initial screening. Subsequently, the MAG lipids were varied for the MdfA–YN1074 complex using lipid mixing ratios of 1:1 [7.7 MAG [1-(7Z-tetradecenyl)-*rac*-glycerol] and 7.8 MAG [1-(7Z-pentadecenyl)-*rac*-glycerol]] and 2:3 [7.9 MAG [1-(7Z-hexadecenyl)-*rac*-glycerol] and 8.8 MAG [1-(8Z-hexadecenyl)-*rac*-glycerol]]. All crystallization trials were performed at 20°C.

2.3. Data collection and processing

Prior to data collection, single crystals of MdfA and the MdfA–YN1074 complex were harvested and flash-cooled directly in liquid nitrogen without additional cryoprotection. All data were collected on beamline PXI (X06SA) at the Swiss Light Source (SLS). For the MdfA and MdfA–YN1074 complex crystals grown using vapour diffusion, diffraction data sets were collected at 100 K using a PILATUS 6M detector, whereas diffraction data for the MdfA–YN1074 complex obtained from LCP were collected using an EIGER 16M detector. Diffraction data were processed and integrated using *XDS* (Kabsch, 2010). Molecular replacement was performed with *Phaser* (McCoy *et al.*, 2007) to analyse crystal packing using the coordinates of MdfA (PDB entry 4zp0; Heng *et al.*, 2015) and, where appropriate, a Fab fragment (PDB entry 1ibg; Jeffrey *et al.*, 1995) as search models (details of the structure solution and analysis will be presented elsewhere). Buried surface areas were calculated using the *PISA* server (Krissinel & Henrick, 2007) and crystallographic figures were prepared using *PyMOL* (Schrödinger).

3. Results and discussion

3.1. Cloning, expression and purification of MdfA

The PCR fragment coding for MdfA was successfully inserted into the XhoI and KpnI sites of pWaldo-GFPe, which was then transformed into *E. coli* C43 (DE3) cells (Table 1). The expression level of MdfA-GFP was monitored by GFP fluorescence emission at 512 nm (excitation wavelength of

488 nm) using an ImageQuant LAS 4000 (GE Healthcare). Following isolation of MdfA-GFP by single-step immobilized metal-affinity chromatography (IMAC), untagged MdfA was obtained *via* TEV cleavage and a subsequent second IMAC step, resulting in >90% purity (Fig. 1). Approximately 0.3–0.4 mg of purified MdfA was routinely obtained from 1 l of 2× YT medium.

3.2. Effect of Fab fragments on MdfA stability

At pH 7.0, the melting curve of MdfA shows an apparent transition temperature T_m of ~58°C in the CPM assay, which is increased by ~4°C in the complexes with Fabs YN1006, YN1010 and YN1082 and by ~12°C in the presence of Fab YN1074 (Jaenecke *et al.*, 2017). The thermostability of purified MdfA and the isolated MdfA–Fab YN1074 complex were

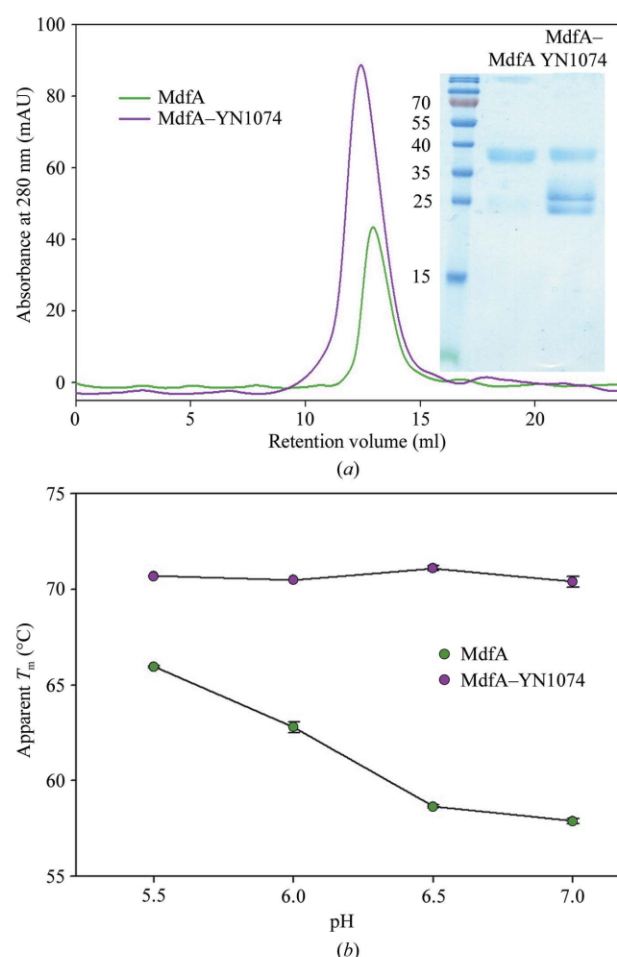


Figure 1
Purification of the MdfA–YN1074 complex and pH-dependent thermostability analyses of MdfA and the MdfA–YN1074 complex. (a) Size-exclusion chromatograms of MdfA (green) and MdfA–YN1074 (purple) on a Superdex 200 10/300 GL size-exclusion column. Inset: SDS-PAGE analysis of the main SEC peaks. (b) Thermostability of MdfA/the MdfA–YN1074 complex as a function of pH was assessed using the CPM thermal denaturation assay. Apparent T_m values for MdfA and the MdfA–YN1074 complex were evaluated from the first derivative of the melting curve.

Table 2
Crystallization of MdfA and MdfA–YN1074.

Protein	MdfA	MdfA–YN1074	MdfA–YN1074
Method	Hanging-drop vapour diffusion	Hanging-drop vapour diffusion	Lipidic cubic phase
Temperature (K)	289	289	293
Protein concentration (mg ml ⁻¹)	5	2.5	2.5
Buffer composition of protein solution	10 mM MES, 20 mM NaCl, 0.02% DDM pH 7.0	10 mM MES, 20 mM NaCl, 0.02% DDM pH 7.0	10 mM MES, 20 mM NaCl, 0.02% DDM pH 7.0
Composition of reservoir solution	100 mM Tris pH 7.5, 100 mM NaCl, 100 mM Li ₂ SO ₄ , 28–30% PEG 400	100 mM HEPES pH 7, 100 mM CdCl ₂ , 100 mM LiCl, 24–28% PEG 400	100 mM ADA pH 6.5, 100 mM NaCl, 100 mM Li ₂ SO ₄ , 32–36% PEG 300
Volume and ratio of drop	2 µl (1:1)	2 µl (1:1)	100 nl
Volume of reservoir	1 ml	1 ml	1 µl

further analysed as a function of pH (Fig. 1*b*). Interestingly, the antiporter exhibits an increased thermostability at lower pH values (T_m of $\sim 66^\circ\text{C}$ at pH 5.5). In contrast, the complex of MdfA with the YN1074 Fab possesses a near-constant T_m of $\sim 71^\circ\text{C}$ at all tested pH values, demonstrating a stabilization of MdfA by the Fab of 5–12°C. The lack of variation of the T_m of the complex with pH suggests that YN1074 stabilizes the low-pH form of the antiporter and that MdfA–YN1074 may be suitable for crystallization screening in a wide range of pH conditions.

3.3. Crystallization of MdfA

In the initial crystallization trials, we used commercially available screening kits with the sitting-drop vapour-diffusion method (Supplementary Fig. S1). Microcrystals of MdfA were observed after 1–2 weeks from a number of conditions containing PEG 400 as the precipitant (*e.g.* 0.1 M MES pH 6.0,

0.2 M Li₂SO₄, 25–30% PEG 400). These conditions were optimized to improve the crystal morphology using the hanging-drop vapour-diffusion method. The largest crystals were obtained in 100 mM Tris pH 7.5, 100 mM NaCl, 100 mM Li₂SO₄, 28–30% PEG 400 (MdfA-VD; Fig. 2*a*, Table 2), which diffracted to resolutions lower than 7 Å (Supplementary Fig. S2*a*). Processing of the diffraction data demonstrated that the MdfA-VD crystal belonged to the hexagonal space group $P6_122$ or $P6_522$, with unit-cell parameters $a = b = 94.5$, $c = 663.1$ Å (Table 3).

In parallel, crystallization conditions for MdfA in complex with the four Fabs were screened using vapour diffusion, and (with the exception of Fab YN1010) crystals were obtained (Supplementary Fig. S1). Nevertheless, the crystals of MdfA–YN1006 and MdfA–YN1082 diffracted poorly, with a maximum resolution of ~ 30 Å. Only those of the MdfA–YN1074 complex, obtained in 100 mM HEPES pH 7, 100 mM CdCl₂, 100 mM LiCl, 24–28% PEG 400 within 3–5 d

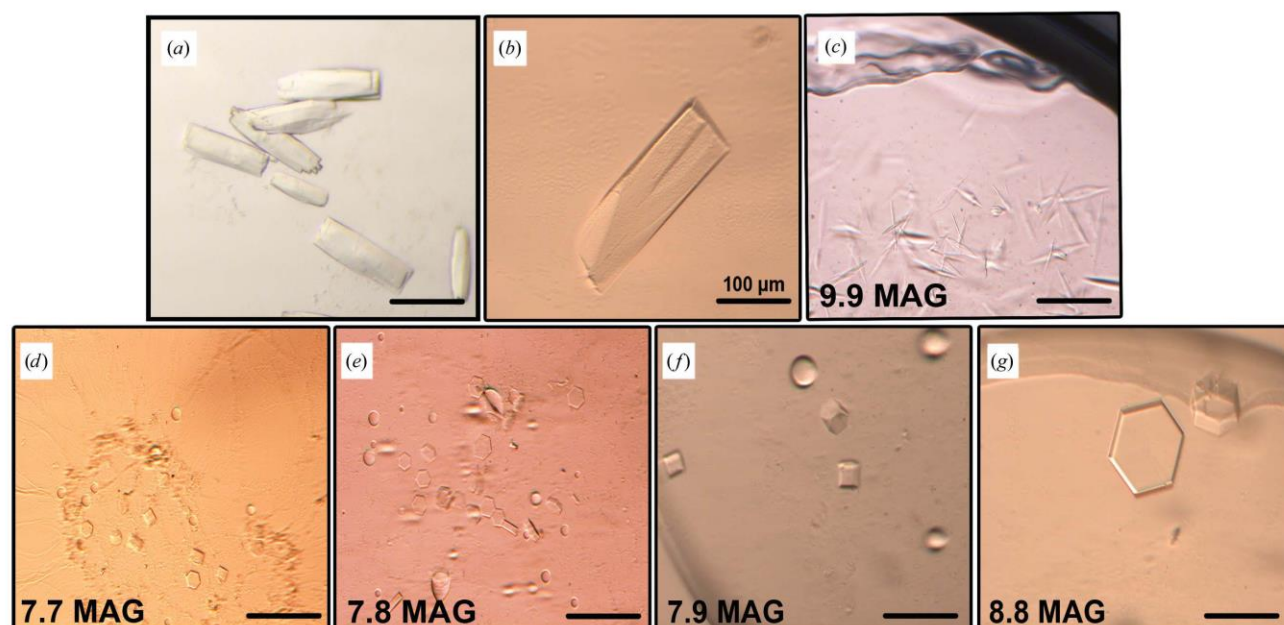


Figure 2
Crystals of MdfA and MdfA–YN1074. Crystals of (a) MdfA and (b) the MdfA–YN1074 complex grown by the hanging-drop vapour-diffusion method, as well as of the MdfA–YN1074 complex grown using the LCP method with various host lipids: (c) 9.9 MAG, (d) 7.7 MAG, (e) 7.8 MAG, (f) 7.9 MAG and (g) 8.8 MAG.

research communications

Table 3

Data collection and processing.

Values in parentheses are for the outer shell.

Protein	MdfA-VD (hanging-drop vapour diffusion)	MdfA-YN1074-VD (hanging-drop vapour diffusion)	MdfA-YN1074-LCP (lipidic cubic phase method)
Diffraction source	PXI (X06SA), SLS	PXI (X06SA), SLS	PXI (X06SA), SLS
Wavelength (Å)	1.000	1.000	1.000
Temperature (K)	100	100	100
Detector	PILATUS 6M	PILATUS 6M	EIGER 16M
Space group	$P6_522$	$P2_12_12_1$	$P6_522$
a, b, c (Å)	94.5, 94.5, 663.1	76.6, 141.6, 296.6	73.2, 73.2, 927.9
α, β, γ (°)	90, 90, 120	90, 90, 90	90, 90, 120
Resolution range (Å)	50–7.82 (8.28–7.82)	50–7.06 (7.48–7.06)	49–3.40 (3.61–3.40)
Total No. of reflections	39028	32684	384466
No. of unique reflections	3376	9469	22224
$CC_{1/2}$ (%)	100 (69.0)	99.9 (76.5)	100 (58.3)
R_{meas} (%)	9.7 (122.2)	6.0 (61.4)	26.2 (172.4)
$\langle I/\sigma(I) \rangle$	9.04 (1.65)	11.49 (2.01)	11.57 (1.59)†
Completeness (%)	99.1 (98.4)	98.3 (94.3)	99.9 (99.9)
Multiplicity	9.97 (9.77)	3.45 (3.44)	17.3 (16.03)
Mosaicity (°)	0.229	0.286	0.097
Solvent content (%)	74.5	71.6	68.1
No. of molecules/complexes per asymmetric unit	2	2	1

† The $\langle I/\sigma(I) \rangle$ falls below 2.0 at 3.4 Å resolution. The resolution cutoff was determined by the $CC_{1/2}$ value (Karplus & Diederichs, 2012), which is 58.3% (our cutoff value is below 50%).

(MdfA-YN1074-VD; Fig. 2*b*, Table 2), diffracted to a maximal resolution between 6 and 7 Å (Supplementary Fig. S2*b*). The MdfA-YN1074-VD crystal belonged to the orthorhombic space group $P2_12_12_1$, with unit-cell parameters $a = 76.6$, $b = 141.6$, $c = 296.6$ Å (Table 3).

The limitations in obtaining diffraction-quality crystals *via* the vapour-diffusion method prompted us to explore the lipidic cubic phase (LCP) technique. The LCP medium is ubiquitously used as an alternative to detergent micelles during the crystallization of membrane proteins (Caffrey, 2015). Needle-shaped crystals of the MdfA-YN1074 complex appeared in LCP using 9.9 MAG (the most frequently used host lipid in initial LCP trials; Caffrey, 2015) in 100 mM Tris pH 7.0, 100 mM NaCl, 100 mM Li_2SO_4 , 40–44% PEG 300 (Fig. 2*c*). These crystals, which belonged to the hexagonal space group $P6_522$ or $P6_522$, with unit-cell parameters $a = b = 73.3$, $c = 950.1$ Å, showed weak diffraction to 8 Å resolution.

We then screened the alkyl-chain length of the host lipid between 14-C and 18-C, which is thought to improve the partitioning of the membrane protein into the lipid and to influence the curvature of the bicontinuous lipidic bilayer to optimize the size of the aqueous channels to accommodate the bound Fab (Li *et al.*, 2013). Selection of lipids was informed empirically by reported membrane-protein structures grown by the LCP method (Caffrey, 2015). Crystallization in 7.7, 7.8 and 7.9 MAG generated small hexagonal crystals (<50 µm) in 100 mM ADA pH 6.5, 100 mM NaCl, 100 mM Li_2SO_4 , 24–26% PEG 300 (7.7 MAG), 100 mM ADA pH 6, 100 mM NaCl, 100 mM Li_2SO_4 , 28–30% PEG 300 (7.8 MAG) or 100 mM ADA pH 6.5, 100 mM NaCl, 100 mM Li_2SO_4 , 32–36% PEG 300 (7.9 MAG) (Figs. 2*d*, 2*e* and 2*f*), yet the diffraction quality remained limited.

Crystals grown in 8.8 MAG as a host lipid appeared within one week in 100 mM ADA pH 6.5, 100 mM NaCl, 100 mM

Li_2SO_4 , 32–36% PEG 300 and matured to full size within between five and seven weeks, when they were harvested (MdfA-YN1074-LCP; Fig. 2*g*, Table 2). The morphology of these larger crystals was hexagonal, and their maximal size was 80–100 µm. These crystals diffracted to a resolution of slightly over 3.0 Å (Supplementary Fig. S2*c*). Owing to the presence of a very long c axis, the crystals were mounted perpendicular to the beam with a slight tilt to best resolve the closely spaced diffraction spots. Anisotropy of the diffraction data restricted the resolution of the data set to 3.4 Å. The MdfA-YN1074-LCP crystal belonged to the hexagonal space group $P6_522$ or $P6_522$, with unit-cell parameters $a = b = 73.2$, $c = 927.9$ Å (*i.e.* related to those obtained using 9.9 MAG but with a 22 Å shorter c axis). Data-collection and processing statistics are summarized in Table 3.

The crystal packing in three of the crystal forms was analysed following molecular replacement (details of the structure solution and analysis will be presented elsewhere). Two MdfA molecules (solvent content of 74.5%) could be located in the asymmetric unit of the MdfA-VD crystal (Fig. 3*a*), two transporter–Fab complexes (solvent content of 71.6%) in that of MdfA-YN1074-VD (Figs. 3*b* and 3*c*) and one complex (solvent content 68.1%) in the asymmetric unit of MdfA-YN1074-LCP (Figs. 3*d* and 3*e*). In each crystal form, individual MdfA molecules associate laterally *via* their trans-membrane regions (although the residues that contact each other differ), with adjacent monomers facing in opposite directions (Fig. 3).

In the MdfA-VD crystal (Fig. 3*a*), hydrophobic TM-helix residues are responsible for most intermolecular contacts, with buried surface areas of 800 Å² between monomers within the asymmetric unit and 614 Å² between crystallographically related monomers. This results in the formation of super-helical ‘chains’ of MdfA molecules with their helix axes parallel to the crystallographic sixfold screw axis. The contacts

between adjacent chains, involving residues from the hydrophilic cytoplasmic and periplasmic surfaces of the transporter, are weak, burying a surface area of only 97 \AA^2 . The large spaces observed between the chains are presumably occupied by detergent micellar structures.

As expected, the intermolecular contacts in the MdfA–YN1074–VD crystal (Figs. 3*b* and 3*c*) are dominated by multiple Fab–Fab interactions, which bury a total surface area of 1179 \AA^2 . This is comparable to that of the MdfA–YN1074 interface (936 \AA^2). Lateral hydrophobic contacts between MdfA molecules are restricted to the interface within the asymmetric unit, with a buried surface area of 707 \AA^2 , whereas crystal contacts between the periplasmic faces of MdfA bury 307 \AA^2 . The complexes are arranged in rippled stacks within the crystals, with inter-stack contacts provided by the Fabs

(Fig. 3*c*). As in the MdfA–VD crystals, the interlayer spaces between MdfA molecules provide space for (presumably disordered) detergent.

In contrast to the type II membrane-protein crystals formed using vapour diffusion, the MdfA–YN1074–LCP crystal is of type I, with the MdfA molecules forming an infinite two-dimensional array as in a membrane, albeit with alternate facing monomers (Figs. 3*d* and 3*e*). Within this two-dimensional layer, two sets of lateral hydrophobic contacts are made, burying 1189 and 768 \AA^2 . Alternate layers are connected by Fab–Fab interactions that bury a total surface area of 900 \AA^2 . The favourable partitioning of intramembrane and hydrophilic contacts observed in the packing of these crystals is presumably responsible for their superior diffraction qualities.

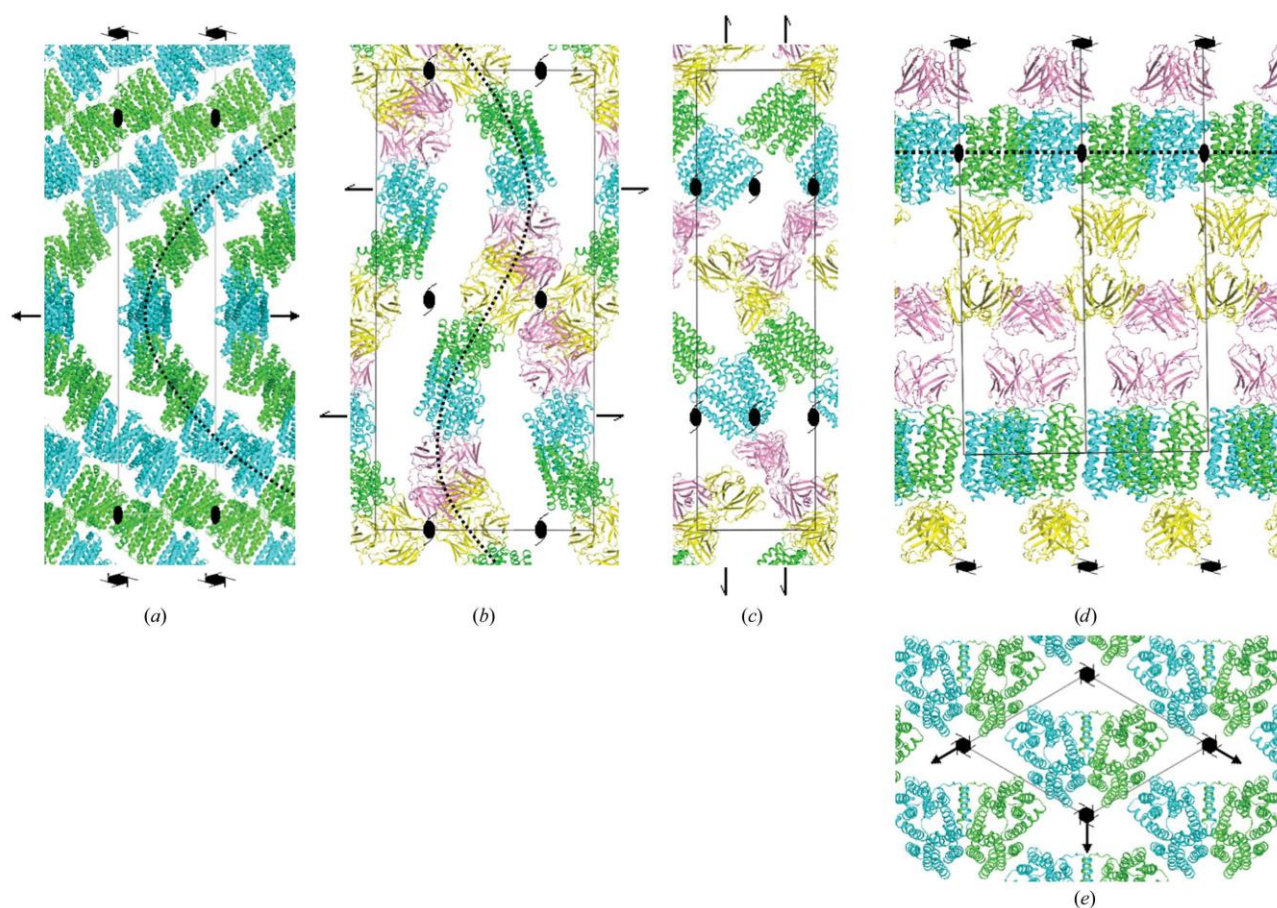


Figure 3

Crystal packing in MdfA crystals. Packing arrangements of (a) the transporter (MdfA–VD), (b, c) the MdfA–YN1074 complex within vapour-diffusion-grown (MdfA–YN1074–VD) crystals and (d, e) the MdfA–YN1074 membrane-protein complex within lipidic cubic phase-grown crystals (MdfA–YN1074–LCP). Selected symmetry-element symbols are shown for orientation. (a) The two MdfA monomers (green, cyan) within the asymmetric unit of MdfA–VD align to form infinite superhelical chains (dotted line) that are stabilized by lateral hydrophobic contacts. Individual chains contact each other *via* a small number of hydrophilic contacts. View parallel to the crystallographic *a* axis. (b) Crystal contacts in MdfA–YN1074–VD are dominated by interactions between the Fabs (yellow, pink) from symmetry-related molecules. Within the lattice, the molecules are arranged in rippled layers (dotted line), with major contacts between the layers provided by the Fabs. The view is parallel to the crystallographic *a* axis. (c) One layer from (b), viewed parallel to the crystallographic *b* axis. (d) In the MdfA–YN1074–LCP crystals, MdfA (green; for clarity, twofold symmetry-related molecules are shown in cyan, although these are crystallographically equivalent) is found in a two-dimensional membrane-like array. MdfA layers sandwich those of the Fab YN1074 (yellow; pink), resulting in a favourable segregation of hydrophobic and hydrophilic crystal contacts. The view is parallel to the crystallographic *a* axis. (e) The MdfA layer from (d), viewed parallel to the crystallographic *c* axis.

research communications

Although the data presented here by no means present a complete picture of the membrane-protein crystallization process, some conclusions may be drawn. Thus, it seems that the lipidic cubic phase facilitates optimal lateral contacts between membrane-protein molecules, supported by the fact that type I crystal formation appears to be typical for crystals obtained in LCP (Caffrey, 2015). In contrast, the arrangements in the vapour-diffusion crystals suggest that masking of the hydrophobic membrane-facing surfaces by detergent molecules prevents such two-dimensional arrangements. Coupled with the need to accommodate bulky disordered detergent micellar structures within the lattice, this results in weak crystal contacts and therefore poor diffraction. As observed previously (Hino *et al.*, 2013), complexation with antibody fragments can (in addition to stabilizing a particular conformation in flexible membrane proteins) increase the likelihood of obtaining three-dimensional crystals. In our case, however, it appears that Fab crystal contacts should be balanced by favourable membrane-protein interactions within the lattice for suitable diffraction properties, as observed in our LCP-grown crystals. Finally, the nature of the host lipid exhibits a pronounced influence both on the morphology and the diffraction quality of the LCP crystals. The fact that we observe a substantial change in the *c* axis for crystals grown using 8.8 MAG and 9.9 MAG suggests that the different lipids influence the two-dimensional packing of the membrane-protein layer and/or the orientation of the MdfA molecules, in turn influencing the positioning of the Fabs and allowing optimization of the crystal packing and diffraction quality.

Structural analyses of MdfA will be presented elsewhere.

Acknowledgements

We thank Martin Caffrey and Dianfan Li for advice concerning the LCP crystallization method, Christoph Parthier for assistance in data reduction and Tina Iverson for critically reading the manuscript. Crystallographic data were collected at the Swiss Light Source (SLS), Villigen with support from the European Community's 7th Framework Programme (FP7/2007-2013) under BioStruct-X (grant agreement No. 283570). The authors declare no conflict of interest.

Funding information

Funding for this research was provided by: Bundesministerium für Bildung und Forschung (BMBF) (ZIK program, award No. FKZ 03Z2HN21 to MT); ERDF (award No. 1241090001 to MTS); the Platform Project for Support in Drug Discovery and Life Science Research (Platform for Drug Discovery, Informatics and Structural Life Science) from the Japan Agency for Medical Research and Development

(AMED) to SI, NN and MT; the ERATO Human Receptor Crystallography Project of the Japan Science and Technology Agency (JST) to SI; the Strategic Basic Research Program, JST to SI and NN; the Research Acceleration Program of the JST to SI and NN; the Targeted Proteins Research Program of the Ministry of Education, Culture, Sports, Science and Technology (MEXT) of Japan to SI; Grants-in-Aids for Scientific Research from the MEXT (award No. 22570114 to NN); BioStruct-X (award Nos. 5450 and 8015 to MT).

References

- Alexandrov, A. I., Mileni, M., Chien, E. Y. T., Hanson, M. A. & Stevens, R. C. (2008). *Structure*, **16**, 351–359.
- Caffrey, M. (2015). *Acta Cryst.* **F71**, 3–18.
- Caffrey, M. & Cherezov, V. (2009). *Nature Protoc.* **4**, 706–731.
- Day, P. W., Rasmussen, S. G. F., Parnot, C., Fung, J. J., Masood, A., Kobilka, T. S., Yao, X.-J., Choi, H.-J., Weis, W. I., Rohrer, D. K. & Kobilka, B. K. (2007). *Nature Methods*, **4**, 927–929.
- Drew, D., Newstead, S., Sonoda, Y., Kim, H., von Heijne, G. & Iwata, S. (2008). *Nature Protoc.* **3**, 784–798.
- Drew, D. E., von Heijne, G., Nordlund, P. & de Gier, J. W. (2001). *FEBS Lett.* **507**, 220–224.
- Edgar, R. & Bibi, E. (1997). *J. Bacteriol.* **179**, 2274–2280.
- Edgar, R. & Bibi, E. (1999). *EMBO J.* **18**, 822–832.
- Fluman, N., Cohen-Karni, D., Weiss, T. & Bibi, E. (2009). *J. Biol. Chem.* **284**, 32296–32304.
- Fluman, N., Ryan, C. M., Whitelegge, J. P. & Bibi, E. (2012). *Mol. Cell*, **47**, 777–787.
- Heng, J., Zhao, Y., Liu, M., Liu, Y., Fan, J., Wang, X., Zhao, Y. & Zhang, X. C. (2015). *Cell Res.* **25**, 1060–1073.
- Hino, T., Iwata, S. & Murata, T. (2013). *Curr. Opin. Struct. Biol.* **23**, 563–568.
- Jaenecke, F., Nakada-Nakura, Y., Nagarathinam, K., Ogasawara, S., Liu, K., Hotta, Y., Iwata, S., Nomura, N. & Tanabe, M. (2017). In the press.
- Jeffrey, P. D., Schildbach, J. F., Chang, C. Y., Kussie, P. H., Margolies, M. N. & Sheriff, S. J. (1995). *J. Mol. Biol.* **248**, 344–360.
- Kabsch, W. (2010). *Acta Cryst.* **D66**, 125–132.
- Karplus, P. A. & Diederichs, K. (2012). *Science*, **336**, 1030–1033.
- Köhler, G. & Milstein, C. (1975). *Nature (London)*, **256**, 495–497.
- Krissinel, E. & Henrick, K. (2007). *J. Mol. Biol.* **372**, 774–797.
- Lewinson, O., Padan, E. & Bibi, E. (2004). *Proc. Natl Acad. Sci. USA*, **101**, 14073–14078.
- Li, D., Shah, S. T. A. & Caffrey, M. (2013). *Cryst. Growth Des.* **13**, 2846–2857.
- Liu, M., Heng, J., Gao, Y. & Wang, X. (2016). *Biophys. Rep.* **2**, 78–85.
- McCoy, A. J., Grosse-Kunstleve, R. W., Adams, P. D., Winn, M. D., Storoni, L. C. & Read, R. J. (2007). *J. Appl. Cryst.* **40**, 658–674.
- Nikaido, H. (2009). *Annu. Rev. Biochem.* **78**, 119–146.
- Pontecorvo, G. (1976). *Birth Defects Orig. Artic. Ser.* **12**, 399–400.
- Putman, M., van Veen, H. W. & Konings, W. N. (2000). *Microbiol. Mol. Biol. Rev.* **64**, 672–693.
- Quistgaard, E. M., Löw, C., Guettou, F. & Nordlund, P. (2016). *Nature Rev. Mol. Cell Biol.* **17**, 123–132.
- Sigal, N., Cohen-Karni, D., Siemion, S. & Bibi, E. (2006). *J. Mol. Microbiol. Biotechnol.* **11**, 308–317.
- Yan, N. (2013). *Trends Biochem. Sci.* **38**, 151–159.



STRUCTURAL BIOLOGY
COMMUNICATIONS

Volume 73 (2017)

Supporting information for article:

Crystallization and X-ray diffraction analysis of the multidrug-resistance transporter MdfA from *Escherichia coli*

Kumar Nagarathinam, Frank Jaenecke, Yoshiko Nakada-Nakura, Yunhon Hotta, Kehong Liu, So Iwata, Milton T Stubbs, Norimichi Nomura and Mikio Tanabe

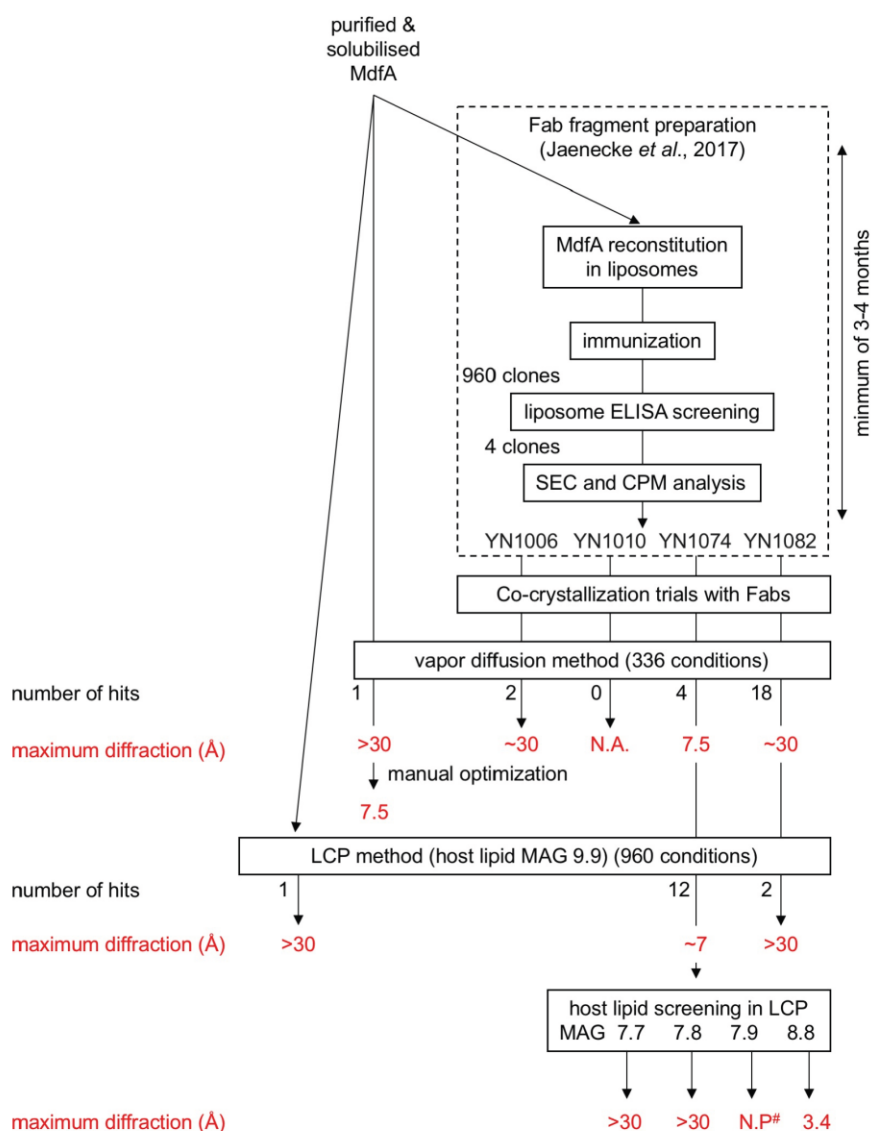


Fig. S1. Flowchart for crystallization of MdfA. The diagram provides a summary of the strategy for generating and optimizing MdfA crystals used in this study. The contribution of Fab for crystallization trials of MdfA were analyzed by 96-well formatted sitting-drop vapor diffusion method. The commercial available screens MemGold2, MemPlus, Wizard I & II, and Wizard III & IV were tested for initial screening for vapor diffusion crystallization trials (336 crystallization conditions in total). MemGold, MemGold2, MemStart & MemSys, MemMeso, JBScreen Membrane, and JBScreen Pentaerythritol, Crystal screen HT, MemFac HT, Index HT and Wizard I & II, were tested for LCP crystallization method (960 crystallization conditions in total). #N.P represents the crystal diffracted more than 7-8 Å (likely 5-6Å) but not processible, because of weak and smear diffraction images.

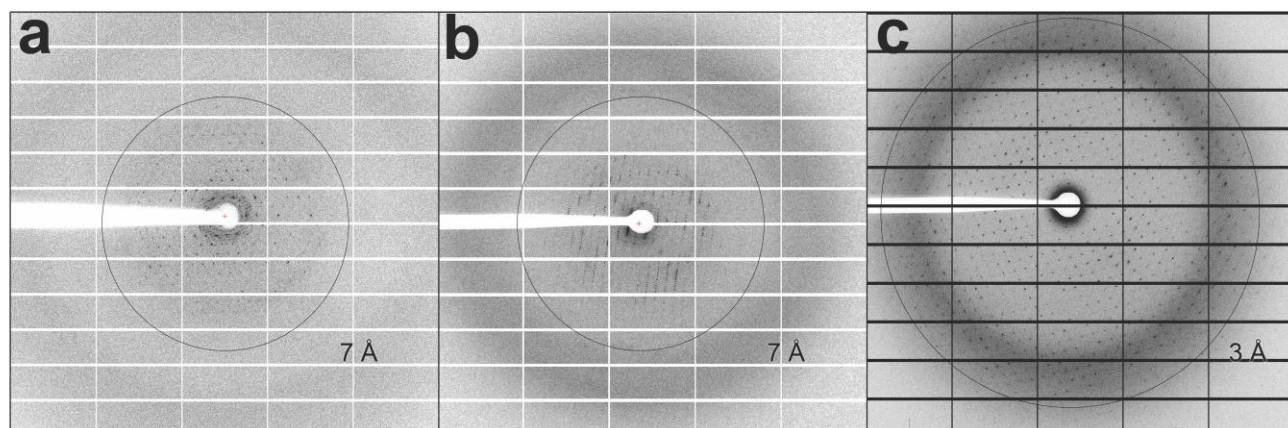


Fig. S2. Representative X-ray diffraction patterns. Diffraction images from crystals of (a) uncomplexed MdfA grown by the vapor diffusion method (**MdfA-VD**), (b) the MdfA-YN1074 complex grown by vapor diffusion (**MdfA-YN1074-VD**) and (c) the MdfA-YN1074 complex using the LCP method with 8.8 MAG (**MdfA-YN1074-LCP**).

III

ARTICLE

DOI: 10.1038/s41467-018-06306-x

OPEN

Outward open conformation of a Major Facilitator Superfamily multidrug/H⁺ antiporter provides insights into switching mechanism

Kumar Nagarathinam^{1,2,9}, Yoshiko Nakada-Nakura³, Christoph Parthier², Tohru Terada⁴, Narinobu Juge⁵, Frank Jaenecke¹, Kehong Liu³, Yunhon Hotta³, Takaaki Miyaji⁵, Hiroshi Omote⁶, So Iwata^{3,7}, Norimichi Nomura³, Milton T. Stubbs^{1,2} & Mikio Tanabe^{1,8}

Multidrug resistance (MDR) poses a major challenge to medicine. A principle cause of MDR is through active efflux by MDR transporters situated in the bacterial membrane. Here we present the crystal structure of the major facilitator superfamily (MFS) drug/H⁺ antiporter MdfA from *Escherichia coli* in an outward open conformation. Comparison with the inward facing (drug binding) state shows that, in addition to the expected change in relative orientations of the N- and C-terminal lobes of the antiporter, the conformation of TM5 is kinked and twisted. In vitro reconstitution experiments demonstrate the importance of selected residues for transport and molecular dynamics simulations are used to gain insights into antiporter switching. With the availability of structures of alternative conformational states, we anticipate that MdfA will serve as a model system for understanding drug efflux in MFS MDR antiporters.

¹ZIK HALOmem, Kurt-Mothes-Straße 3, D-06120 Halle/Saale, Germany. ²Institut für Biochemie und Biotechnologie, Charles-Tanford-Proteinzentrum, Martin-Luther Universität Halle-Wittenberg, Kurt-Mothes-Straße 3a, D-06120 Halle/Saale, Germany. ³Department of Cell Biology, Graduate School of Medicine, Kyoto University, Konoe-cho, Yoshida, Sakyo-ku, Kyoto 606-8501, Japan. ⁴Agricultural Bioinformatics Research Unit, Graduate School of Agricultural and Life Sciences, The University of Tokyo, 1-1-1 Yayoi, Bunkyo-ku, Tokyo 113-8657, Japan. ⁵Advanced Science Research Center, Okayama University, 1-1-1 Kita-ku, Tsushima-naka, Okayama 700-8530, Japan. ⁶Department of Membrane Biochemistry, Okayama University Graduate School of Medicine, Dentistry and Pharmaceutical Sciences, 1-1-1 Kita-ku, Tsushima-naka, Okayama 700-8530, Japan. ⁷RIKEN, SPring-8 Center, 1-1-1 Kouto, Sayo-cho, Sayo-gun, Hyogo 679-5148, Japan. ⁸Structural Biology Research Center, Institute of Materials Structure Science, KEK/High Energy Accelerator Research Organization, 1-1 Oho, Tsukuba, Ibaraki 305-0801, Japan. ⁹Present address: Institute of Virology, Hannover Medical School, Carl-Neuberg-Straße 1, D-30625 Hannover, Germany. Correspondence and requests for materials should be addressed to M.T. (email: mikio.tanabe@kek.jp) or to M.T.S. (email: stubbs@biochemtech.uni-halle.de)

Efflux transport of antibiotics and other potentially harmful compounds from the bacterial cytoplasm by multidrug resistance (MDR) transporters represents an increasing challenge for the treatment of pathogenic bacterial infection^{1–3}. A large number of MDR transporters belong to the Major Facilitator Superfamily (MFS), found in both Gram-positive and -negative organisms^{1,2}. Typical MFS transporters possess 12 transmembrane helices (TMs) divided into two pseudo-symmetrical 6TM N- and C-terminal lobes. Changes in relative orientation of the two lobes within the plane of the bilayer (the rocker-switch mechanism⁴) allow alternating access to the cytoplasmic and extracellular/periplasmic sides of the membrane, facilitating directed transport of substrates across the membrane, with the transporter cycling between outward open (O_o), inward open (I_o) and intermediary occluded states^{5–7}. Despite progress in structural determinations of these states for uniporter and symporter MFS transporters, few such data are available for antiporters.

MdfA, an MFS-MDR transporter from *E. coli* with homologs in many pathogenic bacteria, is an extensively characterized drug/ H^+ antiporter⁸. It transports lipophilic, cationic, and neutral substrates, in each case driven by the proton motive force^{9,10}. Two acidic residues within TM1, Glu26^{TM1} and Asp34^{TM1}, have been implicated in proton (H^+) and substrate transport coupling^{11–13}, and it has been proposed that changes in their protonation could lead to local structural changes within the binding pocket upon H^+ /substrate binding¹¹. The recently reported structure of chloramphenicol-bound MdfA in an inward facing (I_f) conformation¹⁴ reveals the antibiotic bound in the immediate vicinity of Asp34^{TM1}, in line with earlier biochemical data^{12,13}.

In order to gain a complete picture of the efflux mechanism, however, structural data for alternative states are required. Here we report the crystal structure of MdfA in the O_o state and identify conformational changes that accompany transitions between the I_f and O_o states. With the availability of structures of alternative conformational states, we anticipate that MdfA will serve as a model system for understanding drug efflux in MFS MDR antiporters.

Results

Overall structure of MdfA in the outward open (O_o) state. The crystal structure of Fab-bound MdfA presented here reveals the transporter in the outward open (O_o) state, with the N- and C-lobes approaching each other closely at the intracellular face of the transporter (Fig. 1). The N-terminus of TM5 juxtaposes the C-termini of TM8 and TM10 and the N-terminus of TM11 nestles between the C-termini of TM2 and TM4. Access to the transporter cavity from the cytoplasmic face is sealed off by formation of a hydrophobic plug through intercalation of side-chains from each of these helices centered around Phe340^{TM10} (Fig. 2). These contacts are supported by mutually favorable interactions between the side chain of Arg336^{TM10} and the C-terminal dipole of TM4, and Asp77^{TM2} and the N-terminal dipole of TM11. Asp77^{TM2} (from conserved motif A) is in addition part of an electrostatic cluster involving Arg81^{TM3} and Glu132^{TM5}, with an adjacent cluster including Arg78^{TM2} and residues of the intermediate loop (Arg198^{α6–7}) and helix (Asp211^{α6–7}).

In the ligand bound I_f state, in which the two lobes rotate largely as rigid bodies by 33.5° about an axis parallel to the plane of the membrane bilayer, these multiple interactions are replaced by predominantly hydrophobic contacts between the periplasmic halves of TMs 1, 2, and 5 of the N-terminal domain and TMs 7, 8, and 11 of the C-terminal domain. This is effected by a sliding of TM11 along TM2 and a significant rearrangement of TM5 (see below), closing the transporter cavity to the periplasm. The drug binding pocket observed in the I_f state is disrupted in the O_o state through displacement of Ala150^{TM5} and Leu151^{TM5} (see below) as well as lateral movement of C-terminal domain residues from TMs 7 and 8 (Supplementary Fig. 1).

MdfA helix TM5 is kinked and twisted in the O_o state. Superposition of the individual domains of MdfA in the I_f and O_o conformations reveals significant deviations in the N-terminal domain (Supplementary Fig. 2). The largest of these are

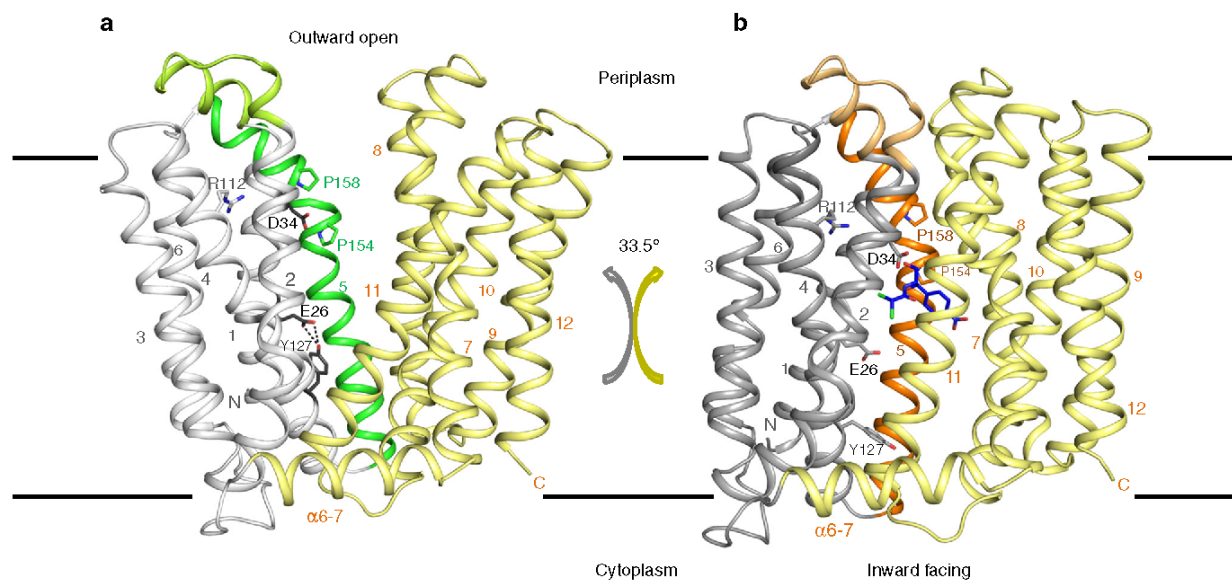


Fig. 1 Overall structure of MdfA in the outward open (O_o) and inward facing (I_f) states. **a** The transporter in the O_o conformation (this work); **b** MdfA in the ligand-bound I_f state (ref. ¹⁴). The N- (white/gray) and C-terminal (yellow) six transmembrane helical domains are shown in ribbon representation, with transmembrane helices (TMs) numbered. Note the difference in relative orientation of the two domains by 33.5° . TM5, whose conformation differs between the two states, is shown in green (O_o) or orange (I_f); the TM1–TM2 termini are in corresponding light colors. The position of chloramphenicol bound in the I_f state is depicted using blue sticks

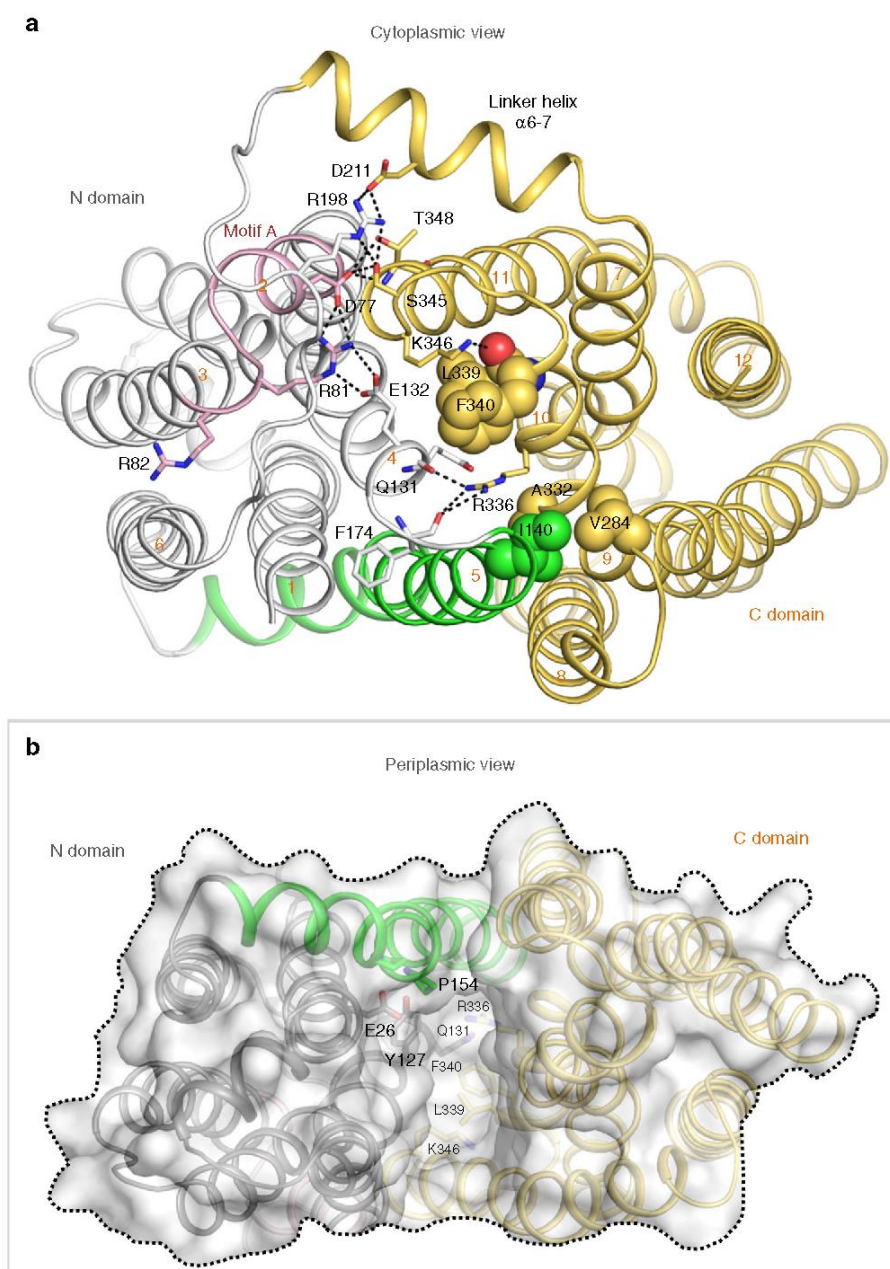


Fig. 2 Cytoplasmic and periplasmic faces of MdfA in the outward open conformation. **a** The cytoplasmic entrance to the ligand-binding pocket is closed in the O_o conformation by numerous interactions between the N- and C-lobes (view obtained by rotating Fig. 1 90° about a horizontal x -axis). The N-terminus of TM5 juxtaposes the C-termini of TM8 and TM10, and the N-terminus of TM11 nestles between the C-termini of TM2 and TM4. Hydrophobic sidechains from each of these helices pack against each other to form a hydrophobic plug that seals off access to the transporter cavity from the cytoplasmic face, supported by additional mutually favorable electrostatic interactions. **b** View from the periplasmic face (following a 180° rotation about a horizontal x -axis), demonstrating the deep cavity between the two domains in the outward open conformation. Dotted line denotes approximate boundary delineated by the bacterial membrane outer leaflet head groups

found in TM5, which ends in the antiporter motif C 153AlaProXaaXaaGlyPro158 that is absent in symporters and uniporters¹⁵. Whereas TM5 in the I_f structure adopts an α -helical conformation of almost ideal geometry up to motif C, residues 136 to 153 in the O_o structure exhibit a profound 15° kink, accompanied by a ca. 45° clockwise twist parallel to the helix axis that terminates with the two-proline-containing motif C (Fig. 3; Supplementary Fig. 3; Supplementary Movie). This results in a

repositioning of the hydrophobic side chains Ile142^{TM5}, Leu145^{TM5}, Met146^{TM5}, and Val149^{TM5} with respect to the N-terminal domain core. Leu145^{TM5}, which in the I_f conformation associates with the N-terminal domain, engages instead with residues of the C-terminal domain in the O_o state. The carboxamide of conserved Asn148^{TM5} is removed from a (presumably hydrophobic) membrane exposed location in the I_f state to form hydrogen bonds with the side chain of Asn272^{TM8} and the main

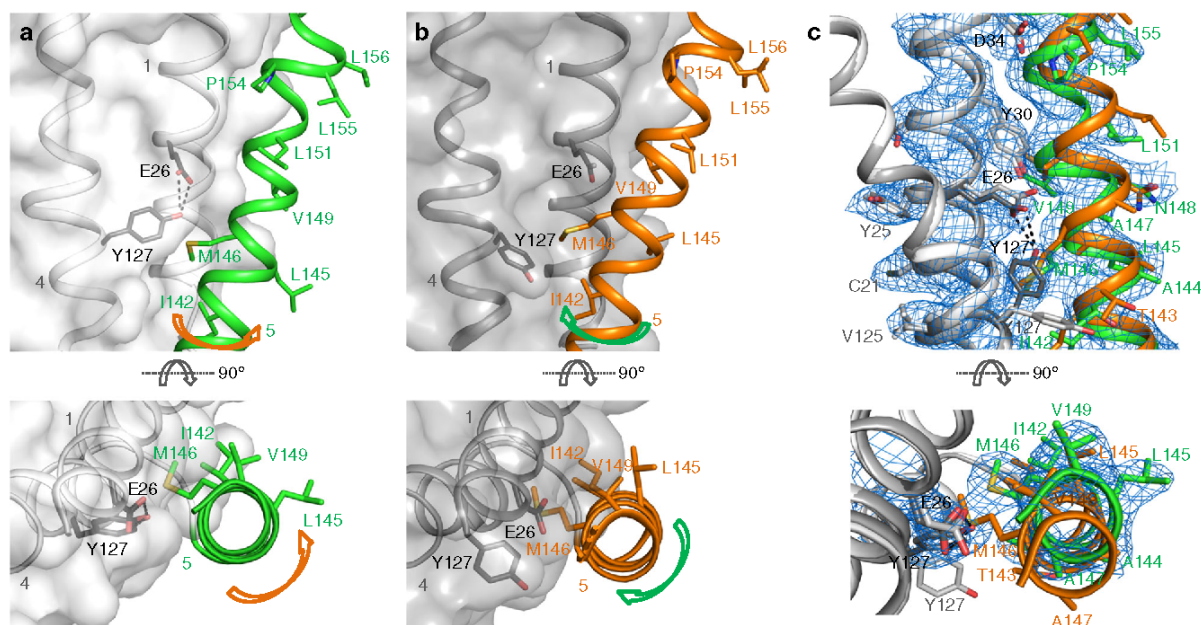


Fig. 3 The O_o and I_f conformations differ by local twisting of TM5. **a** In the O_o state, TM5 (green) in the N-terminal domain is partially distorted, resulting in $C\alpha$ displacements compared to the I_f state of up to 2.9 Å (Met146^{TM5}). The side chain of Met146^{TM5} rests against the phenolic side chain of Tyr127^{TM4}, whose hydroxyl moiety is ca. 2.5 Å from the side chain carboxylate group of Glu26^{TM1}. **b** TM5 adopts an almost ideal α -helical conformation in the I_f state through displacement of the Tyr127^{TM4} side chain by that of Met146^{TM5}. TM5 straightens, rotating around its axis such that its hydrophobic side chains can engage/disengage the C-terminal domain. **c** Electron density for TM5 in the O_o conformation, superimposed with coordinates of the final (green) and initial (orange) models. See also Supplementary Fig. 3 and Supplementary Movie

chain carbonyl of Ile269^{TM8} in the O_o conformation. The largest deviation in TM5 is found at residue Met146^{TM5}, the side chain of which rests against the aromatic moiety of Tyr127^{TM4} in the present structure. In turn, the side chain hydroxyl of Tyr127^{TM4} is found within hydrogen bonding distance (2.5 Å) of the carboxylate of Glu26^{TM1} in the O_o structure. Crucially, the space occupied by the Tyr127^{TM4} side chain in the O_o state is in the I_f structure replaced by that of Met146^{TM5}.

Rearrangements in the N-terminal domain hydrophobic core.

Also of note are small yet significant changes in the region Leu41^{TM1}–Val54^{TM2}, which runs from the C-terminus of TM1 and the N-terminus of TM2 (Supplementary Fig. 4). The side chains of residues Val43^{TM1}, Tyr47^{TM1}, and Trp53^{TM2} form part of a hydrophobic cluster near the periplasmic face of MdfA that includes Met40^{TM1}, Ile105^{TM4}, and Phe108^{TM4} from TM4, and Trp170^{TM6} and Phe174^{TM6} at the N-terminus of TM6. This cluster, which juxtaposes the buried guanidinium moiety of Arg112^{TM4} that is absolutely conserved among MFS homologs (motif B), exhibits a small but significant expansion in the present structure compared to that in the I_f conformation. While the structural differences may appear to be small, we note that the transporter MdfA is stabilized by ligand binding^{14,16}, so that the transporter in the unbound I_o state could well differ from the ligand bound MdfA I_f structures presented by Heng et al.^{14,17}.

In order to test the effect of amino acid substitutions on chloramphenicol transport experimentally, MdfA and its variants were reconstituted in proteoliposomes following procedures described for the chloroquine resistance transporter from *Plasmodium falciparum*¹⁸ (Fig. 4). Purified reconstituted wild-type MdfA was able to transport 50 pmol chloramphenicol (per mg protein per minute), which compares favorably with the 3 pmol $\text{mg}^{-1} \text{min}^{-1}$ determined using crude membrane preparations¹⁹, whereas transport proved unaffected by mutation of

Glu26^{TM1} to Gln, suggesting that the charge state of this residue is not crucial for chloramphenicol transport. The variants Tyr127^{TM4}Phe, Met146^{TM5}Ala, and Trp170^{TM6}Ala of the hydrophobic core all showed significant reductions in transport in the presence of a pH gradient. As expected, chloramphenicol transport was low in the absence of ΔpH , arising from downhill transport due to the initial infinite substrate gradient.

Molecular dynamics simulations. To gain further insights into the transport cycle, molecular dynamics (MD) simulations were performed with all possible combinations of Glu26^{TM1} and Asp34^{TM1} protonation states, starting from either the O_o structure without Fab or the I_f structure without chloramphenicol. Initial trials with the present structure assuming both acidic residues to be deprotonated [O_o (E26⁻/D34⁻)] indicated that the overall structure remained unchanged during the MD simulation. The C-terminal lobe is more rigid than the N-terminal lobe, and the cytoplasmic halves of the TM helices (relative to the center of the lipid bilayer) showed smaller root mean square deviation (RMSD) values than those of the periplasmic halves of the TM helices (Supplementary Table 1)—despite the fact that the Fab binds to the cytoplasmic face of MdfA. We therefore conclude that the outward-open conformation of MdfA is little affected by Fab binding (corroborated by low-resolution data from crystals of MdfA alone²⁰) and is stably maintained in a solvated membrane environment.

To monitor the degree of conformational change, two distances were used to describe the opening and closing of the periplasmic and cytoplasmic sides of the transporter (d_1 and d_2 respectively) (Fig. 5). Starting from the O_o state, the largest divergence from the crystal structure was observed when Asp34^{TM1} was protonated [O_o (E26⁻/D34P) and O_o (E26P/D34P)], resulting in small values of d_1 and d_2 . This state corresponds to an occluded conformation, as both the periplasmic and cytoplasmic entrances

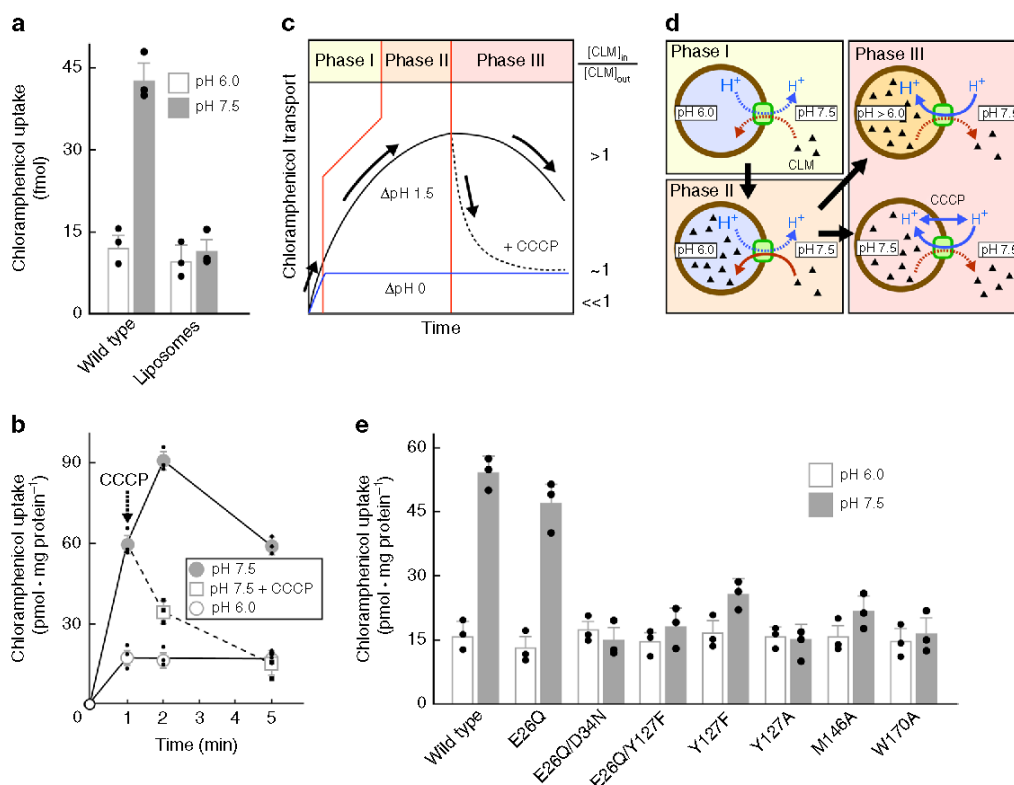


Fig. 4 Chloramphenicol transport by MdfA reconstituted in proteoliposomes. **a** Chloramphenicol transport into reconstituted proteoliposomes is dependent upon the presence of MdfA and a pH gradient. **b** Time course for uptake using reconstituted MdfA. In the absence of a pH gradient (open circles), downhill-like transport (with the substrate gradient) occurs rapidly due to the small volume of the proteoliposomes. In the presence of a pH gradient, however, chloramphenicol uptake (filled circles) involves at least three phases: following a rapid initial downhill transport phase (not visible), uphill accumulation of the substrate in the liposomal lumen against the concentration gradient takes place at the expense of proton export (II). Within a few minutes, the situation is reversed due to lumen acidification, leading to chloramphenicol efflux (phase III). Crucially, collapse of the pH gradient through administration of the H^+ -ionophore CCCP (open squares) results in rapid chloramphenicol efflux (downhill transport) until the luminal concentration reaches that observed in the absence of a pH gradient. **c, d** Schematic diagram illustrating the phases of chloramphenicol (CLM) uptake in the reconstituted system. **e** Uptake by proteoliposomes containing purified MdfA variants in the presence (closed bars) and absence (open bars) of a pH gradient at 1 min. Data are mean values \pm s.d., $n = 3$

are closed. Analysis of the free energy landscape for this transition (Supplementary Fig. 5a) indicates that upon protonation of Asp34^{TM1}, the O_o state is much less stable than the occluded state, suggesting that the transition occurs rapidly and is in effect irreversible. During the simulations, the hydrogen bond between Glu26^{TM1} and Tyr127^{TM4} was for the most part maintained, although the carboxylate at times also hydrogen bonded to Tyr30^{TM1} (Supplementary Fig. 6).

In the occluded state adopted following Asp34^{TM5} protonation, the acidic side chain juxtaposes an internal cavity bounded by the conserved residues Tyr257^{TM8}, Gln261^{TM8} as well as the hydrophobic side chains of Ile239^{TM7} and Phe265^{TM8}; this cavity is also observed in the I_f crystal structure (Supplementary Fig. 7). TM5 is straighter than in the O_o and I_f structures, although it adopts a twisted conformation as in the O_o structure.

Starting from the I_f crystal structure after removal of the ligand and replacement of Arg131^{TM4} by the wild-type Gln, a similar occluded state was obtained during the MD run I_f (E26⁻/D34P). In contrast to the transition from the O_o state, however, the I_f and the occluded states are in a flat free-energy well (Supplementary Fig. 5b), suggesting that these two states can co-exist when Asp34^{TM5} is protonated and that the transition between the I_f state and the occluded state is reversible. As we observed only a one-way transition from the I_f state to the occluded state in the

1 μ s MD simulation, the transition must be slow, presumably due to the complex and rugged nature of the original multi-dimensional energy surface. During this simulation, TM5 twisting was observed due to the close approach of the cytoplasmic halves of TM5 and TM8 (i.e. decreasing d_2), following accommodation of Leu151^{TM5} in the space between Leu268^{TM8} and Ile269^{TM8} (Supplementary Fig. 7). During the simulations where Glu26^{TM1} was protonated [I_f (E26P/D34⁻) and I_f (E26P/D34P)], Tyr127^{TM4} moved toward Glu26^{TM1} (Supplementary Fig. 6).

Discussion

The structure of MdfA presented here reveals features of the O_o conformation and allows comparison with the previously determined ligand bound I_f state¹⁴. Going from the I_f to the O_o state, the N- and C-terminal domains of the transporter reorient in the membrane largely as rigid bodies, with the exception of three regions: (i) transmembrane helix TM5 kinks and twists, (ii) the periplasm-proximal hydrophobic core of the N-terminal domain reorganizes, and (iii) a cytoplasmic loop of the C-terminal domain rearranges to accommodate closure of the cytoplasmic entrance (see Supplementary Movie). The twisting of the helix in the O_o conformation appears to be prevented from transitioning to a straight-form as seen in the I_f state by juxtaposition of the

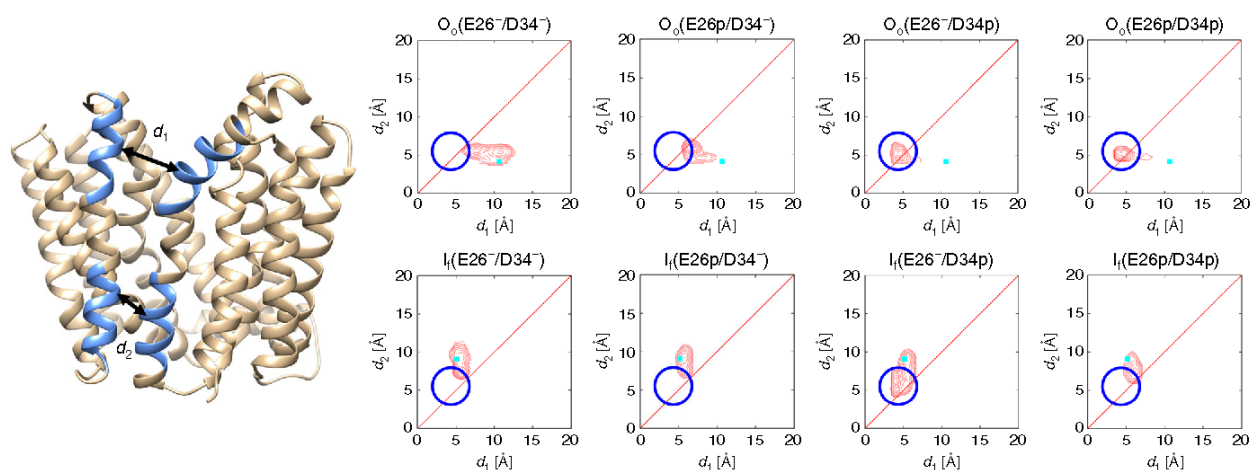


Fig. 5 Conformational distributions of MdfA obtained following MD simulations. Starting from each initial conformation (O_o vs. I_f) and Glu26/Asp34 protonation state, the conformational distributions of the MD simulations were calculated as a function of d_1 and d_2 (d_1 : minimum distance between C α atoms of residues 156–165 (TM5) and those of residues 253–262 (TM8); d_2 : minimum distance between C α atoms of residues 139–148 (TM5) and those of residues 270–279 (TM8)). Cyan squares indicate the corresponding distances in the initial conformations (O_o : this study; I_f : PDB 4ZOW), and the blue circles indicate the position of the peak in the plot for O_o (E26⁻/D34^p)

Tyr127^{TM4} and Met146^{TM5} side chains, with the aromatic side chain hydroxyl of Tyr127^{TM4} held in place by a hydrogen bond to Glu26^{TM1}. Our reconstitution experiments demonstrate the importance of Tyr127^{TM4} and Met146^{TM5} for transport, and suggest that the charge state of Glu26^{TM1} is of little significance for chloramphenicol transport in the presence of a pH gradient, which is consistent with previous results¹⁹. It should be noted that, strictly speaking, the conclusions presented here apply only to chloramphenicol transport (for which structural data of the I_f form are available); whereas we expect them to be generally valid for other neutral MdfA substrates, the situation may differ for other substrates.

To gain further insights into the transport process, we performed MD simulations involving different protonation states of the two acidic residues identified previously as being important in *in vivo* studies^{11,16,21}, Asp34^{TM1} and Glu26^{TM1}. Within the timescale of our simulations, protonation of Asp34^{TM1} through exposure to the low pH periplasmic space leads to an occluded state in which the acidic side chain becomes enclosed in an internal cavity that recapitulates its environment in the I_f conformation. TM5 continues to be twisted in this occluded state and the Glu26^{TM1}–Tyr127^{TM4} hydrogen bond remains intact, although the charge state of Glu26^{TM1} does not appear to play a role in this. Nevertheless, previous *in vivo* studies have shown that Glu26^{TM1} is critical for the transport of cationic substrates^{11,16}, so that the situation may be different for cationic and lipophilic substrates, in which the initial I_f state assumed here might not apply.

MD simulations also demonstrate that an occluded state and a twisted TM5 conformation can be obtained starting from the I_f state. The fact that the transporter is stabilized by ligand binding^{14,16} however means that the I_f structures presented by Heng et al.^{14,17} might not provide an accurate representation of MdfA in the unbound I_o state (moreover, these ligand-bound structures were obtained using a mutated variant Gln131^{TM4}Arg, which has recently been reported to be transport inactive^{22,23}). Thus TM5 untwisting might occur on going from the occluded to the I_o state, or upon ligand binding to form the I_f state.

Recent structure determinations of other transporters^{5–7} indicate that individual helices within each domain can exhibit

significant variability upon conformation switching. For MdfA, the existence of structurally underdetermined I_o and intermediate occluded states (whereby ligand bound and unbound occluded states are likely to be different) thus precludes a detailed description of the complete transport cycle. Nevertheless, the combination of data presented here suggests an important role for the interaction between Glu26^{TM1} and Tyr127^{TM4}. We note that through their common location on helix TM4, the orientation of the Tyr127^{TM4} side chain could couple with the environment of the motif B Arg112^{TM4} side chain. The buried guanidinium moiety is involved in an elaborate hydrogen bonding network involving the even more buried Gln115^{TM4}, the carbonyl carbon of Gly32^{TM1}, and (via a solvent molecule identified in the high-resolution structure¹⁴) Asn33^{TM1} and Asp34^{TM1}. Residues Arg112^{TM4}, Asp34^{TM1}, Gln115^{TM4}, and Gly32^{TM1} have all been shown to be important for MdfA action^{11,14,16,19,24}, and a role of the surrounding hydrophobic cluster is confirmed by the deleterious effect on chloramphenicol transport of the Trp170^{TM6}Ala mutation. Changes in the chemical environment of Asp34^{TM1} (e.g. by ligand binding or changes in protonation) could therefore lead to the observed reorganization of the hydrophobic cluster immediately adjacent to Arg112^{TM4}. In turn, communication of this change through TM4 could influence the orientation of the Tyr127^{TM4} side chain, dictating the position of that of Met146^{TM5} and thereby the degree of TM5 twist. Releasing the twist of TM5 from the O_o to the I_f conformation would result in a repositioning of the hydrophobic side chains Ile142^{TM5}, Leu145^{TM5}, Met146^{TM5}, and Val149^{TM5} with respect to the N-terminal domain core, allowing Leu145^{TM5} to dissociate from the N-terminal domain to engage the C-terminal domain.

Support is provided by MdfA rescue mutants. Selection for drug transport rescue in cells harboring the otherwise inactive TM1 variants Glu26^{TM1}Thr/Asp34^{TM1}Met and Glu26^{TM1}Thr resulted in the detection of mutants containing the acidic side chains Ala150^{TM5}Glu and Val335^{TM10}Glu^{11,25}. These residues would be well positioned to make hydrogen bonds to Tyr127^{TM4} in the outward open structure (Supplementary Fig. 8). Recent thermodynamic calculations and molecular dynamic simulations have led in principle to similar conclusions for the L-fucose/H⁺ symporter FucP²⁶. Using computational methods, it was

Table 1 Data collection and refinement statistics

	MdfA-Fab YN1074
Data collection	
Space group	P6 ₁ 22
Cell dimensions	
<i>a</i> , <i>b</i> , <i>c</i> (Å)	73.26, 73.26, 927.92
α , β , γ (°)	90.00, 90.00, 120.00
Resolution (Å)	49–3.4 (3.61–3.4) ^a
<i>R</i> _{sym} or <i>R</i> _{merge}	25.4 (166.9)
<i>I</i> / σ <i>I</i>	11.57 (1.59)
Completeness (%)	99.9 (99.9)
Redundancy	17.3 (16.03)
Refinement	
Resolution (Å)	49–3.4
No. of reflections	22216
<i>R</i> _{work} / <i>R</i> _{free}	25.8/28.3
No. of atoms	
Protein	6,134
Ion	5
<i>B</i> -factors (Å ²)	
Protein	113.3
Ion	136.8
R.m.s. deviations	
Bond lengths (Å)	0.003
Bond angles (°)	0.596

^aValues in parentheses are for highest-resolution shell

proposed that protonation of FucP Glu135^{TM4} in TM4 allows surmounting of a ca. 2 kcal mol⁻¹ energy barrier between the inward and outward open states. An intermediate state in which TM11 is distorted is postulated, although a causative link between Glu135^{TM4} (de)protonation and TM11 distortion has not been described. Inspection of the FucP structure²⁷ suggests that Glu135^{TM4} could form a hydrogen bond with Tyr365^{TM10} of C-terminal domain TM10 (Supplementary Fig. 8). Interestingly, C-terminal domain TM11 is the counterpart of TM5 in the (inverted topology) N-terminal domain²⁸, reflecting the pseudo-symmetry of the two domains, so that the antiporter MdfA and symporter FucP might be thought of as examples of repeat swapping to yield similar transport mechanisms.

The presence of the MFS-antiporter motif C would appear to be central to transporter switching—restricting the twist of TM5 to a small localized helical segment to facilitate relative rotation of the two domains, and transmitting these perturbations to an adjacent pliable hydrophobic cluster. As other structurally well-characterized antiporter families (such as the amino acid/polyamine/organocation (APC) transporter superfamily²⁹ and cation/H⁺ antiporter family³⁰) have been shown to utilize other mechanisms, this may be a property specific to MFS-antiporters. The O_o structure presented here could serve as a template for the design of novel MFS inhibitors that are able to access their target directly from the bacterial exterior.

Methods

Crystal structure solution. Isolation of Fab fragments that recognize native conformations of MdfA in proteoliposomes has been described elsewhere³¹. Crystals of MdfA in complex with Fab fragments grew in the lipidic cubic phase and diffracted to 3.4 Å resolution^{30,31}. Diffraction data were collected at 100 K at a wavelength of 1.0 Å on the SLS beamline PXI (X06SA) using the 16M Eiger detector. In order to resolve the very long *c*-axis (929 Å), the crystal was mounted so that the rotation axis was ca. 30° to the crystallographic *c*-axis. The synchrotron beam (with beam size increased from 10 to 100 μm) was defocused from the crystal to the detector. Data sets (180° in 0.1° steps) were processed using the program XDS³². The crystal belongs to the space group P6₁22 with one complex in the asymmetric unit. Phases were determined by molecular replacement with PHASER MR³³ using the separated N- and C-lobes of MdfA in the inward open conformation (PDBID: 4ZP0)¹⁴ and an Fab fragment (PDBID: 1IBG)³⁴ as individual

search models. The replacement model was rebuilt manually using COOT³⁵ and refined using PHENIX³⁶ with TLS refinement (three groups per polypeptide chain) to an *R*_{free} value of 28.3%. The final model consists of MdfA residues Gln14–Lys400, Fab heavy chain residues Leu4–Pro216, and Fab light chain residues Asp1–Arg211, as well as one sulfate ion. Ramachandran analysis demonstrates that 94.4% of the residues are in the favorable regions and 5.5% in the allowed regions. One residue (Ser65 in the Fab fragment heavy chain) was in the outlier regions. Atoms for difference density corresponding to solvent molecules, lipids, and/or detergents were not added to the model in accordance with the low resolution of the data. The Fab binds to the cytoplasmic side of MdfA, where it may stabilize the outward open state and enhances crystal contacts²⁰. Data collection and refinement statistics are given in Table 1. RMSDs in Ca in positions between O_o and I_f states (Supplementary Fig. 2) were calculated as a function of residue number after separate superposition of the N- and C-terminal domains using the programme LSQKAB from the CCP4 suite³⁷. The kink of α -helix TM5 was calculated using Kink Finder³⁸. Figures and movies were prepared using PyMOL (Schrödinger, LLC).

Reconstitution of MdfA. MdfA mutants were generated using a PCR site-directed mutagenesis kit (Agilent) with the primers listed in the Supplementary Table 2, and purified as for wild-type MdfA. Forty micrograms of purified wild type or mutant MdfA was mixed with 500 μg of azolectin liposomes (Sigma type IIS), frozen at 193 K for at least 10 min¹⁸. The mixture was thawed quickly by holding the sample tube in the hand and diluted 60-fold with reconstitution buffer containing 20 mM MES-NaOH (pH 6.0), 0.1 M sodium chloride, 5 mM magnesium chloride. Reconstituted proteoliposomes were pelleted by centrifugation at 200,000 × *g* at 277 K for 1 h, and suspended in 0.2 mL of same buffer.

Transport assay. The transport assay mixture (0.2 mL) containing 20 mM MOPS-Tris (pH 7.5) or 20 mM MES-NaOH (pH 6.0), 0.1 M sodium chloride, 5 mM magnesium chloride, and 2 μM [ring-3,5-³H] chloramphenicol (0.5 MBq μmol⁻¹, PerkinElmer) was incubated at 300 K for 3 min. Proteoliposomes containing MdfA (0.5 μg protein per assay) (or liposomes as control) were added to the mixture to initiate transport, and incubated for a further 1 min. Aliquots (130 μL) were taken and centrifuged through a Sephadex G-50 (fine) spin column at 760 × *g* for 2 min. Radioactivity in the eluate was counted using a liquid scintillation counter (PerkinElmer). As a control, the ionophore carbonyl cyanide *m*-chlorophenyl hydrazone (CCCp) was added to the assay (final concentration 1 μM) after 1 min to collapse the pH gradient. Bovine serum albumin was used as a protein concentration standard³⁹.

MD simulations. Initial coordinates of MdfA in the O_o conformation were taken from those of the crystal structure of the MdfA-Fab complex. N- and C-terminal MdfA residues were capped with acetyl and *N*-methyl groups, respectively. All histidine residues were protonated on the Nδ1 atom. All acidic residues (excluding Glu26^{TM5} and Asp34^{TM5}) and all basic residues were deprotonated and protonated, respectively (see Supplementary Table 3). Glu26^{TM5} was protonated in the initial structure of the O_o(E26P/D34⁻) and O_o(E26P/D34P) simulation runs and Asp34^{TM5} was protonated for the O_o(E26⁻/D34P) and O_o(E26P/D34P) simulation runs. After filling the large cavity on the periplasmic side of the protein with water molecules to prevent placement of lipid molecules there, the structure was embedded in a lipid bilayer and solvated with water and ions using CHARMM-GUI⁴⁰. The orientation of MdfA relative to the lipid bilayer was determined analogously to that of MdfA in the I_f state (PDB ID: 4ZP0) as deposited in the Orientations of Proteins in Membranes (OPM) database⁴¹ by alignment of the Ca atoms of residues 203–400. The rectangular simulation system generated by CHARMM-GUI (90.76 Å × 90.76 Å × 96.98 Å) was subjected to periodic boundary conditions. The system was composed of one protein, 223 1-palmitoyl-2-oleoyl-*sn*-phosphatidylethanolamine (POPE), 40 or 41 K⁺, 44 or 45 Cl⁻, and about 14,000 water molecules. The CHARMM36 force-field parameters^{42,43} were used for protein, lipid, and ions, and the TIP3P model⁴⁴ was used for water. Initial coordinates for the simulations starting from the I_f conformation were generated in a similar manner. Here, the coordinates of the chloramphenicol-bound, I_f form of MdfA (PDB ID: 4ZOW) was used after the ligand coordinates were removed and Arg131 was replaced with the wild-type Gln residue. The system size was 92.01 Å × 92.01 Å × 98.11 Å and was composed of 233 POPE, 41 or 42 K⁺, 47 or 48 Cl⁻, and about 14,700 water molecules.

After energy minimization and equilibration, a production MD run was performed for 1.6 μs (starting from the O_o conformation) or 1.0 μs (starting from the I_f conformation). During the simulation, the temperature was kept at 303.15 K using the Nosé–Hoover thermostat^{45,46}, and the pressure was kept at 1.0 × 10⁵ Pa using the semi-isotropic Parrillelo–Rahman barostat^{47,48}. Bond lengths involving hydrogen atoms were constrained using the LINCS algorithm^{49,50} to allow the use of a large time step (2 fs). Electrostatic interactions were calculated with the particle mesh Ewald method^{51,52}. All MD simulations were performed with Gromacs 5.0.5 (ref. 53), with coordinates recorded every 10 ps.

Time evolutions of RMSDs in the O_o(E26⁻/D34P) and I_f(E26⁻/D34P) MD runs were calculated using their respective initial and final structures as reference (Supplementary Fig. 9). The average values of the RMSDs from the final structures

of the $O_{\alpha}(E26^{-}/D34P)$ and $I_{\alpha}(E26^{-}/D34P)$ runs calculated for the last 2.7 μ s trajectory of the $O_{\alpha}(E26^{-}/D34P)$ MD run were 1.24 ± 0.14 and $1.21 \pm 0.08 \text{ \AA}$, respectively. Corresponding values calculated for the last 0.5 μ s trajectory of the $I_{\alpha}(E26^{-}/D34P)$ MD run were 1.48 ± 0.16 and $1.23 \pm 0.26 \text{ \AA}$, respectively. Thus the two simulations converged to similar states.

Data availability

Data supporting the findings of this manuscript are available from the corresponding authors upon reasonable request. Coordinates of the MdfA–Fab complex have been deposited in the Protein Data Bank under the accession number 6GV1 (<https://doi.org/10.2210/pdb6GV1/pdb>).

Received: 18 May 2017 Accepted: 13 August 2018

Published online: 01 October 2018

References

- Pao, S. S., Paulsen, I. T. & Saier, M. H. Major facilitator superfamily. *Microbiol. Mol. Biol. Rev.* **62**, 1–34 (1998).
- Putman, M., van Veen, H. W. & Konings, W. N. Molecular properties of bacterial multidrug transporters. *Microbiol. Mol. Biol. Rev.* **64**, 672–693 (2000).
- Nikaïdo, H. Multidrug resistance in bacteria. *Annu. Rev. Biochem.* **78**, 119–146 (2009).
- Abramson, J. et al. Structure and mechanism of the lactose permease of *Escherichia coli*. *Science* **301**, 610–615 (2003).
- Kaback, H. R. A chemiosmotic mechanism of symport. *Proc. Natl Acad. Sci. USA* **112**, 1259–1264 (2015).
- Jiang, X. et al. Crystal structure of a LacY–nanobody complex in a periplasmic-open conformation. *Proc. Natl Acad. Sci. USA* **113**, 12420–12425 (2016).
- Quistgaard, E. M., Löw, C., Guettou, P. & Nordlund, P. Understanding transport by the major facilitator superfamily (MFS): structures pave the way. *Nat. Rev. Mol. Cell Biol.* **17**, 123–132 (2016).
- Bibi, E., Adler, J., Lewinson, O. & Edgar, R. MdfA, an interesting model protein for studying multidrug transport. *J. Mol. Microbiol. Biotechnol.* **3**, 171–177 (2001).
- Edgar, R. & Bibi, E. MdfA, an *Escherichia coli* multidrug resistance protein with an extraordinarily broad spectrum of drug recognition. *J. Bacteriol.* **179**, 2274–2280 (1997).
- Lewinson, O. et al. The *Escherichia coli* multidrug transporter MdfA catalyzes both electrogenic and electroneutral transport reactions. *Proc. Natl Acad. Sci. USA* **100**, 1667–1672 (2003).
- Sigal, N., Fluman, N., Siemion, S. & Bibi, E. The secondary multidrug/proton antiporter MdfA tolerates displacements of an essential negatively charged side chain. *J. Biol. Chem.* **284**, 6966–6971 (2009).
- Fluman, N., Cohen-Karni, D., Weiss, T. & Bibi, E. A promiscuous conformational switch in the secondary multidrug transporter MdfA. *J. Biol. Chem.* **284**, 32296–32304 (2009).
- Fluman, N., Ryan, C. M., Whitelegge, J. P. & Bibi, E. Dissection of mechanistic principles of a secondary multidrug efflux protein. *Mol. Cell* **47**, 777–787 (2012).
- Heng, J. et al. Substrate-bound structure of the *E. coli* multidrug resistance transporter MdfA. *Cell Res.* **25**, 1060–1073 (2015).
- Varela, M. F., Sansom, C. E. & Griffith, J. K. Mutational analysis and molecular modelling of an amino acid sequence motif conserved in antiporters but not symporters in a transporter superfamily. *Mol. Membr. Biol.* **12**, 313–319 (1995).
- Adler, J. & Bibi, E. Determinants of substrate recognition by the *Escherichia coli* multidrug transporter MdfA identified on both sides of the membrane. *J. Biol. Chem.* **279**, 8957–8965 (2004).
- Liu, M., Heng, J., Gao, Y. & Wang, X. Crystal structures of MdfA complexed with acetylcholine and inhibitor reserpine. *Biophys. Rep.* **2**, 78–85 (2016).
- Juge, N. et al. Plasmodium falciparum chloroquine resistance transporter is a H⁺-coupled polyspecific nutrient and drug exporter. *Proc. Natl Acad. Sci. USA* **112**, 3356–3361 (2015).
- Adler, J., Lewinson, O. & Bibi, E. Role of a conserved membrane-embedded acidic residue in the multidrug transporter MdfA. *Biochemistry* **43**, 518–525 (2004).
- Nagarathinam, K. et al. The multidrug-resistance transporter MdfA from *Escherichia coli*: crystallization and X-ray diffraction analysis. *Acta Crystallogr. F Struct. Biol. Commun.* **73**, 423–430 (2017).
- Sigal, N., Molshanski-Mor, S. & Bibi, E. No single irreplaceable acidic residues in the *Escherichia coli* secondary multidrug transporter MdfA. *J. Bacteriol.* **188**, 5635–5639 (2006).
- Yardeni, E. H., Zomot, E. & Bibi, E. The fascinating but mysterious mechanistic aspects of multidrug transport by MdfA from *Escherichia coli*. *Res. Microbiol.* <https://doi.org/10.1016/j.resmic.2017.09.004> (2017).
- Zomot, E. et al. A new critical conformational determinant of multidrug efflux by an MFS transporter. *J. Mol. Biol.* **430**, 1368–1385 (2018).
- Sigal, N. et al. 3D model of the *Escherichia coli* multidrug transporter MdfA reveals an essential membrane-embedded positive charge. *Biochemistry* **44**, 14870–14880 (2005).
- Adler, J. & Bibi, E. Promiscuity in the geometry of electrostatic interactions between the *Escherichia coli* multidrug resistance transporter MdfA and cationic substrates. *J. Biol. Chem.* **280**, 2721–2729 (2005).
- Liu, Y., Ke, M. & Gong, H. Protonation of Glu135 facilitates the outward-to-inward structural transition of fucose transporter. *Biophys. J.* **109**, 542–551 (2015).
- Dang, S. et al. Structure of a fucose transporter in an outward-open conformation. *Nature* **467**, 734–738 (2010).
- Radestock, S. & Forrest, L. R. The alternating-access mechanism of MFS transporters arises from inverted-topology repeats. *J. Mol. Biol.* **407**, 698–715 (2011).
- Krammer, E.-M., Ghaddar, K., André, B. & Prévost, M. Unveiling the mechanism of arginine transport through AdiC with molecular dynamics simulations: the guiding role of aromatic residues. *PLoS ONE* **11**, e0160219 (2016).
- Drew, D. & Boudker, O. Shared molecular mechanisms of membrane transporters. *Annu. Rev. Biochem.* **85**, 543–572 (2016).
- Jaenecke, P. et al. Generation of conformation-specific antibody fragments for crystallization of the multidrug resistance transporter MdfA. *Methods Mol. Biol.* **1700**, 97–109 (2018).
- Kabsch, W. XDS. *Acta Crystallogr. D Biol. Crystallogr.* **66**, 125–132 (2010).
- McCoy, A. J. et al. Phaser crystallographic software. *J. Appl. Crystallogr.* **40**, 658–674 (2007).
- Jeffrey, P. D. et al. Structure and specificity of the anti-digoxin antibody 40-50. *J. Mol. Biol.* **248**, 344–360 (1995).
- Emsley, P., Lohkamp, B., Scott, W. G. & Cowtan, K. Features and development of Coot. *Acta Crystallogr. D Biol. Crystallogr.* **66**, 486–501 (2010).
- Adams, P. D. et al. PHENIX: a comprehensive Python-based system for macromolecular structure solution. *Acta Crystallogr. D Biol. Crystallogr.* **66**, 213–221 (2010).
- Winn, M. D. et al. Overview of the CCP4 suite and current developments. *Acta Crystallogr. D Biol. Crystallogr.* **67**, 235–242 (2011).
- Wilman, H. R., Shi, J. & Deane, C. M. Helix kinks are equally prevalent in soluble and membrane proteins. *Proteins* **82**, 1960–1970 (2014).
- Schaffner, W. & Weissmann, C. A rapid, sensitive, and specific method for the determination of protein in dilute solution. *Anal. Biochem.* **56**, 502–514 (1973).
- Lee, J. et al. CHARMM-GUI Input Generator for NAMD, GROMACS, AMBER, OpenMM, and CHARMM/OpenMM simulations using the CHARMM36 additive force field. *J. Chem. Theory Comput.* **12**, 405–413 (2016).
- Lomize, M. A., Lomize, A. L., Pogozheva, I. D. & Mosberg, H. I. OPM: orientations of proteins in membranes database. *Bioinformatics* **22**, 623–625 (2006).
- Klauda, J. B. et al. Update of the CHARMM all-atom additive force field for lipids: validation on six lipid types. *J. Phys. Chem. B* **114**, 7830–7843 (2010).
- Best, R. B. et al. Optimization of the additive CHARMM all-atom protein force field targeting improved sampling of the backbone ϕ , ψ and side-chain χ (1) and χ (2) dihedral angles. *J. Chem. Theory Comput.* **8**, 3257–3273 (2012).
- Jorgensen, W. L., Chandrasekhar, J., Madura, J. D., Impey, R. W. & Klein, M. L. Comparison of simple potential functions for simulating liquid water. *J. Chem. Phys.* **79**, 926–11 (1983).
- Nosé, S. A molecular dynamics method for simulations in the canonical ensemble. *Mol. Phys.* **52**, 255–268 (2006).
- Hoover, W. G. Canonical dynamics: equilibrium phase-space distributions. *Phys. Rev. A* **31**, 1695–1697 (1985).
- Parrinello, M. & Rahman, A. Polymorphic transitions in single crystals: a new molecular dynamics method. *J. Appl. Phys.* **52**, 7182–7190 (1981).
- Nosé, S. & Klein, M. L. Constant pressure molecular dynamics for molecular systems. *Mol. Phys.* **50**, 1055–1076 (2006).
- Hess, B. P-LINCS: a parallel linear constraint solver for molecular simulation. *J. Chem. Theory Comput.* **4**, 116–122 (2008).
- Hess, B., Bekker, H. & Berendsen, H. LINCS: a linear constraint solver for molecular simulations. *J. Comput. Chem.* **18**, 1463–1472 (1997).
- Darden, T., York, D. & Pedersen, L. Particle mesh Ewald: an N²log(N) method for Ewald sums in large systems. *J. Chem. Phys.* **98**, 10089–10092 (1993).
- Essmann, U. et al. A smooth particle mesh Ewald method. *J. Chem. Phys.* **103**, 8577–8593 (1995).

53. Hess, B., Kutzner, C., van der Spoel, D. & Lindahl, E. GROMACS 4: algorithms for highly efficient, load-balanced, and scalable molecular simulation. *J. Chem. Theory Comput.* **4**, 435–447 (2008).

Acknowledgements

We would like to thank Vincent Oleric and Takashi Tomizaki of the Swiss Light Source (SLS, Villigen) for assistance in data collection and Toshiya Senda for helpful discussions and support. This work was supported by the Bundesministerium für Bildung und Forschung (BMBF) program ZIK HALOmem (FKZ 03Z2HN21 to M.T.), by the European Regional Development Fund ERDF (1241099001 to M.T.S.), and in part by the Platform Project for Supporting in Drug Discovery and Life Science Research (Platform for Drug Discovery, Informatics and Structural Life Science (PDIS) and Basis for Supporting Innovative Drug Discovery and Life Science Research (BINDS)) from the Japan Agency for Medical Research and Development (AMED) under Grant number JP18am0101107 (to T.T.), JP18am0101079 (to S.I. and N.N.), and JP18am0101071 (to M.T.), the ERATO Human Receptor Crystallography Project of the Japan Science and Technology Agency (JST) (to S.I.), by the Strategic Basic Research Program, JST (to S.I. and N.N.), by the Targeted Proteins Research Program of the Ministry of Education, Culture, Sports, Science and Technology (MEXT) of Japan (to S.I.), and by Grants-in-Aids for Scientific Research from the MEXT (No. 22570114 to N.N.). Crystallographic data were collected at the SLS with support from the European Community's 7th Framework Programme (FP7/2007–2013) under BioStruct-X (grant agreement No. 283570, project ID: BioStructx_5450 to M.T.).

Author contributions

K.N., F.J. and M.T. purified and crystallized MdfA and collected diffraction data. Fab YN1074 was produced by Y.N.-N., K.L., Y.H. and N.N. using the antibody production platform for membrane proteins developed by S.I. and N.N. The structure was solved by K.N. and C.P. and analyzed together with M.T.S. and M.T. Reconstitution experiments were performed by N.J., T.M., H.O. and M.T. MD simulations were carried out by T.T. The project was conceived and designed by M.T. and supervised together with M.T.S. All

authors participated in analysis and discussion of the results and contributed to the preparation of the manuscript.

Additional information

Supplementary Information accompanies this paper at <https://doi.org/10.1038/s41467-018-06306-x>.

Competing interests: The authors declare no competing interests.

Reprints and permission information is available online at <http://npj.nature.com/reprintsandpermissions/>

Publisher's note: Springer Nature remains neutral with regard to jurisdictional claims in published maps and institutional affiliations.



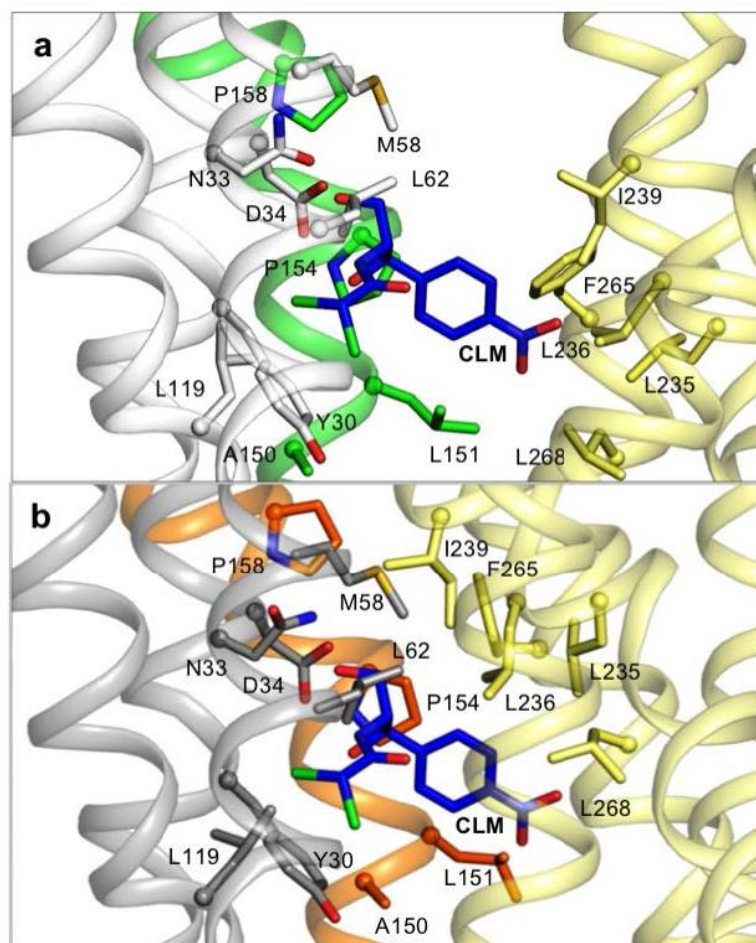
Open Access This article is licensed under a Creative Commons Attribution 4.0 International License, which permits use, sharing, adaptation, distribution and reproduction in any medium or format, as long as you give appropriate credit to the original author(s) and the source, provide a link to the Creative Commons license, and indicate if changes were made. The images or other third party material in this article are included in the article's Creative Commons license, unless indicated otherwise in a credit line to the material. If material is not included in the article's Creative Commons license and your intended use is not permitted by statutory regulation or exceeds the permitted use, you will need to obtain permission directly from the copyright holder. To view a copy of this license, visit <http://creativecommons.org/licenses/by/4.0/>.

© The Author(s) 2018

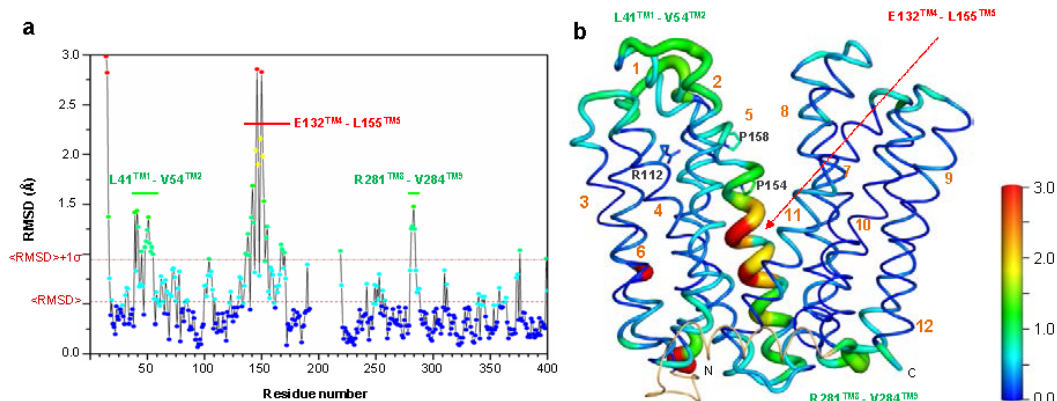
Supplementary Information

Outward open conformation of a Major Facilitator Superfamily multidrug/H⁺ antiporter provides insights into switching mechanism

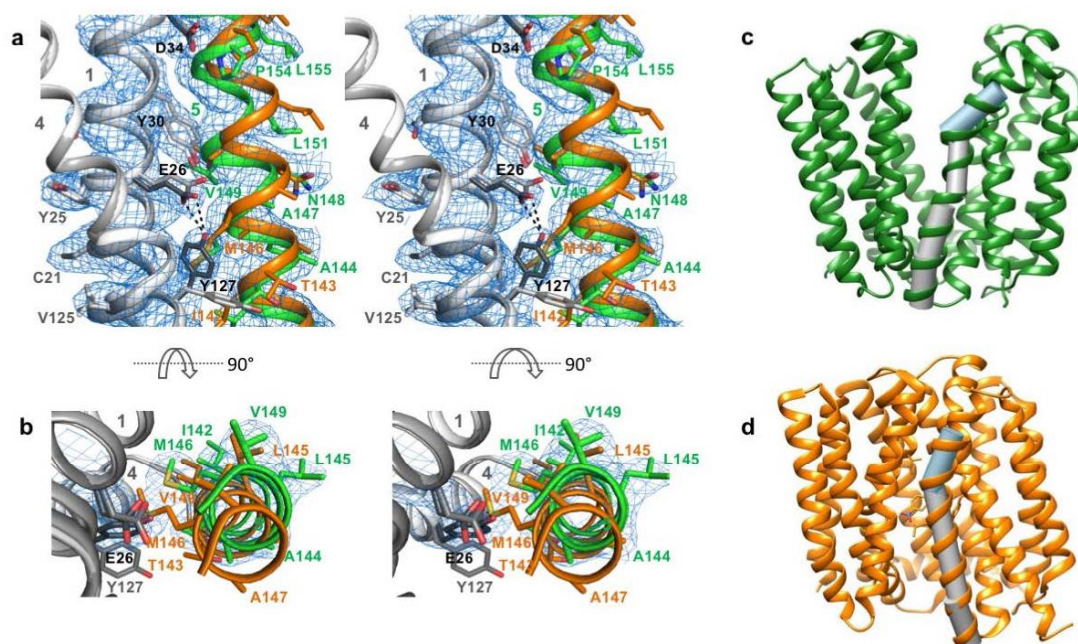
Kumar Nagarathinam *et al.*



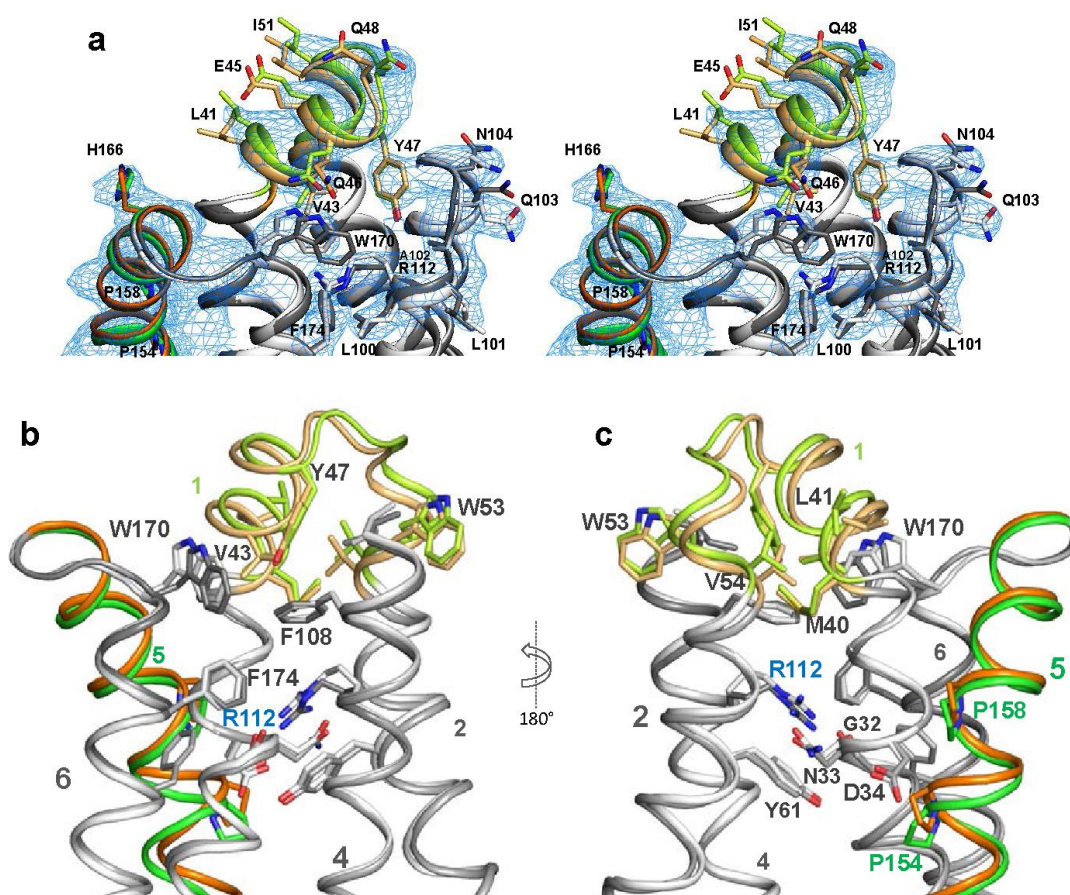
Supplementary Figure 1: The drug binding site is open to the periplasmic space in the outward open conformation (a; orientation as in Figure 1). The chloramphenicol binding site (obtained by superposition of the N-terminal domain of PDB coordinates 4ZOW¹ in the inward open conformation (b) on the present structure) is not only accessible to the periplasm, but is disrupted in the O_o state. Due to a distortion in TM5, N-terminal domain residues A150^{TM5} and L151^{TM5} disengage from the ligand, and rotation of the C-terminal domain results in displacement of residues from TM7 and TM8 by up to 8 Å (C α – C α distance).



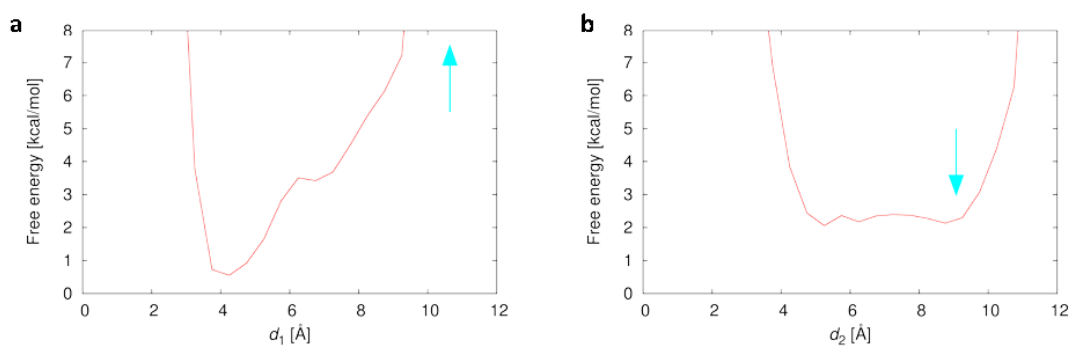
Supplementary Figure 2: Superposition of the individual domains of MdfA in the I_f and O_o conformations reveals significant deviations in the N-terminal domain. (a) $C\alpha$ distance plots between O_o and I_f states as a function of residue number after separate superposition of the N- and C-terminal domains. Lines marking the mean $\langle \text{RMSD} \rangle$ (0.5211 Å) and $\langle \text{RMSD} \rangle + 1\sigma$ ($\sigma = 0.4242$ Å = standard deviation of RMSD values from the mean) values are shown. Three regions of the sequence show significant deviations between the O_o and I_f structures: Glu132^{TM4}-Leu155^{TM5}, Leu41^{TM1}-Val54^{TM2} and Arg281^{TM8}-Val284^{TM9}. The latter region, which represents the contact site for the TM5 N-terminal residues in the O_o state (see Figure 2), shows structural variation in the I_f conformation in the presence of different ligands^{1,2}, so that we assume that this exhibits inherent plasticity and does not play a major role in transitioning between the two states. (b) Projection of the $C\alpha$ distance values per residue on the O_o structure described here using the PyMOL programme. Regions with large and small distances are depicted using thick and thin radii respectively, colored as a spectrum from blue (0.1 Å) to red (3.0 Å).



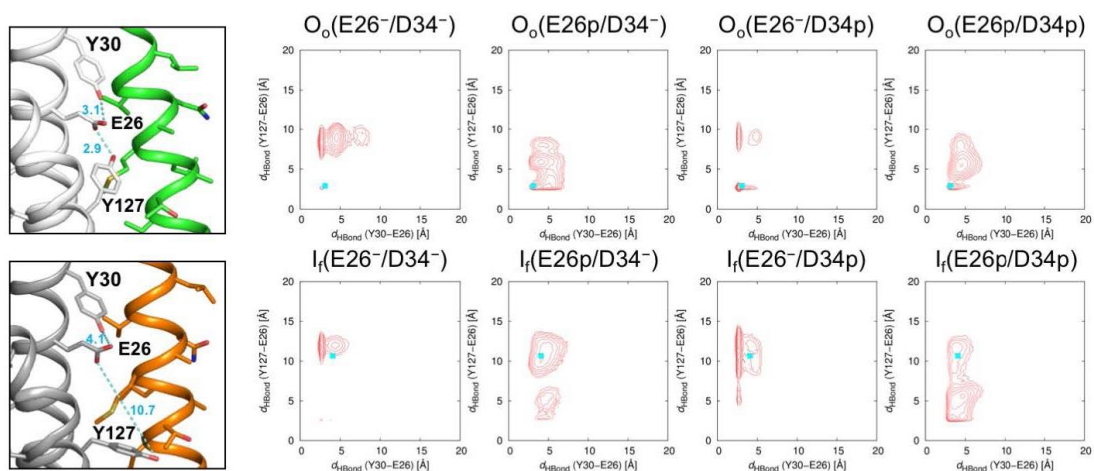
Supplementary Figure 3: Electron densities ($2F_o-F_c$ contoured at 1σ , in stereo) for MdfA in the O_o conformation, superimposed with coordinates of the final (O_o, green) and initial (I_f, orange) models. (a) Electron density for TM5 in the O_o conformation, oriented as in Figure 1. Overlay of the N-terminal domain from the I_f conformation (light grey, green) fails to satisfy electron density for TM5. (b) As in (a), rotated 90° about a horizontal axis. See also accompanying Supplementary Movie 1. (c, d) Depiction of TM5 helix direction in the O_o (orange) and I_f (green) crystal structures calculated using the program Kink Finder³; the two-proline-containing antiporter motif C "153AlaProXaaXaaGlyPro158" of TM5 is shown as a blue cylinder.



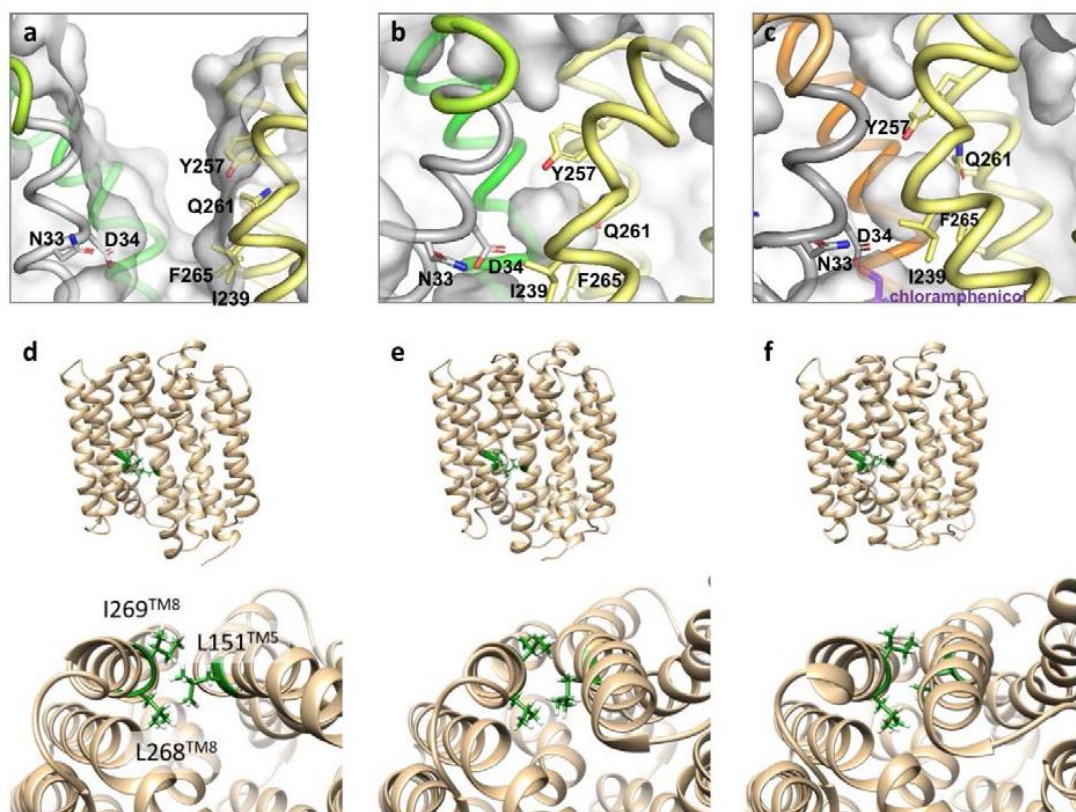
Supplementary Figure 4: Small but significant differences are observed in the hydrophobic core near the periplasmic face of the N-terminal domain. (a) Electron density ($2F_o - F_c$ contoured at 1σ , in stereo) for the hydrophobic core in stereo representation. **(b, c)** The core is in contact with the buried guanidinyli moiety of conserved Arg112^{TM4} (motif B), which in turn is connected to Asn33^{TM1}-Asp34^{TM1} by a hydrogen bond network (not shown). View **(b)** from the “left” of **Figure 1** and **(c)** rotated 180° about a vertical axis.



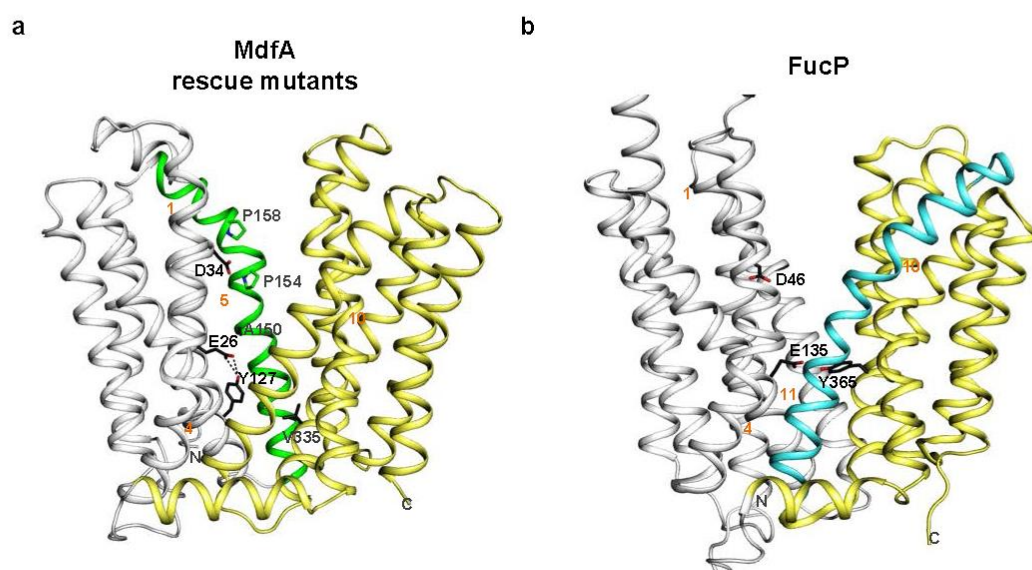
Supplementary Figure 5: Free energy profiles calculated from the distribution of (a) α_1 in the MD run $O_o(E26^-/D34p)$ and (b) α_2 in the MD run $I_t(E26^-/D34p)$. The cyan arrows indicate the d_1 and d_2 values in the initial structures respectively.



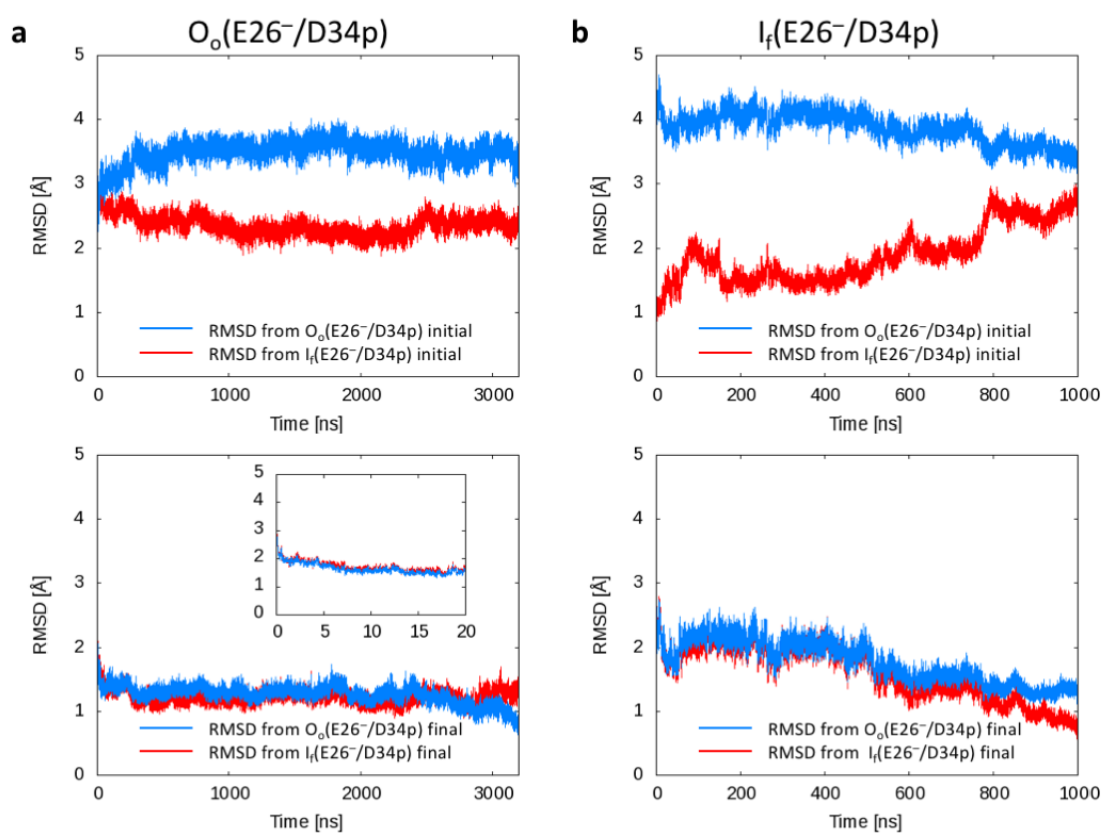
Supplementary Figure 6: Conformational distributions of the transporter during molecular dynamics simulations as a function of starting conformation (O_o vs. I_i) and Glu26/Asp34 protonation states. Plotted are the distances between the Glu26^{TM1} carboxylate and the hydroxyl groups of Tyr127^{TM4} (vertical axes) and Tyr30^{TM1} (horizontal axes). Cyan squares depict distances in the respective initial crystal structures (left).



Supplementary Figure 7: Snapshots from the MD simulation trajectories. (a-c) Protonation of Asp34^{TM5} in the O_o state (a) results in an occluded state (b) in which the Asp34^{TM5} side chain juxtaposes an internal cavity (closed surface) bounded by Tyr257^{TM7}, Gln261^{TM8}, Ile239^{TM7} and Phe265^{TM8}. A similar cavity is found in the chloramphenicol-bound I_f structure (c). (d-f) TM5 undergoes twisting during the transition from the I_f structure to the occluded state. Lateral and cytoplasmic views of the snapshot structures at 0.5 (d), 0.6 (e), and 1.0 μs (f) of the I_f(E26⁻/D34^p) runs are shown in the upper and lower panels, respectively. Sidechain atoms of L151^{TM5}, L268^{TM8} and I269^{TM8} are shown in a stick representation. Carbon and hydrogen atoms are colored green and white, respectively.



Supplementary Figure 8: Similarities in MdfA rescue mutants and the symporter FucP. (a) Selection for drug transport rescue in cells harboring the otherwise inactive TM1 variants Glu26^{TM1}Thr/Asp34^{TM1}Met and Glu26^{TM1}Thr resulted in the detection of mutants containing the acidic side chains Ala150^{TM5}Glu and Val335^{TM10}Glu^{4,5}. These residues would be well positioned to make hydrogen bonds to Tyr127^{TM4} in the outward open structure. (b) Recent thermodynamic calculations and molecular dynamic simulations have led in principle to similar conclusions for the L-fucose/H⁺ symporter FucP⁶. Using computational methods, it was proposed that protonation of FucP Glu135^{TM4} in TM4 allows surmounting of a ca. 2 kcal mol⁻¹ energy barrier between the inward and outward open states. An intermediate state in which TM11 is distorted is postulated, although a causative link between Glu135^{TM4} (de)protonation and TM11 distortion has not been described. Inspection of the FucP structure⁷ suggests that Glu135^{TM4} could form a hydrogen bond with Tyr365^{TM10} of C-domain TM10.



Supplementary Figure 9. Time evolution of the RMSDs from the initial (upper panels) and final (lower panels) structures of the $O_o(E26^-/D34p)$ (blue lines) and $I_f(E26^-/D34p)$ (red lines) MD runs. (a) $O_o(E26^-/D34p)$ and (b) $I_f(E26^-/D34p)$. The inset shows the RMSDs from the final structures of the MD run $O_o(E26^-/D34p)$ for the time from 0 to 20 ns. RMSDs were calculated for C α atoms.

Supplementary Table 1. RMSDs of MD simulation snapshots from the crystal structure

Aligned residues ^a	RMSD ^b [Å]
All ^c	2.59 ± 0.27
TM helices ^d	2.46 ± 0.22
N-lobe TM helices ^e	1.45 ± 0.21
C-lobe TM helices ^f	1.08 ± 0.11
Periplasmic halves of TM helices ^g	2.84 ± 0.29
Cytoplasmic halves of TM helices ^h	1.77 ± 0.14

^aBefore calculating RMSD, the coordinates of the C α atoms of the designated residues of each snapshot structure in the trajectory were aligned with those of the corresponding atoms of the crystal structure.

^bMean ± standard deviation.

^cResidues 14–400.

^dResidues 14–46, 53–79, 81–101, 105–133, 136–164, 171–191, 219–246, 254–278, 284–308, 313–340, 346–398.

^eResidues 14–46, 53–79, 81–101, 105–133, 136–164, 171–191.

^fResidues 219–246, 254–278, 284–308, 313–340, 346–398.

^gResidues 33–46, 53–63, 99–101, 105–113, 155–164, 171–171, 233–246, 254–264, 298–308, 313–321, 361–387.

^hResidues 14–32, 64–79, 81–98, 114–133, 136–154, 172–191, 219–232, 265–278, 284–297, 322–340, 346–360, 388–398.

Supplementary Table 2. Primers used for site direct mutagenesis

	Sequence (5' to 3')
E26Q-Fw	CTGTCTGGTGCTTTACCAATTTTCAACCTATATCGG
E26Q-Rv	CCGATATAGGTTGAAAATTGGTAAAGCACCCAGACAG
D34N-Fw	TTTCAACCTATATCGGCAACAATATGATTCAACCCGGTATG
D34N-Rv	CATACCGGGTTGAATCATATTGTTGCCGATATAGGTTGAAA
Y127A-Fw	CATTGGCGCTGTGGGAGCGGCCGCAATTCAGG
Y127A-Rv	CCTGAATTGCGGCCGCTCCCACAGCGCCAATG
Y127F-Fw	CATTGGCGCTGTGGGATTTGCCGCAATTCAGG
Y127F-Rv	CCTGAATTGCGGCAAATCCCACAGCGCCAATG
M146A-Fw	TCAAGATCACCGCGCTGGCGGCGAACGTGGCGCTGATTG
M146A-Rv	CAATCAGCGCCACGTTCCGCCGCCAGCGCGGTGATCTTGA
W170A-Fw	GTGGATCCATGTGCTGCCCGCGGAGGGGATGTTTGTGTTTGG
W170A-Rv	CAAAACAAACATCCCCTCCGCGGGCAGCACATGGATCCAC

Supplementary Table 3. Conditions for MD simulations

Run	Initial conformation	State of Glu26 ^{TM1}	State of Asp34 ^{TM1}
O _o (E26 ⁻ /D34 ⁻)	O _o	negatively charged	negatively charged
O _o (E26 ^P /D34 ⁻)	O _o	protonated	negatively charged
O _o (E26 ⁻ /D34 ^P)	O _o	negatively charged	protonated
O _o (E26 ^P /D34 ^P)	O _o	protonated	protonated
I _f (E26 ⁻ /D34 ⁻)	I _f	negatively charged	negatively charged
I _f (E26 ^P /D34 ⁻)	I _f	protonated	negatively charged
I _f (E26 ⁻ /D34 ^P)	I _f	negatively charged	protonated
I _f (E26 ^P /D34 ^P)	I _f	protonated	protonated

Supplementary References

1. Heng, J. *et al.* Substrate-bound structure of the *E. coli* multidrug resistance transporter MdfA. *Cell Res.* **25**, 1060–1073 (2015).
2. Liu, M., Heng, J., Gao, Y. & Wang, X. Crystal structures of MdfA complexed with acetylcholine and inhibitor reserpine. *Biophys Rep* **2**, 78–85 (2016).
3. Wilman, H. R., Shi, J. & Deane, C. M. Helix kinks are equally prevalent in soluble and membrane proteins. *Proteins* **82**, 1960–1970 (2014).
4. Sigal, N., Fluman, N., Siemion, S. & Bibi, E. The secondary multidrug/proton antiporter MdfA tolerates displacements of an essential negatively charged side chain. *J. Biol. Chem.* **284**, 6966–6971 (2009).
5. Adler, J. & Bibi, E. Promiscuity in the geometry of electrostatic interactions between the *Escherichia coli* multidrug resistance transporter MdfA and cationic substrates. *J. Biol. Chem.* **280**, 2721–2729 (2005).
6. Liu, Y., Ke, M. & Gong, H. Protonation of Glu135 Facilitates the Outward-to-Inward Structural Transition of Fucose Transporter. *Biophysical Journal* **109**, 542–551 (2015).
7. Dang, S. *et al.* Structure of a fucose transporter in an outward-open conformation. *Nature* **467**, 734–738 (2010).

7 CONTRIBUTIONS

Contributions to each of the manuscripts are stated in terms of percentage (%) and are also tabulated:

- A:** I designed, performed the experiments and analyzed the data.
B: I also significantly contributed to the writing of the manuscript and prepared the figures, tables and movies.

Contributions of my work shared by the co-authors are stated within brackets and overall contributions from each of the co-authors are mentioned in a separate paragraph. Co-authors contribution of figures, tables and movies are also mentioned separately.

The academic position of the authors in the manuscripts during the course of this project work:

Co-authors	Position
<u>Kumar Nagarathinam (K.N.)</u>	Ph.D. student @ Mikio Tanabe Lab
Frank Jaenecke (F.J.)	Postdoc @ Mikio Tanabe Lab
Christoph Parthier (C.P.)	Postdoc @ Milton.T.Stubbs Lab
Mikio Tanabe (M.T.)	Project Leader / Research group leader, ZIK-HALOmem, Halle (Saale), Germany
Milton.T.Stubbs (M.T.S.)	Professor / Research group leader, Dept. Physikalische Biotechnologie, MLU, Halle (Saale), Germany
Yoshiko Nakada-Nakura (Y.N.)	Postdoc @ So Iwata Lab
Satoshi Ogasawara (S.O.)	Postdoc @ So Iwata Lab
Keihong Liu (K.L.)	Lab Assistant @ So Iwata Lab
Yunhong Hotta (Y.H.)	Lab Assistant @ So Iwata Lab
Narinobu Juge (N.J.)	Ph.D. student @ Takaaki Miyaji Lab
Takaaki Miyaji (T.M.)	Associate Professor, Advanced Science Research Center, Okayama University
Hiroshi Omote (H.O.)	Associate Professor, Dept. of Membrane Biochemistry, Okayama University
Norimichi Nomura (N.N.)	Assistant Professor @ So Iwata Lab
So Iwata (S.I.)	Professor / Research group leader, Dept. Cell Biology, Kyoto University, Japan
Tohru Terada (T.T.)	Associate Professor, Agricultural Bioinformatics Research Unit, University of Tokyo, Japan

Manuscript I

Generation of conformation-specific antibody fragments for crystallization of the multidrug resistance transporter MdfA.

Frank Jaenecke*, Yoshiko Nakada-Nakura*, **Kumar Nagarathinam**, Satoshi Ogasawara, Keihong Liu, Yunhong Hotta, So Iwata, Norimichi Nomura, Mikio Tanabe.

Own contribution: **A = 50%** **B = 20%**

Identification of my own share of the results for this publication:

A: Design, execution and analysis of the data:

- 3.0 Expression and Purification of MdfA (F.J., K.N.)
- 3.5 Purification of the MdfA-Fab complexes (F.J., K.N.)
- 3.6 Thermostability analysis of MdfA-Fab complexes
- 3.7 Crystallization trials of MdfA-Fab complexes

B: Contributions to the writing of the manuscript and figures, tables, movies:

- 3.7 Crystallization trials of MdfA-Fab complexes

Figure: Fig. 4

Contributions from co-authors for the sections, figures, tables and movies:

Methods

- 3.1 Reconstitution of MdfA Protein into Liposomes (F.J.)
- 3.2 Generation of Hybridoma-Producing Abs Against MdfA (Y. N-N., K.L., Y.H.)
- 3.3 Liposome ELISA and Denatured MdfA-Targeted ELISA (Y.N-N., K.L., Y.H.)
- 3.4 Preparation of Fab fragments (Y. N-N., K.L., Y.H.)

Fig. 1, Fig. 2, Fig. 3 and Table. 1

Contributions by co-authors for this publication:

F.J. cloned MdfA. F.J. and **K.N.** overexpressed and purified MdfA, MdfA-Fab complex. F.J. and Y.N. performed the reconstitution of MdfA into the liposome. F.J. and **K.N.** designed and optimized the experiments of thermostability analysis (CPM assay) and purification of the MdfA-Fab complex. F.J. and **K.N.** performed vapour diffusion crystallization and data collection under the supervision of M.T. **K.N.** performed the lipidic cubic phase crystallization under the supervision of M.T. Y.N., S.O. and N.N. designed the experiments and performed experiments of Fab fragments generation. Y.N. performed all the Fab generation experiments with the assistance of K.L. and Y.H. N.N. and S.I. organized the research environment of antibody generation for membrane proteins. M.T. initiated and supervised the overall project.

F.J., Y.N., **K.N.** (Section 3.7 and Fig. 4), N.N. and M.T. wrote the manuscript. All authors contributed to the editing and approval of the manuscript.

Manuscript II

The multidrug-resistance transporter MdfA from *Escherichia coli*: crystallization and X-ray diffraction analysis.

Kumar Nagarathinam*, Frank Jaenecke, Yoshiko Nakada-Nakura*, Keihong Liu, Yunhong Hotta, So Iwata, Milton.T.Stubbs, Norimichi Nomura, Mikio Tanabe.

Own contribution: **A = 75%** **B = 75%**

Identification of my own share of the results for this publication:

A: Design, execution and analysis of the data:

2 Materials and methods

2.1. Macromolecule production

MdfA expression and purification (F.J., K.N), Preparation of MdfA-Fab fragment YN1074 complexes (F.J., K.N), Thermostability assays of MdfA and MdfA-Fab complex, Crystallization, Data collection and processing

2.2. Crystallization

2.3. Data collection and processing

3. Results and discussion

Expression and purification of MdfA, Effect of Fab fragments on MdfA stability (M.T.S, M.T., K.N), Crystallization of MdfA (M.T.S, M.T., K.N)

B: Contributions to the writing of the manuscript and illustrations, tables, movies:

Contributed to the writing of the manuscript along with M.T. and M.T.S except the section: 2.1.4 Preparation of Fab fragments.

Figure: Figure 1, Figure 2, Figure 3 (with M.T.S), Fig. S1. (with M.T), Fig. S2.

Table: Table 1, Table 2, Table 3

Contributions by co-authors for this publication:

F.J. cloned MdfA. F.J. and **K.N.** overexpressed and purified MdfA, MdfA-Fab complex. F.J. and **K.N.** designed and performed thermostability analysis, optimization of conditions for purification of the MdfA-Fab complex. F.J. and **K.N.** performed vapour diffusion crystallization method for MdfA and MdfA-Fab. **K.N.** performed lipidic cubic phase and bicelle crystallization of MdfA and MdfA-Fab complex. **K.N.** collected the data for both MdfA, MdfA-Fab complex and processed the diffraction data under the supervision of M.T. **K.N.**, M.T. and M.T.S analysed the data. Y.N. and N.N. designed and performed the experiments of Fab fragments generation with the assistance of K.L. and Y.H. with the support from N.N. and S.I. M.T. initiated and supervised the overall project. The manuscript was

written by **K.N.**, M.T., and M.T.S. All authors contributed to the editing and approval of the manuscript.

Manuscript III

Outward open conformation of a Major Facilitator Superfamily multidrug/H⁺ antiporter provides insights into switching mechanism.

Nagarathinam K*, Nakada-Nakura Y*, Parthier C, Terada T, Juge N, Jaenecke F, Liu K, Hotta Y, Miyaji T, Omote H, Iwata S, Nomura N, Stubbs M.T., Tanabe M.

Own contribution: **A = 40%** **B = 40%**

Identification of my own share of the results for this publication:

A: Design, execution and analysis of the data:

Methods Crystal structure solution (C.P., K.N.)

Results and Discussion

- Overall structure of MdfA in the outward open (O_o) state (M.T.S, M.T., K.N.)
- MdfA helix TM5 is kinked and bent in the O_o state (M.T.S, M.T., K.N.)
- Rearrangements in the periplasm-proximal N-terminal domain hydrophobic core (M.T.S, M.T.)

B: Contributions to the writing of the manuscript and illustrations, tables, movies:

Contributed to the writing of the manuscript partly along with M.T. and M.T.S as quoted above under results and discussion

Figure: Figure 1, Figure 2, Figure 3, Figure S1 (M.T.S, K.N.), Figure S2, Figure S3 (M.T.S, K.N.), Figure S4, Figure S8

Table: Table 1, Table S2

Movie: Movie S1

Contributions from co-authors for the sections, figures, tables and movies:

Methods Reconstitution of MdfA (M.T., N.J., T.M. and H.O.)

Transport assay (N.J., T.M. and H.O.)

MD simulations (T.T.)

Results and Discussion

Molecular dynamics simulations (M.T.S., T.T.)

Fig. 4, Fig. 5, Fig. S5, Fig. S6, Fig. S7, Fig. S9, Table S1 and Table S3

Contributions by co-authors for this publication:

K.N., F.J. and M.T. purified and crystallized MdfA and collected diffraction data. Fab YN1074 was produced by Y.N.-N., K.L., Y.H. and N.N. using the antibody production platform for membrane proteins developed by S.I. and N.N. The structure was solved by **K.N.** and C.P. and analyzed together with M.T.S. and M.T. Reconstitution experiments were performed by N.J.,

T.M., H.O. and M.T. MD simulations were carried out by T.T. The project was conceived and designed by M.T. and supervised together with M.T.S. All authors participated in analysis and discussion of the results and contributed to the preparation of the manuscript.

8 CURRICULUM VITAE

Education

- 07.2017 – present **Research Associate.**
 Advisor: Prof. Dr. Thomas Krey Lab
*Structural Virology, Institute of Virology,
 Medizinische Hochschule Hannover (MHH), Germany*
- 03.2013 – 06.2017 **Doctoral study (Ph.D.).**
 Advisors: Prof. Dr. Milton T. Stubbs, Dr. Mikio Tanabe Lab
*ZIK-HALOMem Membrane protein structure and dynamics
 Martin-Luther-University Halle-Wittenberg, Halle (Saale), Germany*
- 10.2009 – 02.2012 **Master of Science Pharmaceutical Biotechnology**
Martin-Luther-University Halle-Wittenberg, Halle (Saale), Germany
- 09.2004 – 10.2008 **Bachelor of Pharmacy**
Madras Medical College, Chennai, India
- 06.2003 – 03.2004 **12th standard**
Holy Cross Matriculation Higher Secondary School, Salem, India

Publications (reverse chronological order)

- Klamt A*, **Nagarathinam K**, Tanabe M, Kumar A, Balbach J. *Hyperbolic Pressure-Temperature Phase Diagram of the Zinc-Finger Protein apoKti11 Detected by NMR-Spectroscopy.* **J. Phys. Chem. B**, 2019, **123**, 4, 792-801.
- **Nagarathinam K***, Nakada-Nakura Y*, Parthier C, Terada T, Juge N, Jaenecke F, Liu K, Hotta Y, Miyaji T, Omote H, Iwata S, Nomura N, Stubbs M.T., Tanabe M. *Outward open conformation of a Major Facilitator Superfamily multidrug/H⁺ antiporter provides insights into switching mechanism.* **Nature Communications** 9, Article number: 4005 (2018).
- **Ströh LJ, Nagarathinam K***, Krey T. *Conformational flexibility in the CD81-Binding site of the Hepatitis C Virus Glycoprotein E2.* **Front. Immunol.**, 18 June 2018.
- Jaenecke F*, Nakada-Nakura Y*, **Nagarathinam K**, Ogasawara S, Liu K, Hotta Y, Iwata S, Nomura N, Tanabe M. *Generation of conformation-specific antibody fragments for crystallization of the multidrug resistance transporter MdfA. Bacterial Multidrug Exporters.* **Methods in Molecular Biology**, vol 1700, 2018. Humana Press, New York, NY.
- **Nagarathinam K***, Jaenecke F, Nakada-Nakura Y*, Liu K, Hotta Y, Iwata S, Stubbs M.T., Nomura N., Tanabe M. *The multidrug-resistance transporter MdfA from Escherichia coli: crystallization and X-ray diffraction analysis.* **Acta Crystallogr F Struct Biol Commun.** 2017 Jul 1;73(Pt 7):423-430.

Awards / Fellowships / Scholarships

2017	DAAD-STIBET, Ph.D. finalization Grant, Halle (Saale), Germany
2016	Best Presentation Prize - Heart of Europe Bio-Crystallography, 19th HEC meeting, Burg Warberg, Germany
2011	Master study scholarship, Martin Luckner Stiftung Martin-Luther-University Halle-Wittenberg Halle (Saale), Germany
2004 – 2008	Government Merit Scholarship Bachelor study scholarship, Madras Medical College, Chennai, India
2004 – 2008	Venkatammal charitable trust scholarship, Salem, India

Supervision and Teaching

1. Mara Riechmann (Bachelor student project), Martin Luther University, Halle (Saale), Germany
Topic: *Thermostabilization of multidrug resistance transporter MdfA*
2. Shrivatsan Sampathkumar (Master student project), Martin Luther University, Halle (Saale), Germany
Topic: *Interaction studies by cross-linking of the multidrug resistance EmrAB-TolC tripartite complex.*
3. Practical training of Bachelor and Master students on protein crystallization, crystallography softwares.

9 DECLARATIONS

DECLARATION BY THE CANDIDATE

I, Kumar Nagarathinam, hereby declare that the research work described and presented in this cumulative dissertation, entitled “Structural and functional characterization of a Major Facilitator Superfamily multidrug resistance transporter (MdfA) from Escherichia coli”, are my own and was conducted under the guidance of Dr. Mikio Tanabe and Prof. Dr. Milton.T.Stubbs at the ZIK HALOmem – Membrane Protein Structure and Dynamics, Martin Luther University, Halle (Saale), Germany.

In addition, I confirm that no part of this dissertation will be used in a submission in my name, for any other degree at another university or a research institute.

Date:

Halle (Saale), Germany

Kumar Nagarathinam

DECLARATION BY THE SUPERVISORS

We, Prof. Dr. Milton.T.Stubbs and Dr. Mikio Tanabe, certify that the above statements made by the candidate are true to the best of my knowledge.

Prof. Dr. Milton.T.Stubbs



Dr. Mikio Tanabe

Date:

Halle (Saale), Germany

DECLARATION BY THE CANDIDATE FOR SUBMISSION OF A CUMULATIVE DISSERTATION

I, Kumar Nagarathinam, hereby declare that the manuscripts included in this cumulative dissertation are all published. My own contributions to each of the manuscript are mentioned under the section 7 in terms of percentage which were calculated based on the contributions made to the experiments and writing of each manuscript.

Date:

Halle (Saale), Germany

Kumar Nagarathinam

DECLARATION BY THE SUPERVISORS

We, Prof. Dr. Milton.T.Stubbs and Dr. Mikio Tanabe, certify that the above statements made by the candidate are true to the best of my knowledge.

Prof. Dr. Milton.T.Stubbs



Dr. Mikio Tanabe

Date:

Halle (Saale), Germany

10 ACKNOWLEDGEMENTS

I feel overwhelmed when I think of the path that I have travelled through to achieve of what I am today and this would not have been possible without the help of many that I had come across during my research stay in Halle (Saale).

I like to express my deepest gratitude to my direct supervisor **Dr. Mikio Tanabe**. Thanks for giving me the opportunity to work under your mentorship. You were a pillar of support both personally and professionally, since the time I started working as a HiWi for you. Though the projects that you gave me were not easy to get through. I am very happy that we worked it out before you left Halle. This was an unfortunate situation but you left me back as a student with a lot of confidence to work independently. Thanks for being very kind, tolerating me all the time and getting my scientific views in the right direction. Thanks for everything and hope to be nice to people so as you were to me that I can never forget.

I like to thank my other direct supervisor **Prof. Dr. Milton T. Stubbs** for all his guidance and mentorship. Thanks for absorbing me into your research group and letting me finish my Ph.D. work. I have to also thank you very much for your positive criticism and making me think more about how to script down a scientific draft. It was great to see the transformation of the initial manuscript to the published one. I have to also place on the record of your inputs for the scientific presentation which made me win the best presentation prize at the HEC 19th meeting, Burg Warberg and I owe you a lot of gratitude for everything. I really enjoyed the time working in your lab.

Dr. Frank Jaenecke, Post Doc @ AG Tanabe. Thanks for fostering me with the membrane biochemistry techniques, right from my Master thesis. I grew over time under your supervision that I later started to complement the MdfA work along with you. It was an amazing time although the research work was slowly progressing. Thanks for being friendly and for all the personal, scientific discussions that we had.

Dr. Caroline Haupt, Post Doc @ AG Tanabe. Though my project was in no way connected with your research work, you were always there to sort out all scientific troubles and always open for discussions.

Dr. Christoph Parthier, Post Doc @ AG Stubbs. Determining the crystal structure of MdfA would not have been possible without your guidance. Thank you very much for the constructive discussions and for all the protein crystallography you have taught me. You have also taught me indirectly about how should one be self-driven in learning more of protein crystallography if one wants to be a proficient crystallographer.

Employees and students of AG Tanabe; **Dr. Peter Simeonov, Dr. Christoph Kattner, Mara Riechmann**. Thank you for providing me a friendly environment and creating an atmosphere to do good science. With a special mention to **Prof. Dr. Kirsten Bacia** and your team for allowing me to work @ ZIK-**HALO**mem even after Mikio left to Japan. **Dr. Sebastian Daum**, Post Doc @ AG Bacia. You were super friendly, and thank you very much for the interesting discussions that we had.

Not to forget I have to thank the technicians **Ines Jakob** (AG Tanabe) and **Claudia Müller** (AG Bacia) who were of immense help for my experiments, ordering chemicals as and when needed and at times helping me out to get organized in the lab. With the stringent bureaucratic process in Germany, Claudia Müller you were the German voice of me. I do not know how many times I would have walked up to your desk for getting an issue sorted out, either filling in forms or calling someone up on phone.

Dr. Ulla Niesbach-Klösigen, Rositta Mothes, Katja Möritz coordinators of ZIK-**HALO**mem. Thanks for all the administrative things and sorting out my bureaucratic issues from time to time.

I would like to also thank the collaborators at this time point especially **Dr. Yoshiko-Nakadu Nakura**, Kyoto University, Japan for supplying Fab as and when requested without which the project would have not progressed within the stipulated time frame.

I would like to dedicate this thesis to my brother-in-law **Dr. B.R. Srinivasan**, my elder sister **Vanitha** and my **bachelor college mates** who had been the root cause for my career in Germany. I owe the deepest gratitude to them lifelong.

I would like to thank my mother for the constant support and my father. I would like to also thank my eldest sister **Poornima** and brother-in-law **Vivek. Murali** my cousin thanks for your continuous support.

Many good hearts here in Germany during my master and Ph.D. studies have made my life easier. My friends in Halle; **Senthil, Karthi, Dinesh, Mohan, Amit, Sarada, Tamil** and many more had been of great support and strength. My bachelor college mates **Muthu, Kabilan, Ram, Vimal, Sharmila, Saranya, Uma Shankari .etc.**, and my childhood classmates **Bilal, Suganya** for their constant support and encouragement.

I like to also thank my parents-in-law and **Saravana** for everything. Last but not least, I would like to thank my wife **Visha** for all her support right from the day one before the time we got married and for making our life successful so far. **Magilthiran**, a tiny tot and a toy for me at the moment have brought in immense happiness in our life. May he be inspired by my work and apply the same in his endeavours.